University of Stellenbosch

Design Optimisation of Cageless Flux Barrier Rotor Reluctance Synchronous Machine

Maarten J. Kamper

Dissertation accepted for the Degree of
Doctor of Philosophy in Electrical Engineering at
the University of Stellenbosch

Promoter:

Prof. F.S. van der Merwe. University of Stellenbosch

December 1996

Declaration:

The work presented in this dissertation was carried out in the Department of Electrical and Electronic Engineering, University of Stellenbosch, during the period January 1994 to March 1996 under the supervision of Prof. F.S. van der Merwe.

The author wishes to declare that, except for commonly understood and accepted ideas, or where specific reference is made to the work of others, the work in this dissertation is his own and includes nothing which is the outcome of work done in collaboration. It has not been submitted, in part or in whole, to any other university for a degree, diploma or other qualification.

M.J. Kamper

Date: December 1996

Acknowledgements

I would like to express my sincere appreciation to:

- My promoter Prof. F.S. van der Merwe for his supervision and constant encouragement and his efforts to ensure the availability of financial resources.
- Dr A.F. Volschenk, who developed the basic finite element software program at the University of Cambridge. I can only say thank you for everything.
- Dr J.D. Buys for his guidance regarding the mathematical algorithms and his interest in the project.
- Prof. A. Basson for his help with the mechanical strength analysis.
- ESKOM, SPOORNET and the FRD for providing financial assistance.
- All the people of the workshop, the students and the Centre for Mechanical Services for the assembling and testing of the prototype system.
- My family, in particular my mother for her keen interest and my father in memory.
- My wife, Fransien, for her love and understanding of the situation and her encouragement.
- My Lord and my God and may I say, in the words of Ps. 103:1, "Praise the Lord, O my soul; all my inmost being, praise his holy name."

Synopsis

The focus of this thesis is on the overall (stator and rotor) design optimisation of the current vector-controlled reluctance synchronous machine and the evaluation of the steady-state performance of this machine in motoring operation. The rotor considered is the cageless normal laminated flux barrier-type of rotor.

The absolute optimum-designed electrical machine can at best be obtained by using the finite element method in the design optimisation process. This thesis proposes a multidimensional finite element-based design optimisation method for the optimum design of the reluctance synchronous machine. The thesis stresses the explanation and understanding of the optimum-designed reluctance machine. A simple approximate magnetic circuit calculation method is used to show and explain design tendencies and to do preliminary stator design optimisations. Goodness factors for the reluctance synchronous machine are also derived. The optimised results of a number of reluctance synchronous machines that are designed according different criteria in the 3 - 10 kW power range are given and explained. A great deal of attention is also given to the performance capability of the reluctance synchronous machine in the medium power range (sub 500 kW).

The thesis shows that the proposed optimisation method can be applied with success to optimise the design of the reluctance synchronous machine. The optimum steady-state performance of the reluctance synchronous machine found in this study shows that this machine can no longer be considered as a bad machine. Although the power factor of this machine is still on the low side, the advantages of high power density and high efficiency, even in the upper-medium power range, are attractive characteristics for any variable speed drive.

Sinopsis

Die fokus van hierdie tesis is op die totale (stator en rotor) ontwerp-optimering van die stroom vektor beheerde reluktansie sinchroonmasjien en die evaluering van die bestendige toestand vermoë van hierdie masjien in motorwerking. Die tipe rotor onder beskouing is die koulose, normaal gelamelleerde vloedbarrière tipe rotor.

Die absoluut optimum ontwerpte elektriese masjien kan op sy beste verkry word deur die eindige element metode in die ontwerp-optimeringsproses te gebruik. Hierdie tesis stel 'n multidimensionele eindige element gebaseerde optimeringsmetode voor vir die optimum ontwerp van die reluktansie sinchroonmasjien. Die tesis lê nadruk op die verduideliking en verstaan van die optimum ontwerpte reluktansiemasjien. 'n Eenvoudige benaderde magnetiese stroombaan berekeningsmetode is gebruik om ontwerp tendense te verduidelik en om voorlopige stator-ontwerpe te doen. Goedheidsfaktore is ook vir die reluktansie sinchroonmasjien afgelei. Die geoptimeerde resultate van 'n aantal reluktansie sinchroonmasjiene wat volgens verskillende kriteria in die 3 - 10 kW drywingsgebied ontwerp is, word gegee en verduidelik. Heelwat aandag word ook gegee aan die vermoë van die reluktansiemasjien in die medium drywingsgebied (sub 500 kW).

Die tesis toon dat die voorgestelde optimeringsmetode met sukses toegepas kan word om die ontwerp van die reluktansie sinchroonmasjien te optimeer. Die optimum bestendige toestand vermoë van die reluktansie sinchroonmasjien wat in hierdie studie gevind is, toon dat die masjien nie langer meer as 'n swak masjien beskou kan word nie. Alhoewel die arbeidsfaktor van die masjien nog steeds aan die lae kant is, is die voordele van hoë drywingsdigtheid en hoë benuttingsgraad, selfs in die boonste medium drywingsgebied, aantreklike karakteristieke vir enige veranderlike spoed aandryfstelsel.

To my wife Fransien and
my children Herman, Francois and Marina

You may think that designing electric generators (motors) is no longer an interesting subject, that it is a dead subject because they are all designed. Almost perfect generators or motors can be taken from a shelf. Even if this is true, we can admire the wonderful accomplishment of a problem solved to near perfection. But there remain as many unfinished problems. Even generators and transformers are returning as problems. The study of the design of electrical machinery is a life work in itself.

Feynman Lectures on Physics

Table of Contents

Glossary of Symbols

$\mathbf{A}$	magnetic vector potential, **Wb/m**
A_{cu}	active copper area of a stator slot, **m²**
B	flux density, **Wb/m²**
B_{mf}	maximum airgap flux density, **Wb/m²**
B_{mt}	maximum tooth flux density, **Wb/m²**
B_{my}	maximum yoke flux density, **Wb/m²**
b_p or bp	flux barrier pitch, **m**
b_w or bw	flux barrier width, **m**
e_{abc}	instantaneous values of the fundamental induced EMF in phases *a*, *b* and *c*, **V**
E_d, E_q	steady-state values of the d- and q-axis induced EMF components, **V**
d_i or di	stator inner diameter, **m**
d_o or do	stator outer diameter, **m**
F	magnetomotive force (MMF), **At**
f	function value
$\mathbf{G_r}$	function's gradient vector
G	overall goodness factor
G_{eff}	efficiency goodness factor
G_{pd}	power density goodness factor
G_{pf}	power factor goodness factor
G_{pva}	output power / kVA goodness factor
g_d or gd	airgap length of d-axis magnetic circuit, **m**
g_q	airgap length of q-axis magnetic circuit, **m**
H	magnetic field strength, **At/m**
$\mathbf{H_r}$	quasi-Newton approximation of the inverse Hessian matrix
$\mathbf{I_s}$	space phasor of stator currents, **A ∠ rad.**
$\hat{I}_s$	magnitude of the current space phasor, **A**
I_d, I_q	steady-state values of d- and q-axis stator current components, **A**
iw	inner barrier width, **m**
J	current density, **A/m²**
$[K_p]$	Park's transformation
K_s	stacking factor
K_{w1}	winding factor for the fundamental
k_{sd}	saturation factor for the d-axis magnetic circuit
k_{sq}	saturation factor for the q-axis magnetic circuit
k_c	Carter's factor
L_d, L_q	d- and q-axis synchronous inductances, **H**
L_{dm}, L_{qm}	d- and q-axis inductances due to the space-fundamental airgap flux, **H**
L_e	endwinding leakage inductance, **H**
L_ℓ	per phase stator leakage inductance, **H**
$L_{s\ell}$	per phase stator leakage inductance excluding L_e, **H**

l	axial length of the stator/rotor stack, **m**
l_e	average length of a coil end, **m**
M	mass, **kg**
M_t	iron mass of the teeth, **kg**
M_y	iron mass of the stator yoke, **kg**
m	number of phases
N_{bp}	number of flux barriers per pole (including the cutouts)
N_{sl}	number of stator slots
ow	outer barrier width, **m**
n_a	number of parallel circuits of the stator winding
P	multidimensional vector point
P	power, **W**
P_f	power factor
p	number of pole pairs
q	number of slots per pole per phase
r_s	resistance of all the conductors of a stator slot in parallel, **Ω**
R_c	per phase core loss resistance, **Ω**
R_s	per phase stator resistance, **Ω**
s	slip
T	torque, **Nm**
t_p or tp	tooth pitch, **m**
t_w or tw	tooth width, **m**
v_{abc}	instantaneous values of fundamental supply phase voltages *a*, *b* and *c*, **V**
$\mathbf{V}_s$	space phasor of stator voltages, **V ∠ rad.**
V_d, V_q	steady-state values of d- and q-axis stator voltage components, **V**
W	number of turns in series per phase
yh	yoke height, **m**
X	multidimensional vector containing machine variables
Z	vector direction
z	number of conductors per slot, alternatively the z-direction (axial direction)
η	efficiency
Λ	permeance ratio
ℜ	magnetic reluctance, **At/Wb**
λ_{abc}	instantaneous values of total flux linkages of phases *a*, *b* and *c*, **Wb**
λ_{abc1}	instantaneous values of fundamental flux linkages of phases *a*, *b* and *c*, **Wb**
λ_{abc3}	instantaneous values of 3rd harmonic flux linkages of phases *a*, *b* and *c*, **Wb**
$\boldsymbol{\lambda}_m$	space phasor of the fundamental airgap flux linkage, **Wb ∠ rad.**
λ_{dm}, λ_{qm}	d- and q-axis airgap fundamental stator flux linkage components, **Wb**
$\boldsymbol{\lambda}_s$	space phasor of stator flux linkages, **Wb ∠ rad.**
λ_d, λ_q	d- and q-axis fundamental stator flux linkage components, **Wb**
$\boldsymbol{\lambda}_l$	space phasor of the stator leakage flux linkage, **Wb ∠ rad.**
μ_0	absolute permeability, **H/m**

ρ_t	resistivity of conductor at temperature t, **Ωm**
σ	L_d/L_q
τ_p	pole pitch, **m**
ϕ	angle between current space phasor and rotor d-axis, **rad**
Φ	flux, **Wb**
ω_r	electrical speed of rotor reference frame, **rad/s**
ξ	fractional tolerance

Abbreviations

AMC	Approximate Magnetic Circuit
FE	Finite Element
HMF	Hybrid Magnetic Circuit / Finite Element
RSM	Reluctance Synchronous Machine
nor	normalised

1 Introduction

Reluctance machines can be classified as either single-salient or double-salient reluctance machines. The double-salient reluctance machine has saliency on both the stator and the rotor. Examples of this category are the stepping reluctance machines and the so-called switched reluctance machines. The other category of reluctance machines have non-salient-pole stators but salient-pole rotors or rotors (non-salient or salient) with magnetic asymmetry. These machines are sometimes referred to as simply single-salient reluctance machines. The focus of this thesis is on the latter type of reluctance machine. The machine under consideration has a standard, non-salient stator with a three-phase winding and an unexcited rotor with magnetic asymmetry. The machine is a type of synchronous machine that was previously referred to as a "reaction synchronous machine", an "unexcited synchronous machine" and later a "polyphase reluctance machine". The author prefers to use the name "*reluctance* synchronous machine" (RSM) (not synchronous reluctance) because it describes the machine as a type of synchronous machine like the *permanent magnet* synchronous machine and the *wound-rotor* (wound-field) synchronous machine. Note that all reluctance machines are synchronous machines and this includes the double-salient reluctance machines.

One may ask the question why is research still necessary on the single-salient type of reluctance machine. Has it not been well-known for a long time already that this machine is inherently a bad machine with a poor power density and a low power factor? Kostko said in 1923, "... it can hardly be expected that reaction motors will ever be extensively used". While this is true for reluctance machines that are designed and used for single-speed, open-loop operations, it can simply not been said for reluctance machines that are designed for closed-loop, current vector control. As the first vector-controlled reluctance synchronous machine drives were reported only at the end of the 1980s, surely the research on closed-loop reluctance synchronous machines is still very much in an initial phase.

Furthermore, the advantages of single-salient reluctance machine drives are sometimes not fully recognised. These advantages can be summarised as follows:

- Vector control of the single-salient reluctance machine is very simple as there are no rotor parameters to be identified. The machine has also a distinct advantage over the induction machine in that it runs at exactly synchronous speeds.

- The single-salient reluctance machine is free from the torque ripple problem of double-salient reluctance machines. The rotating field allows for extremely smooth torque and good operation at low speeds.

- There are basically no losses on the rotor, if the rotor is designed correctly. Note that the double-salient reluctance machine suffers from rotor iron losses. The rotor stack, shaft and bearings, therefore, run cooler than machines with rotor windings.

- The cooling of the machine is in principle much less of a problem than is the case with wound-rotor or cage-rotor machines as all the losses are on the stator.

- With no brushes and rotor windings, the reluctance machine requires less maintenance and is in principle more reliable than wound-rotor or cage-rotor machines.

In the past these advantages were completely overshadowed by the poor power density of the reluctance machine due to the fact that the machine was used in an open-loop mode, operating from fixed mains frequency and voltages supplies. With the use of power electronics and current vector control, however, it is clear today that the performance and specifically the power density of the machine can be improved. This justifies further research on the single-salient reluctance machine.

In the following section an overview of the history of the reluctance machine is given and the important publications on single-salient reluctance machines are highlighted. In section 1.2 the problem statement for the research necessary on the reluctance synchronous machine is considered and in section 1.3 the approach to solving the problem is given. The thesis layout is given in section 1.4.

1.1 The history of the reluctance machine

Reluctance and permanent magnet machines were among the first electrical machines built. The observation that an electromagnetic coil attracts a piece of iron led to the idea of using this force to obtain mechanical motion. The first reluctance machines (from 1840) were basically double-salient machines with electromagnets that were switched according to the position of moving iron in very much the same way as with the switched reluctance machine today. These "electromagnetic engines" as they were called were heavy, bulky machines with amazingly low efficiencies. The result was that they were used very little in practice. The development of these machines came to an abrupt halt in the early 1870s when the first electric generator/motor with wound field coils was developed.

From that time and due to the development of the induction and synchronous machines in the 1880s, research on double-salient stepping reluctance machines and single-salient "reaction" machines (unexcited salient-pole synchronous machine) remained in the background. The research on alternating current machines was focused almost completely on the induction machine and the wound rotor synchronous machine, as is very much the case today. The single-salient reluctance synchronous machines, operating from fixed mains frequency and voltage supplies, were used only in low power applications, as the performance of these machines was poor compared to other a.c. machines.

The paper by Kostko (1923) on a new rotor structure for single-salient reluctance machines is remarkable for that time. Kostko's rotor structure is shown in Fig. 1.1(a). It can be seen that Kostko moved away from the salient-pole type of rotor to the more round rotor with inner flux barriers and cutouts. It must be mentioned that the idea of using flux barriers or slits in the poles of machines to reduce quadrature-axis flux was proposed long before in 1904 by Thompson (1911). Thompson's proposal showed a d.c. machine with slitted field poles to reduce the armature reaction effect. Kostko

mentioned that the maximum torque of his "polyphase reaction" machine with the new rotor structure was about 80% of an equivalent induction machine.

Between the 1920s and 1950s the publications on polyphase reluctance machines, as they were called generally, were very much on the theory and analysis of these machines. The important publications on reluctance machines for that time are those by Bruderlin (1924), Trickey (1933, 1946), Talaat (1951), Lin (1951) and Douglas (1956).

The research on the single-salient reluctance machines between 1960 and the early 1970s was mainly on the design of the rotor and on the stability problem of the machine. No attempt was made to conduct research on the stator design of the machine and standard induction machine stators were used throughout. The important research work done during this time can be summarised as follows:

- The work of Lawrenson (1963, 1967) on segmental-rotor reluctance motors.
- The work of Kurscheidt (1961) and Brinkman (1965) on flux barrier rotors with saturation bridges (the rotor investigated by Brinkman is shown in Fig. 1.1(b)).
- The work of Cruickshank (1966, 1971) on axially laminated rotors (the rotor structure is shown in Fig. 1.1(c)).
- The work of Lipo (1967) and Krause (1968) on the stability of the reluctance machine.
- The analysis of Honsinger (1971) on a two flux barrier per pole rotor (structure shown in Fig. 1.1(d)).

In these research works there was the attempt on the one hand to improve the power density, efficiency and power factor of the machine by increasing the reactance ratio of the machine; on the other hand a too high reactance ratio leads to instability, i.e. rotor oscillation about synchronous speed, when operating from fixed mains frequency and voltage supplies. These are conflicting requirements that limit the performance capability of the machine. Little was gained in using new types of rotors for the single-speed, open-loop reluctance machine drive.

From the mid 1970s the research on reluctance machines took a new direction due to the advent and intensive use of power electronics. It was possible to vary the frequency and thereby the speed of the open-loop, single-salient reluctance synchronous machine by means of an inverter (Krause, 1969 and Ong, 1977). More important, for the first time the machine is used in a closed-loop manner, i e the rotor position and the phase current are fed back and the current spatially placed in the machine according to the position of the rotor (Faucher, 1979). A cage-rotor in this case is no longer necessary due to the direct current control of the machine by means of an inverter and control system. The machine can also be designed to obtain the largest difference and ratio of the two-axis inductances - there is in this case no danger of instability when a too high reactance ratio is used.

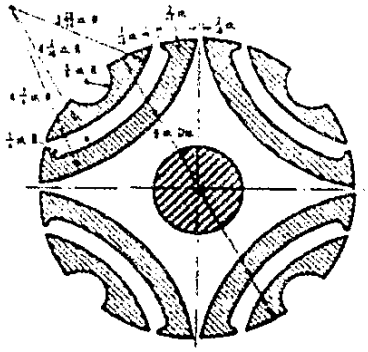

(a) Kostko (1923)

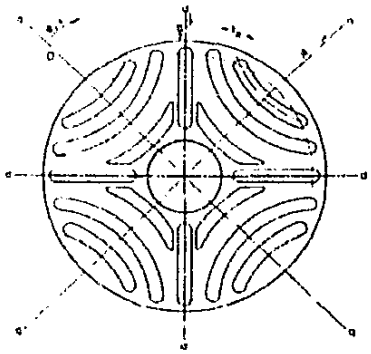

(b) Brinkman (1965)

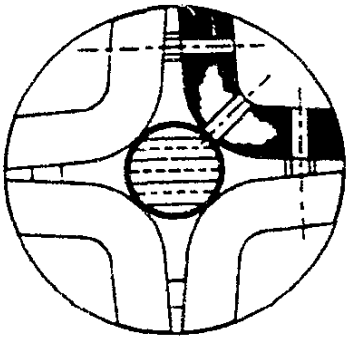

(c) Cruickshank (1971)

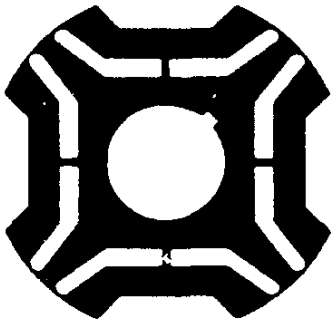

(d) Honsinger (1971), Kamper (1994)

Fig. 1.1. Single-salient reluctance machine rotors

Surprisingly, the research on the design and control of the single-salient, closed-loop reluctance machine drive during the 1970s and the beginning of the 1980s moved entirely to the background. This was even more the case for the open-loop reluctance machine drive. In contrast with this, the double-salient switched reluctance machine received considerable research attention, first in the UK and later worldwide. This machine was the first type of reluctance machine that demonstrated good power density characteristics. Note that this was made possible due to closed-loop switching.

From the mid-1980s till 1990 the single-salient reluctance synchronous machine under closed-loop control received more attention. Research work that can be referred to includes:

- The work of Weh (1985) on a special multi-phase reluctance machine with an axially laminated rotor.
- The work of El-Antably (1985(a), 1985(b)) on the design and control of a 3-phase, axially laminated rotor reluctance machine with the laminations mounted on a fiber glass intermediate rotor piece.
- The important work of Fratta (1987) on a high-performance reluctance machine drive with an axially laminated rotor.

Fratta (1987) for the first time applied a full vector control scheme to control the reluctance synchronous machine. He and Weh showed for the first time that the single-salient reluctance machine under closed-loop control has high power density characteristics.

From 1990 until now considerable research attention has been given to both the single- and double-salient reluctance machine drive systems. Research on the single-salient reluctance synchronous machine focused almost completely on the use of axially laminated rotors. Vagati (1992) moves away from using this type of rotor, due to iron loss problems, to the use of punched flux barrier-type of rotors. During this time, little work has been done on the design of the reluctance synchronous machine and the focus was and still is more on the control-side of the machine. With regard to the control of the machine one can refer to the research work of Boldea (1991) on torque vector control, Xu (1991) which includes the effect of saturation and iron losses, Matsuo (1993) on field-oriented control, Fratta (1994) on flux weakening control and Kamper (1995) on an optimum steady-state control method. Much attention is currently being given to position sensorless control of the single- and double-salient reluctance machines.

On the design-side, research work has been done by Vagati (1992) on the flux barrier rotor reluctance synchronous machine. Other published works that can be referred to on the design aspects of reluctance synchronous machines are: Miller (1991) and Matsuo (1994) on axially laminated rotors and Kamper (1994) on a flux barrier-type of rotor. A comparison between the reluctance synchronous machine and the induction machine has been done by Fratta (1992) and Franceschini (1994). In these publications it is shown that the reluctance synchronous machine has a higher torque per volume capability than the induction machine counterpart in the 10-100 Nm torque range. A review of the reluctance synchronous machine drive as an alternative a.c. drive is given by Vagati (1994).

To summarise, the history of the reluctance machine can be divided into basically three periods. The first period lasts from, say, 1840 till 1870 during which time the double-salient electromagnet type of reluctance machines were used. These machines were considered in general as very bad machines. The second period lasts from, say, the 1880s till 1970 where the single-speed, open-loop reluctance synchronous machine was used for low-power applications in cases where a constant speed was either desirable or necessary. The machine was characterised as not a good machine with a low power factor and a poor power density. The double-salient stepping machine was used only in very low-power applications. During the third period from 1970 until now the converter-fed, double-salient switched reluctance machine drive received considerable attention and revealed itself to have good power density capabilities. The single-salient, closed-loop reluctance synchronous machine drive initially received no attention during this period and it was mentioned only recently that this drive could be a viable alternative for a.c. drives.

1.2 Problem statement

As the focus of this thesis is on the single-salient, current-controlled reluctance synchronous machine (RSM), it is important to mention some aspects about the design and analysis of the RSM that are

prominent from the literature. These are the following:

(i) It is clear that the axially laminated rotor is not the way to go in any further research due to the difficult (unconventional) rotor structure and the problem with iron losses if a large number of insulation layers are used. It is also difficult to skew these rotors if necessary. The iron loss problem was one of the main reasons why Weh (1990) and Vagati (1992) moved away from axially laminated rotors to normal transverse-laminated rotors with a limited number of flux barriers.

(ii) It is amazing that the stator-design of the RSM (a machine used from the beginning of this century) received for all practical purposes no attention in the research. The only exception to this is, to some extent, the work of Vagati (1992), who considered an overall (stator and rotor) design of the machine. To quote from Vagati (1992), "... the rotor cannot be optimised by itself, but stator and rotor laminations have to be optimised as a whole." The importance of this statement cannot be over-emphasised as the optimum performance of the reluctance machine is greatly dependent on the stator design. It is absolutely invalid and unfair to compare the performance of the RSM with other machines using an induction machine stator.

(iii) Most of the design analysis of the RSM is done by means of the lumped circuit method. The finite element method is merely used to investigate the effect of the variation of a single dimension on e.g. the inductances of the machine (Matsuo, 1994; Kamper, 1994) and not to do an overall optimum design. There thus seems to be a deficiency in this regard.

By keeping these aspects in mind, the question to be answered today, despite the research that has been done, is what the performance capability or goodness is of the optimum designed RSM. Note that the optimum design of the machine implies also the optimum spatial placement of the current in the machine with respect to the rotor. The latter concerns the optimum control of the machine. Another question to be answered is what the performance capability of the RSM is in the higher power levels, say in the sub 500 kW power level.

To fully investigate these questions, recalling the remarks made in paragraphs (i), (ii) and (iii) above, it is necessary to do an overall (stator and rotor) design optimisation and to use an analytical model of the machine in the optimisation process which is representative of the real machine. The latter is particularly important for the RSM where the calculation of the q-axis inductance e.g. has to be very accurate and where the effect of cross magnetisation has to be taken into account (Kamper, 1994). The effect of cross magnetisation may be ignored for reluctance machines with axially laminated rotors (Matsuo, 1993), but not for reluctance machines with normal transverse-laminated rotor with punched flux barriers and iron saturation bridges. If cross magnetisation is ignored in any design optimisation then the optimisation will not be true. The lumped circuit method will not give absolute optimisation results. The absolute optimum-designed machine can at best be obtained by using the finite element method in the optimisation process.

To do a design optimisation of the RSM an objective function, like e.g. the torque of the machine,

must be maximised subject to constraints, if any. An optimisation algorithm is therefore necessary to optimise in multidimensions the design of the machine. It must be emphasised that all the machine variables must be optimised to put the objective function value at a minimum (maximum). It is simply not good enough to focus only on single variables in the design of the machine and to reach certain conclusions from that. All the variables must be looked at in the design optimisation. Typically, the number of variables for an electrical machine to be optimised is 10. Furthermore, different objective functions must be minimised (maximised), or in other words the machine must be optimised according to different design criteria to obtain the best answer about the performance capability of the machine.

From the preceding two paragraphs there is the requirement that the finite element analysis method be used in some way together with the multidimensional optimisation algorithm to optimise the design of the machine. As far as the author is aware this has not been done before for the current-controlled, single-salient reluctance machine (in fact not for any electrical machine) and it is the focus of this thesis. Note that Ramamoorty (1979) optimised the overall design of a reluctance machine, but this was for a segmented-rotor machine, for open-loop fixed frequency operation and he used the inaccurate lumped circuit approach. In addition, there is a need today to explain on a simple basis, low on maths and high on understanding, the operation, the characteristics and the goodness of the RSM. It is the aim of the thesis to provide this explanation.

1.3 Approach to problem

As a first step in the design optimisation of the RSM only the steady-state is considered in this thesis. To solve the problem mentioned in section 1.2, the approach followed in the thesis is to try to use the finite element method directly in the optimisation procedure. This approach may be explained by the flow diagram of Fig. 1.2. Here, the optimisation algorithm finds the multidimensional vector [X], i.e. the values of the machine variables (*the machine variables include amongst other things the physical dimensions of the machine*) that minimise (maximise) the function value Y or performance parameter of the machine. In this process with each iteration r the algorithm determines directions of search in a multidimensional space along which Y is minimised (maximised). Each time the optimisation algorithm needs an output function value Y, like torque or efficiency, for a given multidimensional input vector [X], it calls the finite element program. The finite element program generates a new mesh according to the changed input variables. The program then does the pre-processing and the nonlinear solution to find the magnetic vector potentials. The flux linkages and flux densities are calculated, followed by the calculation of the output performance parameters (Y) of the machine. The finite element program may be called a number of times by the algorithm during an iteration. At the end of each iteration a test is carried out to determine if an absolute minimum (maximum) is reached. If not, a next iteration is executed.

It is obviously that the process represented in Fig. 1.2 will be time consuming. This necessitates the following:

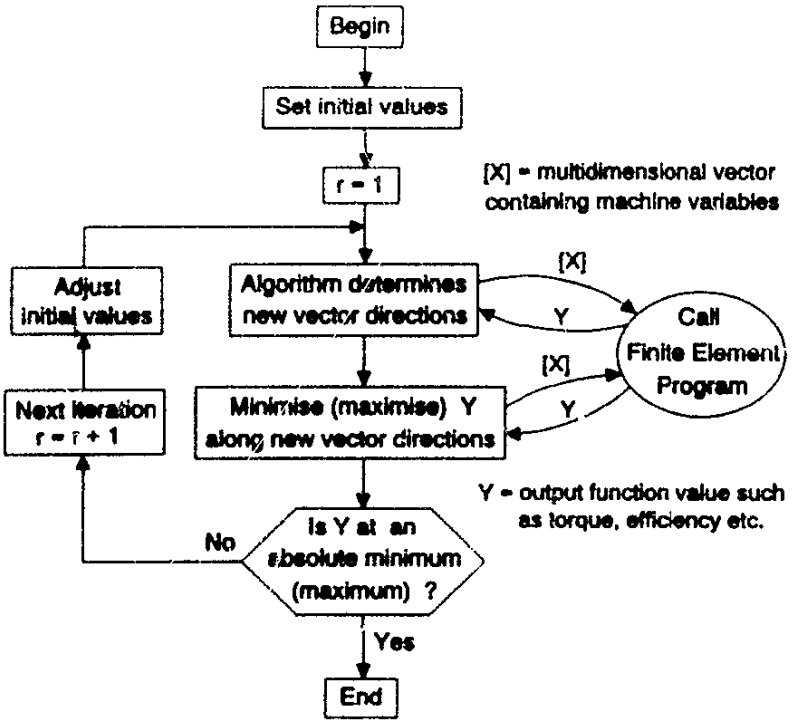

Fig. 1.2. Optimisation procedure using the finite element solution directly.

- The finite element solution must be fast and accurate, i.e. generating the mesh, doing the pre-processing and solving for the vector potentials must be a fast and accurate process.

- As few finite element solutions as possible must be used to calculate all the equivalent circuit parameters and performance data of the machine. For example, it will be beneficial if the performance parameters of the machine can be calculated by using the results of one basic set of finite element solutions.

- The optimisation algorithm must be fast.

These aspects receive considerable attention in the thesis. It will be difficult to realise the process of Fig. 1.2 with a finite element software package of the commercial variety as the source codes are not available. Therefore, the source code of a finite element software program developed at the University of Cambridge (Volschenk, 1993) is used for this study. The software is adapted so that it could be used for the analysis of the current-controlled reluctance machine. With the source code available it was possible to link the finite element and the optimisation algorithm programs with each other. The finite element program is briefly described in Appendix B and will be referred to in the thesis.

It is equally important to explain the outcome of the design optimisation. To do this a very simple calculation method is necessary to show certain tendencies of the design optimisation. This aspect

receives much attention in the thesis as an approximate magnetic circuit calculation method is proposed. The outcome of the design optimisation is also explained by deriving goodness factors for the RSM.

1.4 Thesis layout

The layout of the remainder of this thesis is as follows:

Chapter 2: The method for calculating the performance data of the machine is described. This includes not only the finite element method but also the proposed approximate magnetic circuit method.

Chapter 3: The focus of this chapter is on the multidimensional optimisation algorithms that are used to optimise the design of the RSM. The results of two optimisation case studies are given and discussed in detail.

Chapter 4: The performance calculation methods of Chapter 2 and the optimisation algorithms of Chapter 3 are used to optimise in multidimensions the design of the RSM. The aim of this chapter is to evaluate from calculations but also from measurements the performance capability of the RSM in the 3-10 kW power level.

Chapter 5: This chapter explains the characteristics of the RSM by deriving goodness factors for the machine. Goodness factors are also derived for the induction machine to compare the RSM with the induction machine.

Chapter 6: The performance capability of the machine in the medium power range is considered. The different goodness factors of Chapter 5 are calculated for optimum-designed RSMs in the 10 - 350 kW power range and are compared with those of standard induction machines. Altogether six machines are optimised using the methods of Chapters 2 and 3.

Chapter 7: In this chapter a summary with conclusions is given and recommendations are made for further research.

2 Calculation of Performance Parameters

This chapter describes the calculation of the performance parameters, i.e. the function values such as torque, efficiency, power factor, kVA, etc. of the RSM, by means of the finite element program of Fig. 1.2. In the finite element program the equivalent circuit parameters of the RSM are determined and the performance parameters are calculated. The calculations are done with the machine in the steady-state and only fundamental values of voltage, current and flux linkages are considered. The reason for the latter is that the design optimisation of the machine is done on the basis of fundamental values only.

2.1 Electromagnetic torque production

The space phasor model with the reference fixed to the rotor is used in the analysis of the RSM. Fig. 2.1(a) shows a cross-section of the machine. On the non-salient stator a standard symmetrical three-phase winding is used. No cage or field windings are used on the salient-pole rotor. The angle α_r is the rotor angle between the magnetic axis of phase *a* and the q-axis of the rotor. The reference frame rotates at a speed of $\omega_r = d\alpha_r/dt$. The fundamental current and flux linkage space phasors of the machine, shown in Fig. 2.1(b), are stationary with respect to the rotor in the steady-state. In Fig. 2.1(b) the stator flux linkage space phasor λ_s is the phasor sum of the airgap flux linkage space phasor λ_m and the leakage flux linkage space phasor λ_ℓ. Torque production of the machine is given as the cross-product between λ_s and I_s, i.e.

$$T = k\,\lambda_s \times I_s \tag{2.1}$$

where k is a constant. The same torque is obtained with the cross-product between λ_m and I_s. Equation (2.1) can also be expressed as

$$T = k\,\hat{\lambda}_s \hat{I}_s \sin(\gamma) \tag{2.2}$$

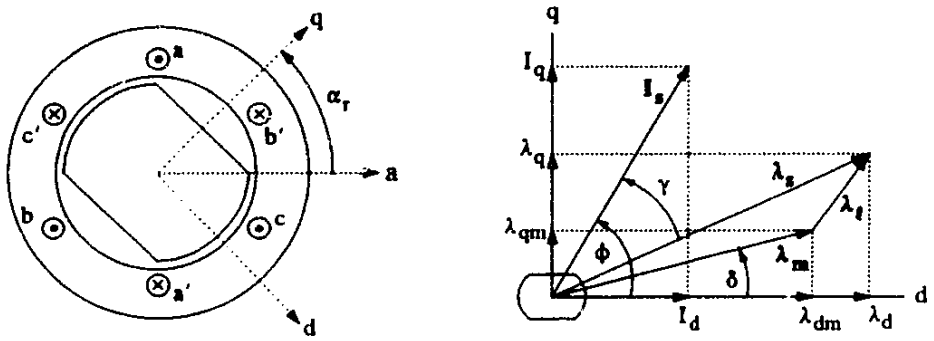

(a) Cross-section (b) Space phasor diagram

Fig. 2.1. Cross-section of the RSM and space phasor diagram fixed in the rotor reference frame

where $\hat{\lambda}_s$ and $\hat{I}_s$ are the amplitudes of the stator flux linkage and current space phasors respectively. The angle γ is the torque angle, which is zero when the current space phasor lies either on the d- or the q-axis of the rotor. Equations (2.1) and (2.2) can be expressed in terms of dq-axis components for a p pole-pair machine as derived in all classical texts on dq-axis theory as

$$T = \frac{3}{2} p (\lambda_d I_q - \lambda_q I_d) . \tag{2.3}$$

λ_d and λ_q are the d- and q-axis fundamental stator flux linkage components and I_d and I_q the d- and q-axis fundamental stator current components. By defining the d- and q-axis inductances L_d and L_q as

$$L_d = \lambda_d / I_d \quad \text{and} \quad L_q = \lambda_q / I_q , \tag{2.4}$$

eqn (2.3) can be expressed in the form

$$T = \frac{3}{2} p (L_d - L_q) I_d I_q \tag{2.5}$$

or

$$T = \frac{3}{4} p (L_d - L_q) \hat{I}_s^2 \sin(2\phi) . \tag{2.6}$$

ϕ is called the current space phasor angle which is the angle between the current space phasor and the d-axis of the rotor. The torque of the RSM is thus a function of the inductance difference L_d-L_q. With L_q relatively small, the torque is sensitive to the value of L_d.

Equation (2.6) can also be written as

$$T = \frac{3}{4} p (L_{dm} - L_{qm}) \hat{I}_s^2 \sin(2\phi) \tag{2.7}$$

where L_{dm} and L_{qm} are the d- and q-axis inductances of the machine due to the d- and q-axis *airgap* fundamental stator flux linkage components. These inductances are given by

$$\begin{aligned} L_{dm} &= \lambda_{dm} / I_d = L_d - L_l \\ L_{qm} &= \lambda_{qm} / I_q = L_q - L_l \end{aligned} \tag{2.8}$$

where L_l is the per phase leakage inductance of the stator winding.

2.2 Equivalent circuits

To calculate the performance parameters of the RSM it is necessary to consider the equivalent circuits of the machine in the *abc* and *dq* reference frames. The fundamental per phase equivalent circuit of the RSM may be represented by the circuit of Fig. 2.2(a), where R_s is the effective stator resistance,

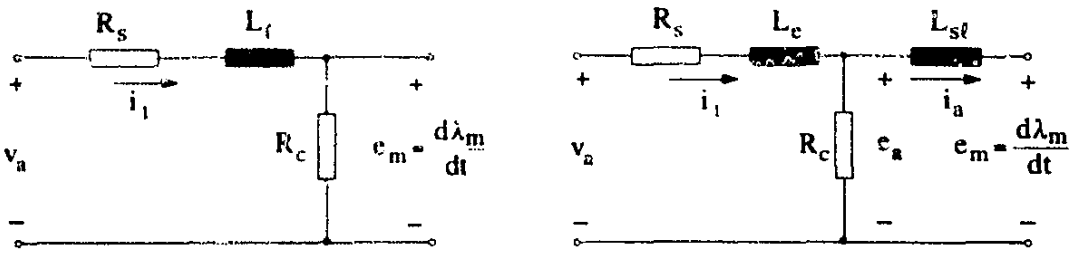

(a) Equivalent circuit (b) Approximate equivalent circuit

Fig. 2.2. Per phase equivalent circuits of the RSM

L_ℓ is the stator leakage inductance and R_c is the stator core loss resistance. v_a is the fundamental instantaneous phase voltage, i_1 is the fundamental instantaneous stator current and e_m is the induced stator voltage due to the fundamental airgap flux linkage λ_m.

With 2-D finite element analysis it is necessary to separate the endwinding leakage inductance L_e from the total stator leakage inductance. L_e, thus, has to be calculated separately. As an approximation the core loss resistance is shifted in the equivalent circuit to the position shown in Fig. 2.2(b). The reason for this is that the total stator flux linkage, excluding the endwinding flux linkage, can then be calculated by means of the 2-D finite element analysis. The inductance $L_{s\ell}$ of Fig. 2.2(b) represents the leakage inductance of the stator winding excluding the endwinding leakage inductance, i.e. $L_\ell = L_e + L_{s\ell}$.

The equivalent circuit of Fig. 2.2(b) in the *abc* reference frame can be transformed to equivalent circuits in the *dq* reference frame fixed in the rotor by using Park's transformation. The transformation of core loss resistances to the *dq* reference frame is described by, amongst others, Xu (1991). The *dq* equivalent circuits are shown in Fig. 2.3. The flux linkages λ_d and λ_q are the d- and q-axis stator flux linkage components, which include the stator leakage flux linkage but not the endwinding flux linkage. The parameter ω_r is the electrical speed of the rotor reference frame. In the phasor diagram the space phasors $\mathbf{V}_s$ and $\mathbf{I}_{s1}$ represent the stator supply voltage and the terminal current of the machine respectively. Note that $\mathbf{I}_{s1} = I_{d1} + jI_{q1}$ includes the *dq* core loss current components (see the *dq* equivalent circuits of Fig. 2.3). The angle θ is the power factor angle. The stator flux linkage phasor $\boldsymbol{\lambda}_s$ originates from the current phasor $\mathbf{I}_s$ and torque is produced when there is a phase shift between these phasors (see eqn 2.2 and Fig. 2.1(b)). The angles ϕ and ϕ_1 are current space phasor angles.

2.3 Calculation of equivalent circuit parameters

This section describes how the *dq* equivalent circuit parameters of Fig. 2.3 are calculated by using, amongst others, the finite element analysis method. The circuit elements R_s and L_e are calculated separately by common analytical formulas.

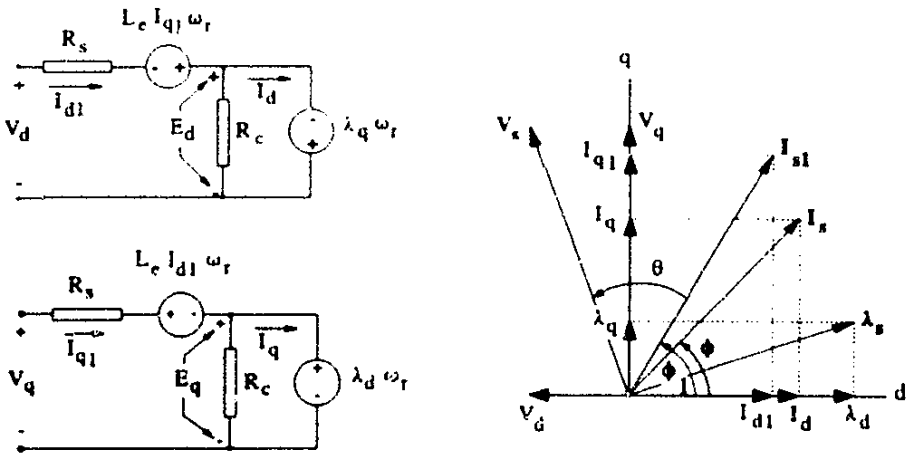

Fig. 2.3. Steady-state d- and q-axis equivalent circuits and space phasor diagram of the RSM

2.3.1 Stator winding resistance and endwinding leakage inductance

The stator winding resistance R_s is calculated from the active copper area at a temperature of, by convention, 75°C. The copper area is determined from the given slot dimensions. The skin effect is ignored in the calculation of R_s. To obtain the correct active copper area of a stator conductor, provision is made in the formula for R_s for the filling of the stator slot using a fill factor. The areas of the slot insulation and conductor insulation are also taken into account. The formula is given in Appendix A, eqn (A.1).

The endwinding leakage inductance, L_e, is calculated according to a formula given by Kamper (1987). This formula is based on a formula derived by Honsinger (1959) for the calculation of the stator endwinding leakage reactance of squirrel-cage induction machines. The formula can be used for single- or double-layer windings and takes into account the shape of the endwinding coils as well as the mutual flux linkage between the endwinding phase groups. The formula can be used very well for small and medium power machines and is given by eqn (A.5).

2.3.2 Calculation of flux linkages and inductances using the finite element method

To calculate the flux linkages using the finite element method (refer to Appendix B for details about the finite element program) it is necessary to specify the phase current $\mathbf{I}_s = \hat{I}_s \angle \phi$ of the machine. Due to the fact that the RSM is under current control, the current space phasor can be set at an angle ϕ with respect to the rotor (Fig. 2.3). The angle ϕ is thus an input variable. The amplitude of the current space phasor, $\hat{I}_s$, is determined from either a given rms current density, J, according to the relation

$$\hat{I}_s = \sqrt{2}\, J\, A_{cu}\, n_a / z \tag{2.9}$$

where n_a is the number of parallel circuits, A_{cu} is the active copper area per stator slot and z is the

number of conductors per slot, or from given copper losses, P_{cu}, according to the relation

$$\hat{I}_s = \sqrt{\frac{2\,P_{cu}}{3\,R_s}} = K\,(n_s/z)\sqrt{\frac{P_{cu}\,A_{cu}}{(l + l_e)}} \qquad (2.10)$$

with $K = \left(\frac{1}{3\,q\,p\,\rho_t}\right)^{1/2}$ (see glossary of symbols and eqns (A.1) and (A.3)) .

Note that the actual current density and copper losses will be slightly higher due to the slightly higher terminal current I_{s1} of the machine (Fig. 2.3).

With the current space phasor known in terms of amplitude and angle, the *dq* current components I_{dq} can be calculated as well as the instantaneous three-phase currents i_{abc} using the inverse Park transformation. Hence, the three-phase winding currents are set in the finite element program according to the rotor position. The finite element analysis method is then called to calculate the total stator flux linkages λ_{abc} that exclude the endwinding flux linkage. Due allowance is made for saturation by using the correct B/H-curve in the finite element program.

The effect of skew is accounted for in the 2-D finite element analysis by using a set of unskewed machines of which the rotors are relatively displaced by an angle that is a fraction of the total skew. The technique, first introduced by Alhamadi and Demerdash (1991), is used in time-stepping finite element analysis by Volschenk (1993) and Williamson (1994). With *k* unskewed machines the phase flux linkages are calculated by eqn (2.11). Here $\lambda_{abc}(\alpha_n)$ denotes the total phase flux linkages of the unskewed machine with the rotor at position α_n and is calculated by means of the finite element analysis method (Appendix B, eqn B.5). In this analysis *k* is taken as 5.

$$[\lambda_{abc}] = \frac{1}{k}\left[\sum_{n=1}^{k} \lambda_{abc}(\alpha_n)\right] \qquad (2.11)$$

Equation (2.11) suggests that *k* time-expensive finite element field solutions are required, but it is only the first non-linear solution at position α_1 which will be expensive due to the unknown reluctivities. At positions $\alpha_2..\alpha_k$, the known reluctivities of previous positions can be used, which will already be close to the new reluctivities, so that the field solution times at these positions will be less (Alhamadi, 1991).

The flux linkages of eqn (2.11) versus position will contain harmonics and it is necessary to find the fundamental total flux linkages. With a distributed double-layer stator winding it is assumed, as an approximation, that the effects of the MMF space harmonics are negligible. The remaining harmonic fluxes are the synchronous harmonic fluxes which stand still with respect to the fundamental rotating flux wave. With the rotor skewed no prominent high-frequency slot ripple will be present in the flux linkage wave (Alhamadi 1991, Volschenk 1993, Williamson 1994). Furthermore, with a distributed winding the quasi-square flux density wave in the airgap, caused by saturation, will be filtered so that a near sinusoidal flux linkage wave is obtained. However, a prominent 3rd and less prominent 5th

and 7th harmonics will still be present in the total flux linkage wave-form. If the 5th, 7th and higher harmonics are ignored, the total flux linkage can be written in terms of a fundamental and a 3rd harmonic, or

$$[\lambda_{abc}] = [\lambda_{abc1}] + [\lambda_{abc3}] . \tag{2.12}$$

The co-phasal 3rd harmonic flux linkages, including the higher order triplen harmonics, can be obtained from the actual three-phase flux linkages as

$$\lambda_{a3} = \lambda_{b3} = \lambda_{c3} = \frac{1}{3}(\lambda_a + \lambda_b + \lambda_c) . \tag{2.13}$$

Thus, with the actual total phase flux linkages and the 3rd harmonic flux linkages known from the finite element analysis, the fundamental total phase flux linkages can be calculated by eqn (2.12). Note that with the use of eqn (2.12) and with the rotor fixed at a certain position, errors are made in the same way each time the finite element program is called in the optimisation process. This implies that the optimised machine will ultimately be almost exactly the absolute optimum machine.

Another way to determine the fundamental total phase flux linkage is to do a Fourier expansion of the total flux linkage wave. This requires that the rotor and the current space phasor be stepped through an angle of at least $\pi/2$ electrical radians. This, however, will undo the idea of using the finite element method directly in the optimisation process due to the long computation time.

The use of eqn (2.12) is thus a key aspect in the whole optimisation process because it enables the fundamental total phase flux linkages of the RSM to be determined by using just one set of finite element solutions. The fundamental total phase flux linkages are necessary, amongst other reasons, for the calculation of the supply voltage and power factor of the machine.

With the fundamental total phase flux linkages and the rotor position known, the *dq* flux linkages of Fig. 2.3 are calculated using Park's transformation, namely

$$[\lambda_{dqo}] = [\mathbf{K}_p][\lambda_{abc1}] . \tag{2.14}$$

From this the speed voltages $E_d = -\lambda_q\omega_r$ and $E_q = \lambda_d\omega_r$ of the equivalent circuits of Fig. 2.3 are determined. The d- and q-axis inductances L_d and L_q are determined from eqns (2.4) and (2.14), but it must be realised that these inductances are subject to a small error due to the approximation of eqn (2.12).

To calculate the d- and q-axis inductances L_{dm} and L_{qm} of eqn (2.8) it is necessary to determine the airgap flux linkage space phasor in terms of amplitude and angle, $\boldsymbol{\lambda}_m = \hat{\lambda}_m\angle\delta$, of the skewed machine. For the unskewed machine the amplitude and the angle of the fundamental airgap flux density space phasor $\mathbf{B} = \hat{\mathbf{B}}\angle\delta$ are determined by a Fourier expansion of the radial component of the airgap flux density. In Appendix B, section B.3 it is shown how this is done using the airgap magnetic vector potentials. The amplitude of the fundamental airgap flux linkage space phasor of the unskewed machine is calculated from

$$\hat{\lambda}_m = \frac{2}{\pi} \hat{B}\, \tau_p\, l\, W\, K_{w1} \tag{2.15}$$

where τ_p is the pole pitch, l is the core length, W is the number of turns in series per phase and K_{w1} is the winding factor.

The effect of skew is accounted for in the same way as in eqn (2.11) by using a set of unskewed machines. For the *n*th machine the amplitude $\hat{\lambda}_{m(n)}$ as well as the space angle $\delta_{(n)}$ of the fundamental airgap flux linkage space phasor is determined. With *k* unskewed machines the *resultant* airgap flux linkage space phasor of the skewed machine is obtained by taking the *phasor* sum (not the arithmetical sum) of $\hat{\lambda}_{m(n)}\angle\delta_{(n)}$, as in eqn (2.16).

$$\boldsymbol{\lambda}_m = \hat{\lambda}_m\angle\delta = \frac{1}{k}\sum_{n=1}^{k} \hat{\lambda}_{m(n)}\angle\delta_{(n)} \tag{2.16}$$

Note that the angles $\delta_{(n)}$ of eqn (2.16) are the space angles with respect to the original or actual d-axis of the rotor and not with respect to the d-axes of the set of unskewed machines. The d- and q-axis components of eqn (2.16) are given by

$$\lambda_{dm} = \hat{\lambda}_m \cos(\delta) \quad \text{and} \quad \lambda_{qm} = \hat{\lambda}_m \sin(\delta) \tag{2.17}$$

and are used in eqn (2.8) to calculate L_{dm} and L_{qm}.

2.3.3 *Core loss resistance*

The only remaining equivalent circuit parameter to be calculated is the core loss resistance, R_c. Core losses in electrical machines are in general difficult to calculate accurately. The core losses in electrical machines occur as, amongst other things, rotational losses (not pure alternating losses), rotor-pole surface losses, additional iron losses with load due to harmonic fluxes, tooth pulsation losses and, in the case of the reluctance machine, rotor-iron-segment pulsation losses if the barrier pitch is less than the stator slot pitch.

The stray-load losses in reluctance machines consist of only iron losses. There are no bar and endring losses due to harmonic-induced rotor currents and also no inter-bar losses, as in the induction machine.

Rotational losses occur specifically in the stator tooth tips and stator yokes where the flux density vectors rotate, rather than to pulsate on the same axis. The calculation of rotational losses is complex. Also, rotational loss curves of laminated steel are very rarely available from suppliers due to the difficulties in measuring these losses.

As an approximation, therefore, only alternating iron core losses due to the main (fundamental) flux are considered in the analysis. This means that the calculated core losses will be somewhat low. The core losses are calculated from measurements on electrical machines and from loss-frequency curves

of the laminations used.

Considering only stator core losses due to the main flux and fundamental supply frequency of the machine, the core losses are calculated from

$$P_c = c\, f_1^x \left(B_{mt}^y M_t + B_{my}^y M_y \right) \tag{2.18}$$

where B_{mt} and B_{my} are respectively the maximum flux densities in the teeth and yoke, M_t and M_y are respectively the iron masses of the teeth and yoke and f_1 is the fundamental supply frequency. The maximum flux densities in the teeth and yoke can be obtained directly from the finite element solution. The constants c, x and y are determined from measurements and from loss-frequency curves (M-36, 26 gage, non-oriented sheet steel) as $c = 0.0337$, $x = 1.32$ and $y = 2$.

From the known core losses of eqn (2.18) the core loss resistance is calculated as

$$R_c = \frac{3 E_a^2}{P_c} \tag{2.19}$$

where E_a is the rms value of the phase EMF and is given by

$$E_a = \sqrt{\frac{E_d^2 + E_q^2}{2}} \,. \tag{2.20}$$

2.3.4 *Effect of cross magnetisation on L_d and L_q inductances*

The torque and power factor of the RSM are both functions of the inductances L_d and L_q. It is therefore important to consider the effects of saturation and cross magnetisation on these inductances. Cross magnetisation or cross coupling is the magnetic coupling between the fictitious d- and q-axis windings of the machine. A number of studies have been done on the cross magnetisation effect in reluctance machines (Anvari 1985, Binder 1989). These studies have been done on reluctance machines with rotor cage windings without rotor flux barriers. Little is published on the cross magnetisation effect in reluctance machines with axially laminated rotors, but it is shown that this effect with these rotors is small (Mayer 1986, Matsuo 1994).

A study was done by Kamper (1994) to investigate the effect of cross magnetisation on the inductances of the RSM using the double barrier rotor of Fig. 1.1(d). The inductances in this study were calculated in the same way as described in section 2.3.2 and were confirmed by measurements. The results of these calculations are shown in Fig. 2.4.

It is clear that saturation and specifically cross magnetisation have a considerable effect on the inductances of the RSM using a flux barrier rotor. Consider e.g. in Fig. 2.4 the case where constant, rated d-axis current of 9 A is used. The d-axis inductance is affected relatively little (10%) by cross magnetisation (or varying q-axis current) as shown in Fig. 2.4(a). The q-axis inductance, however, is greatly reduced by the rated d-axis current particularly at low q-axis currents as shown in Fig.

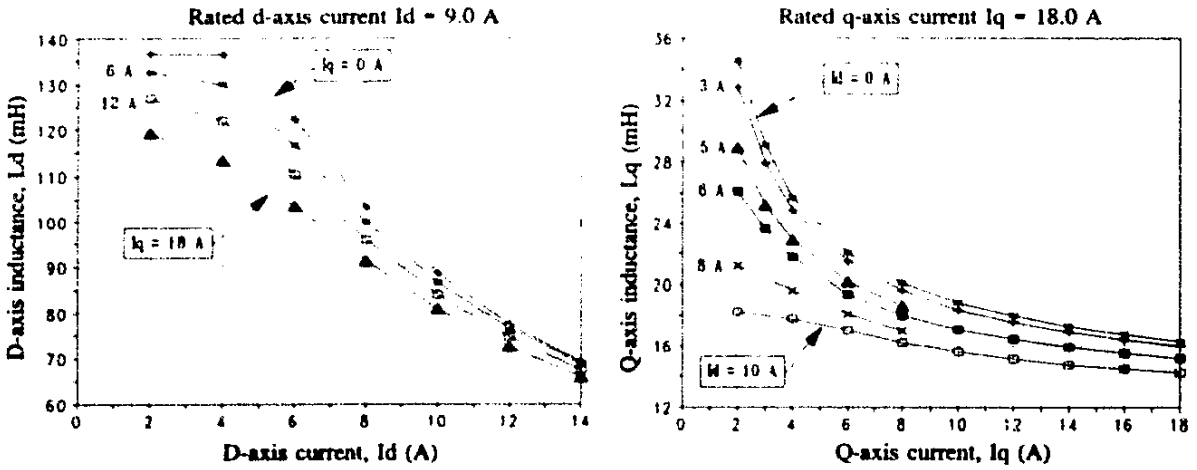

(a) Ld versus Id with Iq as parameter (b) Lq versus Iq with Id as parameter

Fig. 2.4. Finite element results to illustrate the effect of cross magnetisation (Kamper, 1994).

2.4(b). Cross magnetisation in this case therefore leads, amongst other things, to the improvement of the inductance ratio $\sigma = L_d/L_q$ and thus the power factor of the machine. On the other hand, at low d-axis currents (field weakening operation) the d-axis inductance and specifically the q-axis inductance vary significantly with q-axis current. In this case cross magnetisation has a reducing effect on the inductance difference $\Delta L = L_d - L_q$ and the inductance ratio σ, affecting negatively the torque and power factor of the machine.

The effect of cross magnetisation may be ignored with the use of e.g. the lumped circuit analysis method to obtain preliminary, first-order design optimisation results of the RSM. However, in the search for the absolute optimum-designed RSM the effect of cross magnetisation has to be taken into account using the finite element analysis method.

2.4 Performance calculation

From the known *dq* current components, I_{dq}, and from the calculated *dq* speed voltages, E_{dq}, according section 2.3.2 and the calculated core loss resistance according section 2.3.3, the *dq1* current components, I_{dq1}, of Fig. 2.3 and the current amplitude, $\hat{I}_{s1}$, are determined as

$$I_{d1} = I_d + E_d/R_c\,, \qquad I_{q1} = I_q + E_q/R_c \qquad \text{and} \qquad \hat{I}_{s1} = \sqrt{I_{d1}^2 + I_{q1}^2}\,.$$

From this and from the calculated endwinding leakage inductance L_e according eqn (A.5), the endwinding leakage flux linkage speed voltages $L_e I_{q1}\omega_r$ and $L_e I_{d1}\omega_r$ of Fig. 2.3 are determined. The *dq* supply voltage components, V_{dq}, and the voltage amplitude $\hat{V}_s$ are calculated from

$$V_d = E_d + L_e I_{q1}\omega_r + I_{d1}R_s\,, \qquad V_q = E_q + L_e I_{d1}\omega_r + I_{q1}R_s \qquad \text{and} \qquad \hat{V}_s = \sqrt{V_d^2 + V_q^2}$$

where R_s is the stator winding resistance calculated according eqn (A.1).

The power factor angle θ of Fig. 2.3 is easily calculated from the *dq* voltage components V_d and V_q and the *dq1* current components I_{d1} and I_{q1}. By ignoring the stator resistance and the iron loss resistance in the mathematical model of the RSM it is shown by Kamper (1994), amongst others, that the power factor of the machine can be expressed as

$$P_f = \cos\left(\tan^{-1}\left(\frac{\sigma/\upsilon + \upsilon}{\sigma - 1}\right)\right), \tag{2.21}$$

where $\sigma = L_d/L_q$ and $\upsilon = I_q/I_d = \tan(\phi)$. Equation (2.21) shows that the power factor is dependent on the inductance ratio L_d/L_q. With L_q relatively small the power factor is sensitive to the value of L_q.

The supply kVA and the copper losses of the machine are respectively calculated as

$$S = \frac{3}{2}\hat{V}_s \hat{I}_{s1} \qquad \text{and} \qquad P_{cu} = \frac{3}{2}\hat{I}_{s1}^2 R_S .$$

The steady-state torque of the RSM is calculated from either eqn (2.6) or (2.7). It must be realised that the calculated torque, using eqns (2.7), (2.8) and (2.14) is subject to a small error due to the approximation of eqn (2.12). The torque may also be calculated as a function of the radial and tangential components of the airgap flux density or from the vector potential nodal values in the airgap as shown by Abdel-Razek (1981).

Finally, the wind and friction losses as an approximation are taken to be the same as that of a standard induction machine with equal volume. From this the shaft torque and efficiency are calculated.

This concludes the calculation of the performance parameters of the RSM, i.e. the function value Y of Fig. 1.2. It is important to emphasise that the effects of cross magnetisation, saturation and skew are taken into account in the above calculation of the performance parameters by using the results of only one set of finite element solutions.

2.5 Effect of current angle control on torque and power factor

Both the torque and power factor of the RSM are functions of the current space phasor angle, ϕ. The torque equation of the RSM (eqn 2.7),

$$T = \frac{3}{4}p(L_d - L_q)\hat{I}_s^2 \sin(2\phi), \tag{2.22}$$

suggests that maximum torque per ampere will be obtained with a current phasor angle of 45°. However, the inductance difference $\Delta L = L_d - L_q$ is not a constant but varies with both the d- and q-axis currents of the machine due to saturation and cross magnetisation (Fig. 2.4). In effect ΔL is some function of the current space phasor angle ϕ for a given current amplitude $\hat{I}_s$. This is shown for example in Fig. 2.5 for the double barrier rotor RSM of Fig. 1.1(d), using the inductance curves of Fig. 2.4.

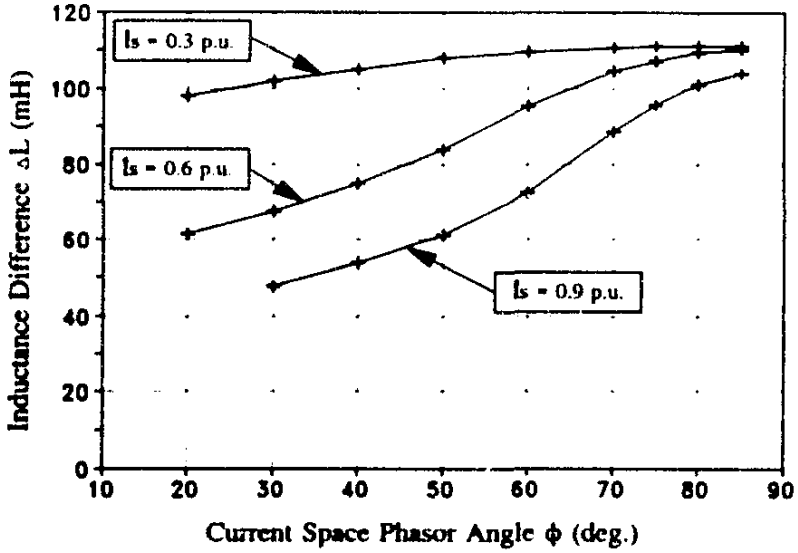

Fig. 2.5. Calculated inductance difference versus current angle with $\hat{I}_s$ as parameter

For a given current amplitude $\hat{I}_s$ eqn (2.22) can be written as

$$T = K\,\Delta L(\phi)\sin(2\phi)\,. \tag{2.23}$$

The maximum torque is developed where the derivative of eqn (2.23) is zero. By differentiation and simplification the following equation is obtained:

$$\frac{\partial \Delta L(\phi)}{\partial \phi} = -2\cot(2\phi)\,\Delta L(\phi) \tag{2.24}$$

From Fig. 2.5 it is clear that the inductance derivative of eqn (2.24) is always positive at 45° for a given current amplitude $\hat{I}_s$, except at perhaps very low currents. Thus, for eqn (2.24) to be valid the current space phasor angle ϕ must be between $45° < \phi < 90°$. Maximum torque per ampere, therefore, is not obtained with a current angle of 45° as some authors expressly state. Kamper (1995) shows that the current angle for maximum torque per ampere of the RSM using the rotor of Fig. 1.1(d) is between 60° and 65°.

The power factor of the RSM, in contrast with the torque, is dependent on the inductance ratio (eqn 2.21) which also varies with both the d- and q-axis currents due to saturation and cross magnetisation. The inductance ratio σ therefore is also some function of the current space phasor angle ϕ for a given current amplitude $\hat{I}_s$. This implies, amongst other things, that there will be some current angle where the power factor becomes a maximum for a given current $\hat{I}_s$. The calculated and measured results of Kamper (1995) show for the RSM using the rotor of Fig. 1.1(d) that maximum power factor and minimum kVA are obtained with current angles between 72° and 75°.

The current angle, therefore, is an important design and control parameter of the RSM. It has to be used in the design optimisation of the RSM as one of the machine variables to be optimised.

2.6 Calculation of L_{dm} and L_{qm} using an approximate magnetic circuit method

Both the d- and q-axis inductances L_{dm} and L_{qm} can be considered as magnetising inductances of the RSM. The only difference in the equations for these inductances is the difference in the resultant airgap lengths of the d- and q-axis magnetic circuits. Let the machine operate e.g. with only d-axis current, then a constant magnetising reactance will be "seen" by the supply. The magnetising inductance in this case is equal to the d-axis magnetising inductance L_{dm} and is given by

$$L_{dm} = \frac{m\,(W\,K_{w1})^2\,d_i\,l\,\mu_0}{\pi\,p^2\,g_d\,k_{sd}} \tag{2.25}$$

where m is the number of phases,
W is the number of turns in series per phase,
K_{w1} is the winding factor for the fundamental,
d_i is the airgap diameter or approximately taken here as the stator inner diameter,
g_d is some resultant airgap length of the d-axis magnetic circuit
and $k_{sd} \geq 1$ is the saturation factor for the d-axis magnetic circuit.

With a smooth airgap reluctance machine with a round flux barrier rotor, g_d will be equal to the actual airgap length between the stator and the rotor.

Similarly, the q-axis magnetising inductance is given by

$$L_{qm} = \frac{m\,(W\,K_{w1})^2\,d_i\,l\,\mu_0}{\pi\,p^2\,g_q\,k_{sq}} \tag{2.26}$$

where g_q is some resultant airgap length of the q-axis magnetic circuit and $k_{sq} \geq 1$ is the saturation factor for the q-axis magnetic circuit. Defining the *effective* d- and q-axis airgap lengths as

$$g_d' = g_d\,k_{sd} \quad \text{and} \quad g_q' = g_q\,k_{sq}\,, \tag{2.27}$$

the inductance difference and inductance ratio are respectively

$$\Delta L = L_{dm} - L_{qm} = K_m\left(\frac{1}{g_d'} - \frac{1}{g_q'}\right) \tag{2.28}$$

and

$$\sigma = \frac{L_{dm}}{L_{qm}} = \frac{g_q'}{g_d'} \tag{2.29}$$

where K_m is

$$K_m = \frac{m\,(W\,K_{w1})^2\,d_i\,l\,\mu_0}{\pi\,p^2}\,. \tag{2.30}$$

The d-axis inductance L_{dm} of eqn (2.25) is a function of two important parameters, namely the stator inner diameter d_i and the airgap length g_d. The tooth width and yoke height of the stator and the widths of the rotor iron segments will also have an effect indirectly on the saturation factor k_{sd} and thus on L_{dm}.

The q-axis inductance L_{qm} of eqn (2.26) is also a function of the diameter d_i and further of the airgap length g_q. g_q is determined by, amongst other things, the widths of the flux barriers. The ratio of the inner diameter d_i to the barrier width, therefore, is an important factor in the value for L_{qm}. Note further that both the saturation factors k_{sd} and k_{sq} of respectively eqns (2.25) and (2.26) are affected by cross magnetisation.

With the torque of the RSM proportional to the inductance difference and the power factor dependent on the inductance ratio, eqns (2.28) and (2.29) show that a high torque and a high power factor can be obtained by making g_d' small and g_q' large. This implies, amongst others, that the saturation factors k_{sd} and k_{sq} have to be respectively small and large for the d- and q-axis magnetic circuits. Equation (2.28) shows further that the torque is proportional to K_m, which is, amongst other things, proportional to the square of the winding factor, K_{w1}. The latter points out what the effect is of a single-layer versus a double-layer winding on the torque of the machine. With a single-layer winding the torque improvement may theoretically be as much as 10%, depending on what double-layer winding is used. Obviously, with a single-layer winding the space harmonics are less suppressed and a less smooth torque is developed. The power factor is independent of the winding factor according to eqn (2.29).

Description of the approximate magnetic circuit method

Analytical approximations or the lumped circuit analysis method may be used to calculate the effective airgap lengths of eqn (2.27) and the *dq* inductances of eqns (2.25) and (2.26). Recent studies have been done in this regard on RSMs with axially laminated rotors (Fu 1991, Vagati 1992, Platt 1992, Soong 1993, Luo 1994). These calculation methods can be used in the design optimisation of the machine to obtain fast, preliminary optimum design results and to investigate the tendencies of the optimum dimensions of the machine. However, the analytical and lumped circuit models can not be used to obtain a near-absolute ("near-true") optimum design of the reluctance machine. The latter is due to the inaccurate calculation of particularly the q-axis effective airgap length, g_q', of eqn (2.27), especially for roters with punched flux barriers and saturation bridges. Furthermore, these methods do not take into account the effect of cross magnetisation and ignore in general the effect of saturation.

The aim of this section is to propose a very simple, approximate magnetic circuit (AMC) analysis method which can be used to partly optimise the design of the RSM. The aim of using the AMC method is to get an idea quickly of some of the optimum dimensions of the RSM and to use the method to explain the optimum design of the machine. The procedure is as follows:

→ Calculate the values for L_{dm} and L_{qm} of the machine using the lumped circuit approach.
→ Calculate approximately the leakage inductance L_{sl} (Fig. 2.2).

→ Obtain values from the lumped circuit analysis for the maximum flux densities B_{mt} and B_{my}.
→ Calculate the core losses and core loss resistance by means of eqns (2.18) - (2.20).
→ Calculate R_s and L_e as in section 2.3.1.
→ Calculate the performance parameters as in section 2.4.

To make the analysis of the AMC method as simple as possible the following approach is followed:

1) The d-axis inductance L_{dm} is calculated with due allowance for saturation but not cross magnetisation.
2) A round rotor is assumed with uniformly distributed flux barriers with equal barrier widths. An example of such a rotor and a stator structure is shown in Fig. 2.6.
3) The flux barrier width of the rotor of Fig. 2.6 is not optimised and the normalised width of the barrier is set constant in the analysis. The focus of using the AMC method, thus, is to optimise the stator parameters of the machine. The rotor structure is optimised in the final analysis by means of the finite element method.
4) The q-axis inductance, L_{qm}, is set constant at some realistic value. This approach is explained in detail in section (ii) below.
5) The current angle ϕ is set constant at $\phi = 65°$ which is a realistic value to use (from section 2.5 and Kamper, 1995).

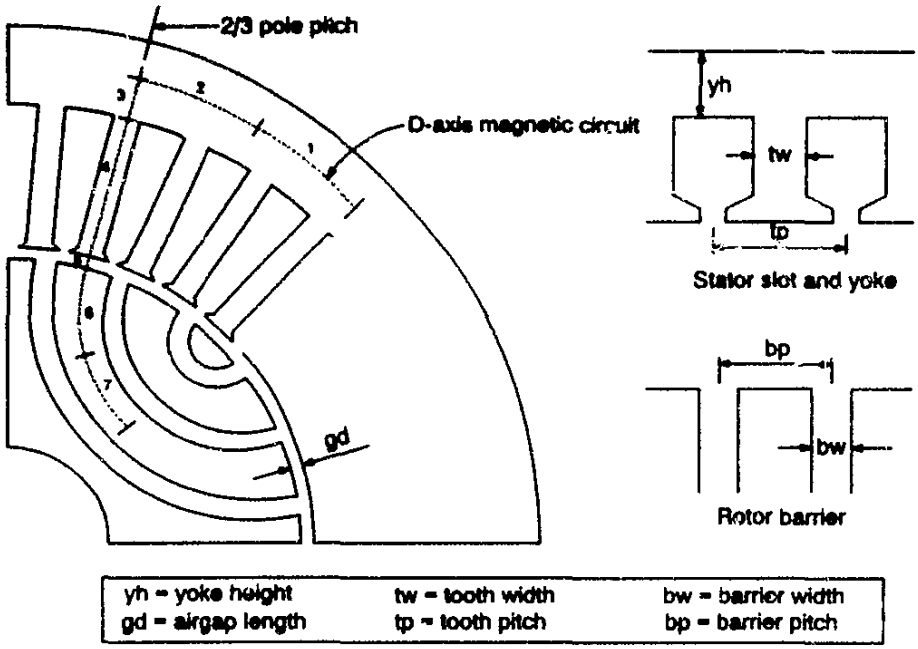

Fig. 2.6. Stator and rotor structure with d-axis magnetic circuit

(i) *The d-axis inductance, L_{dm}:*

For the calculation of the d-axis inductance, L_{dm}, of the machine eqn (2.25) is used. The effective d-axis airgap length, g_d', is calculated by

$$g_d = g_d k_{sd} k_c \tag{2.31}$$

where g_d is the actual airgap length between the stator and the round rotor of Fig. 2.6,
k_{sd} is the saturation factor
and k_c is the Carter factor to take account of stator slotting (assuming closed rotor slots).

The saturation factor k_{sd} is dependent on the extent of d-axis current or d-axis MMF and further on the yoke height, the tooth width (or tw/tp ratio) and the barrier width (or bw/bp ratio) (see Fig. 2.6).

The saturation factor is determined by calculating the fundamental total MMF drop, F_{tot}, of the d-axis magnetic circuit divided by the fundamental airgap MMF, F_f, i.e.

$$k_{sd} = \frac{F_{tot}}{F_f} \tag{2.32}$$

Half of the d-axis magnetic circuit used in the analysis is shown in Fig. 2.6. The analysis is done at an operating point in the airgap that is at ⅔ (or ⅓) of the pole pitch where the fundamental flux density wave intersects more or less with the actual flux density wave. The total and airgap MMFs of the magnetic circuit are determined by means of an iteration procedure using the correct B/H-curve of the lamination steel to account for saturation. The bisection method is simply used in the iteration procedure for the non-linear solution. The iteration procedure and the entire calculation method is described in detail in Appendix C, section C.1.

The effect of cross magnetisation is not taken into account as only d-axis current and d-axis flux are considered in the determination of k_{sd} of eqn (2.32). The effect of skew on the value for L_{dm} is also not taken into account.

(ii) *The q-axis inductance, L_{qm}:*

The calculation of L_{qm} is much more complex than L_{dm}. It is in this case not possible to use just one equivalent magnetic circuit, as with the d-axis, to obtain the fundamental values of the saturated q-axis airgap flux density and the q-axis airgap MMF. The reason for this is the highly non-linear airgap flux density waveform with only q-axis current flowing. The only way to solve this problem is to either use a complex network of lumped elements and solve the network by some iterative procedure to take saturation into account or to use a non-linear finite element field solution.

To avoid the complexity of these calculation methods another approach is followed in the AMC method. In this method the normalised values of the rotor dimensions are kept constant. The rotor is optimised in the final analysis by means of the finite element method. In the AMC method thus the bw/bp ratio of Fig. 2.6 is set constant. The immediate question then is what realistic value for the bw/bp ratio must be used. Both Miller (1991) and Matsuo and Lipo (1994) investigated this for axially laminated rotors. They found in general that an optimum ratio of bw/bp = 0.5 must be used, i.e. the iron segment width must be equal to the barrier width. However, from their graphs it is clear

that the optimum ratio depends on what design criteria are under consideration. The graphs of Matsuo and Lipo (1993) show clearly that for maximum inductance difference, ΔL, which is the same as for maximum torque (eqn 2.7), the optimum ratio is between 0.26 and 0.33. In the case of a maximum inductance ratio $\sigma = L_{dm}/L_{qm}$, which is closely related to maximum power factor or maximum torque/kVA of the machine, the optimum ratio from the graphs of Miller (1991) is about bw/bp = 0.55.

This difference in the optimum ratio can be explained as follows. With L_{qm} relatively small, ΔL is most sensitive to the value of the d-axis inductance L_{dm}. To increase L_{dm}, more iron has to be used on the rotor to make the saturation effect less, i.e. the bw/bp ratio must be less. On the other hand, the inductance ratio $\sigma = L_{dm}/L_{qm}$ is most sensitive to the value of L_{qm}. To decrease L_{qm}, i.e. to maximise σ, large barrier widths have to be used with less iron on the rotor, i.e. the bw/bp ratio must be increased. Note that the bw/bp ratio will seldom be higher than 0.5, because with a peak airgap flux density of say 0.9 tesla, the iron segment flux density will then be higher than 1.8 tesla, which will drive the rotor iron deep into saturation.

To conclude, it is realistic to choose values for the bw/bp ratio between 0.3 and 0.5. There is no reason to believe that the same ratios cannot be applied to the simpler rotor structure of Fig. 2.6. If the design optimisation of the RSM is focused on maximising the torque of the machine, then a ratio of bw/bp = 0.33 (⅓ air and ⅔ iron) can be used. If focused on maximising the power factor or maximising the torque/kVA then a ratio of bw/bp = 0.5 (½ air and ½ iron) can be used. Note that the effect of different ratios on the optimum design can also be quickly investigated.

With the bw/bp ratio constant the d_i/bw ratio is constant. Hence, the d_i/g_q ratio is more or less constant because g_q is some function of the barrier width. From eqn (2.26), this implies that for the same saturation factor, k_{sq}, the q-axis inductance, L_{qm}, will be more or less constant per given stack length of the machine. The approach in the proposed AMC method is to assume a constant value for L_{qm} in the design optimisation based on the fact that the bw/bp ratio is constant.

The question, however, is what value must be taken for L_{qm} in the AMC method. It is known from measurements on flux barrier rotors (e.g. Kamper, 1994) that the inductance ratio of the RSM can typically vary between, say, 4 and 7. If a value of $\sigma = 5$ is assumed in the analysis, then L_{qm} can be calculated from $L_{qm} = L_{dm}/5$ and L_{dm} from eqn (2.25). Assume a normalised value for the stator inner d_i of eqn (2.25) of say $d_i/d_o \approx 0.55$. Furthermore, take the saturation factor as $k_{sd} \approx 2$ and the Carter factor as $k_c \approx 1.2$, then an analytical equation for L_{qm} may be

$$L_{qm} = \frac{m\,(W\,K_{w1})^2\,l\,\mu_0\,d_o}{22\,\pi\,p^2\,g_d} \qquad (2.33)$$

Eqn (2.33) gives a first-order estimate of what the value for L_{qm} may be. The approach in the design optimisation, however, must be to use different values for L_{qm} to see what the effect is on the optimum design of the machine. This effect is investigated in Chapter 4.

It is clear from the above that keeping I_{qm} constant in the proposed AMC method is a *very rough approach* in the design optimisation of the RSM. It will be shown in Chapter 4, however, that using this simple method gives quite remarkable results.

It must once again be emphasised that in using the AMC method in the design optimisation, the rotor is not optimised but only the stator parameters. The AMC method can, however, be used to explain design aspects of the RSM, as will be shown in Chapter 4.

(iii) *The leakage inductance, $L_{s\ell}$*

The leakage inductance $L_{s\ell}$ defined in Fig. 2.2 consists of the slot leakage inductance and the harmonic flux leakage inductance, but not the endwinding leakage inductance. The slot leakage inductance, L_{slot}, can be calculated in the same way as for the induction machine. A formula for the slot leakage inductance per phase is given in Appendix C, eqn (C.19), and is

$$L_{slot} = \left(\frac{2 \mu_o l W^2}{p q} \right) (k_\ell \Lambda_\ell + k_g \Lambda_g) \qquad (2.34)$$

where Λ_ℓ and Λ_g are permeance ratios of the slot sections that hold air (eqn C.22) and conductors (eqn C.23) respectively

and k_ℓ and k_g are double-layer winding correction factors for the slot section that hold air (eqn C 20) and conductors (eqn C.21) respectively.

The formula for L_{slot} is further described in Appendix C, section C.2. It does not take into account the skin effect and the effect of saturation.

The harmonic leakage flux inductance, sometimes called the differential leakage inductance, L_{diff}, is due to the higher order rotating harmonic MMFs. These harmonic MMFs rotate asynchronously with the rotor. In the case of the induction machine with a rotor with magnetic symmetry the effect of the harmonic MMFs and harmonic fluxes can easily be accounted for by simply considering all the harmonic equivalent circuits of the machine taking into acount the damping effect. In the case of the RSM with a cageless rotor with magnetic asymmetry, however, the analysis is much more complex. The stator differential leakage inductance coefficient without damping for the induction machine (Richter 1954, Heller and Hamata 1977, Kamper 1987) cannot just be applied to the reluctance machine. Vagati (1994) considers only the slot harmonic fluxes of the RSM and calculates a zig-zag leakage inductance. A thorough treatment of the harmonic fluxes of the RSM and how they must be accounted for in terms of a harmonic leakage inductance is beyond the scope of this thesis. Even for induction machines there are different views on how to consider the harmonic fluxes (Cheong 1979, Kamper 1987). As an approximation, therefore, L_{diff} is ignored in the AMC method, which means that the total leakage inductance calculated in this way will be somewhat low.

With the inductances L_{dm}, L_{qm} and $L_{s\ell}$ calculated according sections (i) - (iii) above, the *dq* flux linkages are calculated as (see eqns 2.4 and 2.8)

$$\lambda_d = (L_{dm} + L_{sl})\, I_d$$
$$\text{and} \qquad \lambda_q = (L_{qm} + L_{sl})\, I_q \,. \tag{2.35}$$

The other *dq* equivalent circuit parameters of Fig. 2.3 and the performance parameters of the RSM are calculated in the same way as described in sections 2.3 and 2.4.

This concludes the description of the AMC method for calculating the performance of the RSM. As is clear, the method is far from exact, but has the important advantage of taking into account with reasonable accuracy the effect of saturation on L_{dm}. The further advantage of the AMC method is the low computation time, as this design optimisation of the RSM typically takes less than one minute on a SUN 1000 workstation.

2.7. Calculation of L_{dm} and L_{qm} using a hybrid magnetic circuit / finite element method

Another simple but reasonably accurate optimisation approach is to identify from finite element analysis those parameters of the RSM which are difficult to calculate accurately by means of analytical equations or lumped circuit analysis. One such a parameter is the q-axis inductance, L_{qm}, of the RSM, which is taken as constant in the AMC method. The idea of this method is to optimise the stator parameters of the machine using the AMC method and then calculate a new L_{qm} from finite element analysis and use this new L_{qm} in the next optimisation iteration.

It is also possible to optimise the bw/bp ratio or the current angle ϕ using only a few finite element program solutions, as will be shown in Chapter 4. The optimised bw/bp ratio, or optimised current angle ϕ, can then be used in the AMC method to get more accurate optimisation results. This method is, thus, a hybrid magnetic circuit / finite element method (HMF method). The aim of the HMF method is to get more accurate results than in the case of the AMC method but, however, still keeping the computational burden low.

An example of using the HMF method in the optimisation procedure of the RSM using the rotor structure of Fig. 2.6 is as follows:

- → Decide on a design criterion and set either the current density J or the copper losses P_{cu} constant.
- → Select initial values for the stator and rotor dimensions and set ϕ = 65°.
- → Optimise the stator dimensions using the AMC method.
- → With new stator dimensions, calculate L_{qm} using the FE method (section 2.3.2).

→ Optimise the stator design using the AMC method with the new L_{qm}.

→ With new stator dimensions, optimise the current angle ϕ using the FE method. Also, calculate a new value for L_{qm} afterwards.

→ With new ϕ and L_{qm}, optimise the stator using the AMC method.

→ With new stator dimensions, optimise the bw/bp ratio using the FE method. Calculate a new value for L_{qm} afterwards.

→ With new bw/bp ratio and new L_{qm}, optimise finally the stator using the AMC method.

In the HMF procedure some independence is assumed between ϕ and the bw/bp ratio, i.e the optimum value of ϕ is assumed to be independent of what the value is of the bw/bp ratio, and vice versa. The above procedure will typically require 10-15 finite element solutions. An example of using the HMF method will be given in Chapter 4.

Obviously, one can continue with the above procedure to get hopefully more and more accurate results. The idea, however, is to keep the computation time of the preliminary design optimisation low. The preliminary optimum results can be used as a good starting point for the final design optimisation where the FE method is used directly to optimise all the parameters of the machine.

3 Optimisation Algorithms

This chapter describes the optimisation algorithms which can be used to optimise in multidimensions the design of the RSM. As shown in the flow diagram of Fig 1.2, the optimisation algorithm minimises (maximises) the objective function $Y = F(\mathbf{X})$ of the machine subject to inequality and/or equality constraint functions. This is an iterative process where the optimisation algorithm and the line minimisation procedure repeatedly call the lumped circuit or finite element program to calculate the objective function values.

A review of the literature on electrical machine design optimisation reveals that there are a few important aspects that have to be mentioned. These are the following:

(i) Much more attention is given in the literature to the optimum design of the *induction machine* than to other electrical machines.

(ii) The *manufacturing* and *operating costs* of the electrical machine are usually the objective functions to be minimised, subject to performance constraints.

(iii) Only *analytical* or *lumped circuit models* of the electrical machine are used in the optimisation process to calculate the performance parameters of the machine. The finite element method is merely used to investigate the effect of the variation of a single dimension on the performance of the machine and not to do an overall optimum design.

(iv) The constrained optimisation is usually done by converting the constrained problem into an unconstrained one by adding *penalty functions* to the objective function. This modified objective function is then minimised by means of an *unconstrained* optimisation method or algorithm.

From the vast amount of published work on the design optimisation of electrical machines, only some of the work is highlighted here:

- Andersen (1967, 1992) makes use of a Monte Carlo routine, using a random search method, to minimise the objective function with penalty functions. It is not known how fast this method is compared to other methods.

- Ramamoorty and Rao (1979) optimise the design of a segmented rotor reluctance machine using the method of Powell (1964) and Zangwill's (1967) penalty function formulation. In their optimisation of the reluctance machine, the cost of the active materials of the motor is minimised subject to the constraints of pull-out torque and power factor. The optimisation of the voltage-fed, current-controlled reluctance machine was not considered in their work.

- Li (1990) and Parasiliti (1993) make use of the modified Hooke-Jeeves method (based on the direct search method of Hooke and Jeeves (1961) in the optimum design of the induction machine. Li (1990) found that this method is very time efficient compared to other methods.

- An in-depth study was done by Singh and Sarkar (1992) on the optimum design of the induction machine using the methods of Powell (1978) and Han (1977), modified by Schittkowski (1981). These methods suppose that the objective and constrained functions are differentiable and that first derivatives can be calculated. They show that the modified Han-Powell method is very effective using less computation time.

All the above methods prove to be effective in the optimisation of the electrical machine. In this thesis the algorithms of Powell (1964) and the quasi-Newton method are used for the unconstrained design optimisation of the machine. The difference between these two methods is that the Powell method is a non-gradient method which requires only function evaluations, not derivatives, while the quasi-Newton algorithm is a gradient method which requires that the vector of first partial derivatives be calculated. The reasons for using these methods are:

(1) to determine if a gradient method can be used to optimise the design of the machine using the nonlinear finite element field solution to calculate the function value.

(2) to compare the effectiveness of a non-gradient method (Powell) with that of a gradient method (quasi-Newton) and

(3) to verify the optimum design results by using two completely different optimisation algorithms.

Both these methods are described in detail in textbooks and proved to be effective for the minimisation of functions in multidimensions.

The method used in this thesis for the constrained optimisation is the same as that mentioned in (iv) above namely to modify the objective function and solving for the minimum by means of an unconstrained algorithm. Furthermore, the focus of the thesis is on the characterisation of the performance capability of the RSM. The design optimisation, therefore, is on the maximisation of the performance parameters of the machine, such as torque, efficiency and power factor, and not on the minimisation of the cost of the machine, as mentioned in (ii) above. This does not mean that cost and weight are not important factors to be considered. The approach of the thesis also differs from that mentioned in (iii) above, namely to use the *finite element* method in the optimisation procedure instead of less accurate analytical or lumped circuit methods.

Both the Powell and quasi-Newton methods make use of successive line minimisations to minimise (maximise) sequentially a function of n variables along certain lines or vector directions in an n-dimensional space (see the flow diagram of Fig. 1.2). The technique used to do the line minimisation is explained in section 3.1. In sections 3.2 and 3.3 the Powell and quasi-Newton algorithms are

briefly described. The method for the constrained optimisation is described in section 3.4 and in section 3.5 the results of two optimisation case studies are given.

3.1 Line minimisation

For the line minimisation eqn (3.1) is used, i.e. find the scalar y that minimises the function $F(\mathbf{X})$ along a given vector direction $\mathbf{Z}$ from a given starting vector point $\mathbf{P}_o$.

$$\mathbf{X} = \mathbf{P}_o + y\mathbf{Z} \tag{3.1}$$

In the design program each variable x_i to be optimised is given minimum and maximum boundary values wherein the variable is allowed to vary. The boundary values of all the variables are used to determine the minimum and maximum values allowed for y in eqn (3.1). The latter is done to ensure that the minimisation process is within a restricted region in n-dimensional space. If the minimum or maximum of the function is not attained in this region then the program either shifts the boundary values or, if this is not allowed, uses penalty functions to penalise the function value. The region between y_{min} and y_{max} is divided into a number of sections to determine the step size Δy by which y is changed. To bracket the minimum (maximum) of the function, the y-value of eqn (3.1) is changed in steps starting from the initial point P_o as shown in Fig. 3.1. The y-value is changed until the maximum of the function $f(y) = F(\mathbf{P}_o + y\mathbf{Z})$ has been bracketed by the values y_i, y_{i+1} and y_{i+2}. The problem of local minima/maxima was not experienced by the author. The variation of f(y) with y gives very smooth curves for the RSM as is shown e.g. in the graphs of Kamper (1994).

The step size Δy is important because if it is too small then a relatively high number of finite element field solutions will be required to bracket the maximum. The step size, therefore, is taken initially as relatively large in the design program. Closer to the optimum solution the step size can be reduced to bracket the maximum more accurately. With constrained optimisation the step size is taken much smaller to ensure a much closer bracketing of the maximum.

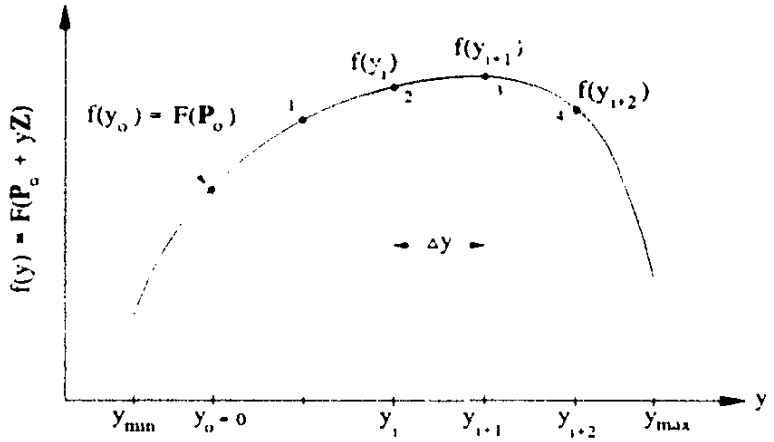

Fig. 3.1. Points 2, 3 and 4 bracket the maximum of f(y) and are used for curve fitting

The last three y-values that bracket the maximum, as shown in Fig. 3.1, are used to do a curve fitting using a second-degree interpolating polynomial of the Newton form. As mentioned, the variation of f(y) with y gives smooth curves so that the use of just three points for curve fitting is justified. Even with the constrained optimisation using the quadratic penalty function method the latter is allowed.

The second degree polynomial $f_2(y)$ of the Newton form is given by

$$f_2(y) = c_1 + c_2(y - y_i) + c_3(y - y_i)(y - y_{i-1}) \tag{3.2}$$

where

$$c_1 = f(y_i), \qquad c_2 = \frac{f(y_i) - f(y_{i-1})}{y_i - y_{i-1}} \qquad \text{and}$$

$$c_3 = \frac{c_2}{y_i - y_{i-2}} - \frac{f(y_{i-1}) - f(y_{i-2})}{(y_{i-1} - y_{i-2})(y_i - y_{i-2})}. \tag{3.3}$$

The minimum (maximum) of the polynomial is obtained by setting the derivative of eqn (3.2) equal to zero and solving for the optimum value y_{optm} from

$$y_{optm} = \frac{1}{2}\left(y_{i-1} + y_i - \frac{c_2}{c_3}\right). \tag{3.4}$$

This solution of y_{optm} is accepted as the location of the minimum/maximum of F(**X**) along the line of eqn (3.1). If a fourth calculated point is available, as shown e.g. in Fig. 3.1, then a third degree interpolating polynomial can be used with a more accurate solution.

3.2 Powell's method

The method of Powell (1964), which is also described in detail by others (Greig 1980, Press *et al* 1986), minimises, with each iteration r of the optimisation process, the function value along a set of n vector directions, where n is the number of variables to be optimised. The initial set of n vector directions is the unit or co-ordinate directions. After each iteration a new direction is defined which is used in the set of vector directions for the next iteration. The basic procedure generates, after n iterations, a set of n mutually *conjugate* vector directions. This implies that after n iterations the minimum of a quadratic function is found. A flow diagram of Powell's method is shown in Fig. 3.3 and is explained briefly in the following paragraphs.

Consider an iteration of Powell's method where the function is minimised along a set of n vector directions, $\mathbf{Z}_1$, $\mathbf{Z}_2$, ..., $\mathbf{Z}_n$, as shown in Fig. 3.2. With each direction $\mathbf{Z}_i$ the function is minimised through a line minimisation using eqns (3.1) and (3.2). This moves the vector point **P** from $\mathbf{P}_{i-1}$ to

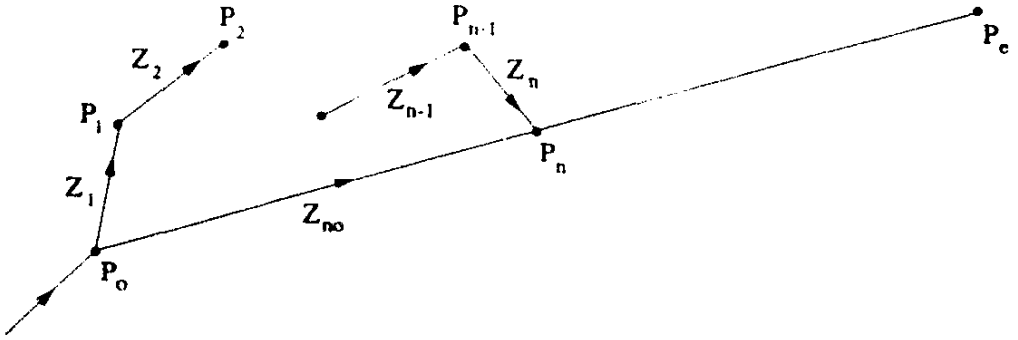

Fig. 3.2. Moving the vector **P** through a set of vector directions $\mathbf{Z}_i$ (Powell's method)

$\mathbf{P}_1$. After n vector directions, thus n line minimisations, the vector point **P** has moved to the point $\mathbf{P}_n$. A new direction is defined $\mathbf{Z}_{no} = \mathbf{P}_n - \mathbf{P}_o$ and the set of vector directions for the next iteration is chosen to be $\mathbf{Z}_2, \ldots, \mathbf{Z}_n, \mathbf{Z}_{no}$. Powell, however, modifies this basic procedure because occasionally the procedure may choose nearly dependent directions which may cause the process to terminate before an optimum is reached. Therefore, tests are done after each iteration to determine whether the new defined direction $\mathbf{Z}_{no}$ is a good direction to be added to the set of directions or not.

Powell recommends two tests to be done to decide if the new defined direction is a good direction or not. The tests are carried out by using an additional calculated vector point $\mathbf{P}_e = 2\mathbf{P}_n - \mathbf{P}_o$ further along the proposed new direction, as shown in Fig. 3.2. For the *maximisation* of the function F, let the values of the function be

$$f_o = F(\mathbf{P}_o), \qquad f_n = F(\mathbf{P}_n) \quad \text{and} \quad f_e = F(\mathbf{P}_e), \quad \text{where} \quad f_n > f_o,$$

and define Δf as the largest increase along one of the directions of the present iteration, i.e.

$$\Delta f = \max_i(f_i - f_{i-1}).$$

Then, if either

$$\begin{aligned} &f_e \le f_o \qquad \text{and\or} \\ &(f_o - 2f_n + f_e)(f_o - f_n - \Delta f)^2 \le \tfrac{1}{2}\Delta f (f_o - f_e)^2, \end{aligned} \tag{3.5}$$

the old directions are for the next iteration used and $\mathbf{P}_n$ for the next $\mathbf{P}_o$. Otherwise, the old set of directions $\mathbf{Z}_1, \mathbf{Z}_2, \ldots, \mathbf{Z}_j, \ldots, \mathbf{Z}_n$, where $\mathbf{Z}_j$ is the direction with the largest increase, is changed to $\mathbf{Z}_1, \mathbf{Z}_2, \mathbf{Z}_{j-1}, \mathbf{Z}_{j+1}, \ldots, \mathbf{Z}_n, \mathbf{Z}_{no}$ and $\mathbf{P}_n$ is moved to the maximum along $\mathbf{Z}_{no}$, and this point is used for the next $\mathbf{P}_o$. The direction with the largest increase is thus discarded, which seems paradoxical, but Powell showed that dropping it gives the best change of avoiding a buildup of linear dependence.

The optimisation procedure is terminated when

$$|f_n - f_o| \le \xi \left(\frac{|f_n| + |f_o|}{2} \right) \tag{3.6}$$

where ξ is the fractional tolerance in the function value and f_o and f_n are the start and final function values on one iteration.

Finally, from the procedure of Fig. 3.3, if it takes an average of m finite element program solutions per line minimisation (actually it is mk program solutions due to skew - eqns 2.11 and 2.16), then mn solutions are necessary per iteration. If, say, n iterations are used to minimise or maximise the function value, then the total number of finite element solutions will be mn^2 (with $n = 10$ and $m = 3$ the number of solutions are 300). Hence, it is clear that with a high average number of finite element solutions per line minimisation, the total number of solutions will be high using Powell's method. The only advantage of Powell's method is that derivatives are not necessary.

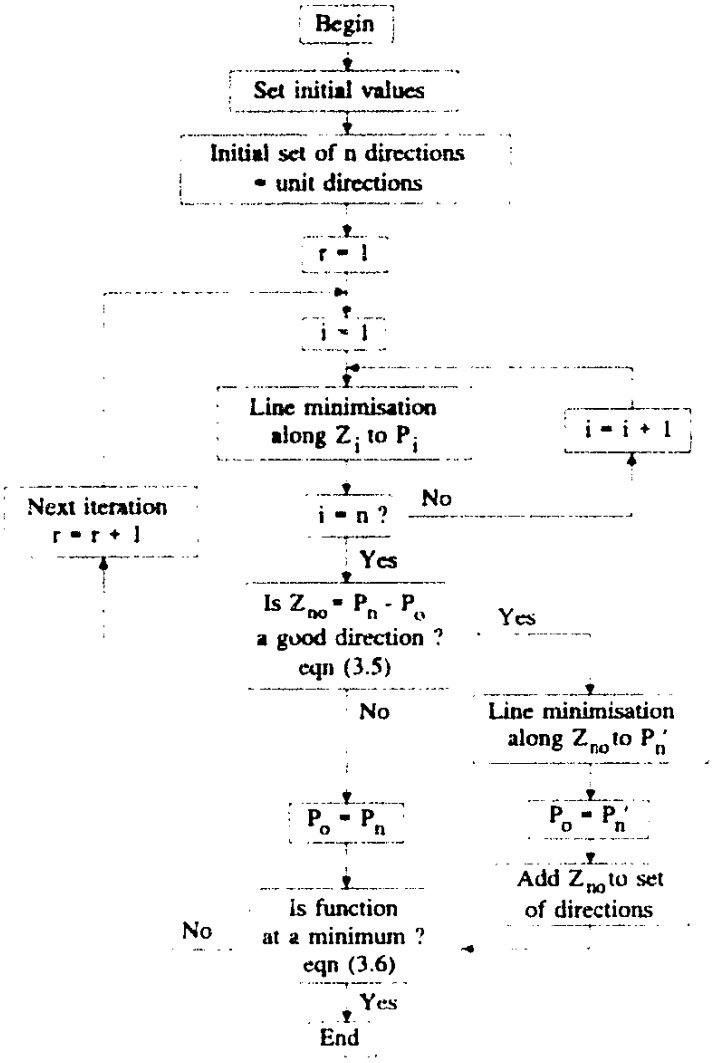

Fig. 3.3. Flow diagram of Powell's optimisation procedure

3.3 Quasi-Newton algorithm

The quasi-Newton method described by, amongst others, Greig (1980), Gill *et al* (1981) and Press *et al* (1986) requires that at each iteration step, r, the function's gradient vector $\mathbf{G}_r$ (vector of first partial derivatives) be calculated at the vector point $\mathbf{P}_r$. The new direction of search, $\mathbf{Z}_r$, from this point is given by

$$\mathbf{Z}_r = \mathbf{H}_r \mathbf{G}_r \tag{3.7}$$

where $\mathbf{H}_r$ is an $n \times n$ matrix which is the quasi-Newton approximation of the inverse Hessian matrix. The Hessian matrix is a second partial derivative matrix of the function at a vector point $\mathbf{P}$. In the quasi-Newton method the matrix $\mathbf{H}_r$ is updated sequentially to build up a good approximation of the inverse Hessian. It can be shown that for a quadratic function the algorithm terminates in at most n steps, where n is the number of variables to be optimised.

The first quasi-Newton method was suggested by Davidon (1959), which was publicised and improved by Fletcher and Powell (1963) - referred to as the *Davidon-Fletcher-Powell* (*DFP*) algorithm. Since 1963 there has been an ever expanding interest in quasi-Newton methods. The *Broyden-Fletcher-Goldfarb-Shanno* (*BFGS*) formula is generally recognized as the most effective formula for updating the approximate inverse Hessian. The BFGS formula, which is implemented in this section, was independently suggested by Broyden (1970), Fletcher (1970), Goldfarb (1970) and Shanno (1970).

The procedure of the quasi-Newton method is described by the flow diagram of Fig. 3.4. Initially, the matrix $\mathbf{H}_1$ is the unit matrix. With each iteration r the function is minimised along the line $\mathbf{P}_r + y\mathbf{Z}_r$ (eqn 3.1) where $\mathbf{Z}_r$ is given by eqn (3.7). This moves the vector point $\mathbf{P}$ from $\mathbf{P}_r$ to $\mathbf{P}_{r+1}$. The approximate inverse Hessian matrix is updated by means of eqn (3.9) and is used for the next iteration $r = r + 1$ to determine $\mathbf{Z}_{r+1} = -\mathbf{H}_{r+1}\mathbf{G}_{r+1}$.

By defining

$$\begin{aligned} \mathbf{S}_r &= \mathbf{P}_{r+1} - \mathbf{P}_r \qquad \text{and} \\ \mathbf{W}_r &= \mathbf{G}_{r+1} - \mathbf{G}_r \,, \end{aligned} \tag{3.8}$$

the BFGS update formula is given by

$$\begin{aligned} \mathbf{H}_{r+1} = \mathbf{H}_r &+ \left(\frac{1}{\mathbf{S}_r^{\mathrm{T}} \mathbf{W}_r}\right) \mathbf{S}_r \mathbf{S}_r^{\mathrm{T}} - \left(\frac{1}{\mathbf{W}_r^{\mathrm{T}} \mathbf{H}_r \mathbf{W}_r}\right) \mathbf{H}_r \mathbf{W}_r \left\{\mathbf{H}_r \mathbf{W}_r\right\}^{\mathrm{T}} \\ &+ \mathbf{W}_r^{\mathrm{T}} \mathbf{H}_r \mathbf{W}_r \left\{\mathbf{U}_r \mathbf{U}_r^{\mathrm{T}}\right\} \end{aligned} \tag{3.9}$$

where

$$\mathbf{U}_r = \left(\frac{1}{\mathbf{S}_r^{\mathrm{T}} \mathbf{W}_r}\right) \mathbf{S}_r - \left(\frac{1}{\mathbf{W}_r^{\mathrm{T}} \mathbf{H}_r \mathbf{W}_r}\right) \mathbf{H}_r \mathbf{Y}_r \,. \tag{3.10}$$

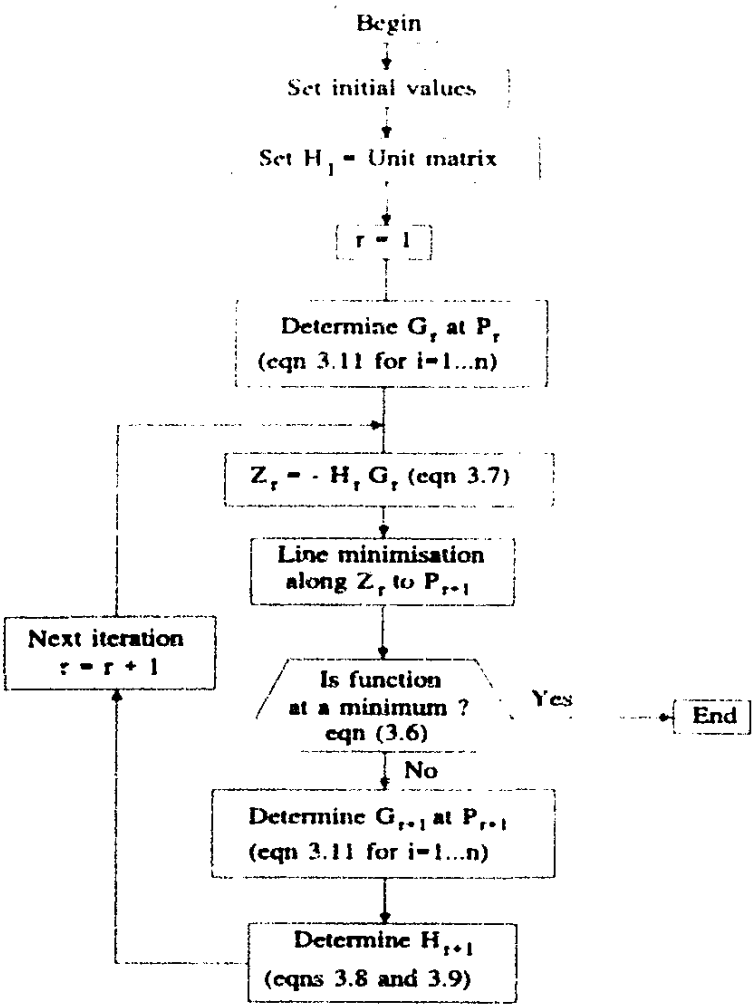

Fig. 3.4. Flow diagram of the quasi-Newton optimisation procedure

The first partial derivative of the function with respect to a variable x_i is determined by the forward-difference approximation as

$$\frac{\partial f}{\partial x_i} \approx \frac{f(x_i + \delta_i) - f(x_i)}{\delta_i} \qquad \text{where} \qquad \delta_i = x_i h \ . \tag{3.11}$$

The choice of h in eqn (3.11) is critical because it determines the quality of the derivative. If h is too large, then the truncation error is large; if too small, then the condition error, due to the error in the computed function value, is large. The usual approximation is to take h as $h = \varepsilon_r^{1/2}$ where ε_r is the relative error in the computed function value. Note that function values are not available to machine precision due to the nonlinear finite element field solution, which uses an iterative method with a convergence criterion to solve for the magnetic vector potentials. The accuracy of the computed function value is approximately estimated by using difference tables as described in Gill (1981). The calculated results of the difference tables are given in Appendix D. Hence, h is found to be equal to

10^{-6}, but faster optimisation results were obtained with h between 10^{-4} and 10^{-5}. In their paper, Singh and Sarkar (1992) found a best value of $h = 10^{-2}$. The error in the finite difference gradient approximation can also be minimised by changing or updating h as the optimisation progresses (Barton, 1992). This, however, was found to be unnecessary and a fixed value of $h = 10^{-5}$ was used throughout the optimisation.

By using eqn (3.11) it is clear that n finite element program solutions (n is the number of variables to be optimised) are necessary to determine the gradient vector. With an average of m solutions to do the line minimisation and with, say, n iteration steps necessary to minimise the function value, the total number of finite element solutions will be $n^2 + mn$ (with $n = 10$ and $m = 3$ the number of solutions are 130). This is dramatically less than the mn^2 solutions necessary with Powell's method, particularly when m is high. However, owing to the inaccuracy of the forward-difference approximation, additional iterations will be performed closer to the optimum.

3.4 Constrained optimisation

Although the focus of the optimisation study is more on the unconstrained condition, constrained optimisation is also done by using penalty functions. The objective function is modified by adding terms or functions that assign a positive 'penalty' for increased constraint violation. The new objective function is defined as

$$\mathbf{F(X,w)} = \mathbf{f(X)} + \sum_{i=1}^{u} \mathbf{w}_i \, \mathbf{c}_i\mathbf{(X)} \tag{3.12}$$

where $\mathbf{f(X)}$ is to be minimised, $\mathbf{w}_i$ are weighting factors and $\mathbf{c}_i\mathbf{(X)}$ are functions which penalise infeasibility. As an example, the quadratic penalty function is used to maximise the power factor, $\mathbf{P}_f\mathbf{(X)}$, of the machine subject to the torque constraint $\mathbf{T(X)} \geq \mathbf{T}_o$ as defined by

$$\mathbf{F(X,w)} = \mathbf{P}_f\mathbf{(X)} - \mathbf{w}\,\epsilon \tag{3.13}$$

where

$$\epsilon = \begin{cases} 0 & : \ \mathbf{T(X)} \geq \mathbf{T}_o \\ (\mathbf{T}_o - \mathbf{T(X)})^2 & : \ \mathbf{T(X)} < \mathbf{T}_o \end{cases}. \tag{3.14}$$

The advantage of the penalty function method is that eqn (3.12) e.g. can now be solved by the use of an unconstrained optimisation algorithm. The disadvantage of this method is that it may require repeated minimisation of $\mathbf{F(X, w_i)}$ for a sequence of $\mathbf{w}_i$ - therefore the name *sequential unconstrained minimisation*. The constrained problem, thus, is solved by means of a sequence of unconstrained subproblems (or possibly a single unconstrained subproblem). A general treatment of penalty functions is given by Zangwill (1967).

The use of weighting functions has also been described by Williamson and Smith (1980) when using optimisation algorithms in electrical engineering.

3.5 Optimisation results of two case studies

In this section two examples are given of the design optimisation of the cageless flux barrier RSM. The aim of these examples is to prove the feasibility in terms of computation time and number of solutions of the proposed finite element design optimisation method. The finite element method is used directly in the optimisation procedure to calculate the performance parameters of the machine, i.e. the function values, as shown in Fig. 1.2. The aim is also to point out the time efficiency of the Powell and quasi-Newton methods described in sections 3.2 and 3.3 respectively and to verify that the same optimum solutions are obtained with these methods. Both methods make use of the line minimisation technique of section 3.1.

3.5.1 Variables and performance parameters

A linearised cross-section of the reluctance machine investigated is shown in Fig. 3.5. Only five variables (dimensions) of the machine are selected to be optimised for the two case studies. These are the tooth width, yoke height, stator inner diameter, inner barrier width and outer barrier width. The stator outer diameter, the stack length and the airgap length of the machine are kept constant in the optimisation procedure namely the same as that of a standard 5.5 kW induction machine. Furthermore, a 7/9 chorded stator winding is used in the analysis. The rotor variables not changed in the optimisation are the rib heights, web widths, barrier positions and cutout dimensions. Some of these variables are optimised in the design examples of Chapter 4.

In the design optimisation either the current density or the copper losses are kept constant in the finite element program (see eqns 2.9 and 2.10). The full-load values of a standard induction machine are used for the current density and total copper losses of the RSM. The current angle ϕ of Fig. 2.3 is also kept constant at certain angles. The performance parameters (function values) that are maximised in the two examples are the torque and the torque/kVA of the machine.

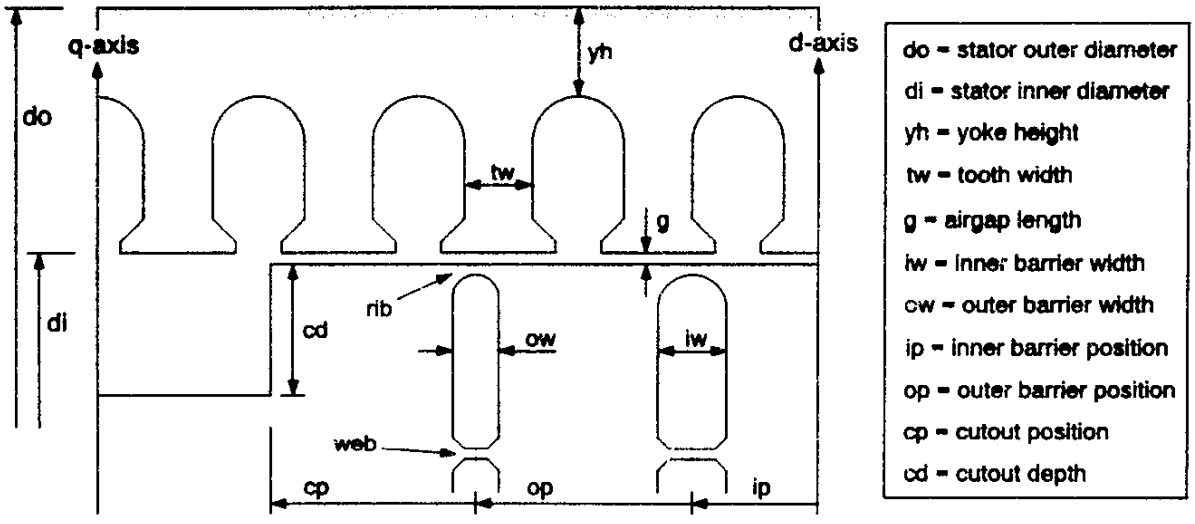

Fig. 3.5. Linearised cross-section of a four barrier per pole rotor RSM

3.5.2 Optimisation results

The optimisation results of the two case studies are given in Table 3.1. In the one case study (machine A) the torque as the function value calculated by the finite element program is maximised unconstrained. The total copper losses are taken as P_{cu} = 700 W and the current angle is set at ϕ = 60°. In the other case study (machine B) the torque/kVA of the machine is maximised unconstrained with the current density J = 6 A/mm² and the current angle ϕ = 70°. These two examples are extreme cases of the optimum design of the machine and as such will yield two totally different machines.

The results of Table 3.1 point out that some of the optimum dimensions of the two optimised machines differ remarkably. This difference is explained in detail in Chapter 4. Both the Powell and quasi-Newton methods give the same optimum values for the variables. This gives confidence in the results specifically if it is taken into account that the two algorithms are totally different, that the one is a gradient and the other a non-gradient method, and that the two unconstrained problems are completely different.

The relatively high number of finite element program solutions required for both optimisation methods is due to the strict termination criterion set in the optimisation program (eqn 3.6).

The other results of Table 3.1 regarding the time efficiency of the Powell and quasi-Newton methods are discussed in section 3.5.4.

	Machine A			Machine B		
Criterion →	Maximise Torque = F(X)			Maximise Torque/kVA = F(X)		
Constants →	P_{cu} = 700 W and ϕ = 60°			J = 6 A/mm² and ϕ = 70°		
Variables [X] ↓	Starting values (mm)	Powell Optimum values (mm)	Q-Newton Optimum values (mm)	Starting values (mm)	Powell Optimum values (mm)	Q-Newton Optimum values (mm)
1. Tooth width	7.5	5.41	5.42	5.0	6.31	6.3
2. Yoke height	15.0	18.32	18.27	20.0	15.95	15.8
3. Inner diameter	133.0	105.7	105.5	105.0	138.9	139.5
4. Outer barrier	4.5	2.89	2.9	2.5	3.41	3.4
5. Inner barrier	3.5	5.84	5.88	6.5	10.3	10.4
F(X)	41.12 Nm	57.993 Nm	57.994 Nm	4.098 Nm/kVA	4.564 Nm/kVA	4.564 Nm/kVA
F(X) after 5 iterations		57.993 Nm	55.967 Nm		4.563 Nm/kVA	4.539 Nm/kVA
No. of iterations with all variables within 5% of optimum values		3	6		4	6
Total number of iterations		5	10		8	10
Total number of solutions		102	98		156	115

Table 3.1. Optimisation results of the Powell and quasi-Newton methods

3.5.3 Some remarks on the finite element analysis

The computation time per finite element program solution is about 5 minutes on a SUN 1000 workstation, using an average of 1800 elements per pole and 1100 vector potential unknowns. This implies that the design optimisation problem requiring, say, 100 solutions can be solved in a day. It was found that for the optimisation of 10 variables the number of solutions required typically vary between 100 and 150 with the computation time between 8 to 12 hours. The latter obviously depends on the load of the workstation, the starting vector point and the termination criterion.

The computation time to solve the design optimisation problem will decrease as the power and speed of workstations increase in the future. Another aspect that influences the computation time is the number of finite elements used. The latter has a dramatic effect on the solution time. The question is to what extent accuracy is lost in using fewer elements. There may be some optimum number of elements where the computation time is reduced whilst accuracy is still maintained. The latter is not investigated and is recommended for further study. Note, however, that for the flux barrier rotor of the RSM, the barriers with their saturation bridges must be meshed well using a relatively high number of elements. The more barriers used the higher the number of elements. This higher number of elements is unavoidable for the punched flux barrier rotor RSM as the saturation of the iron ribs and webs plays an important role in the performance of the machine.

Another question about the proposed finite element optimisation method may be about the mesh that is changing as the optimisation progresses. Is there a possibility that some of the elements become badly shaped or ill conditioned and that accuracy is lost? This is possible but was not experienced by the author. Before and after each design optimisation the mesh was checked and in no case was it found that elements of the new mesh of the optimised machine were badly shaped. The latter can be explained by the fact that the variables (dimensions of the machine) do not change that much in the search for the optimum. A good starting vector point with typical optimum values of the dimensions can always be estimated beforehand. Or else, start with the normalised stator dimensions of a standard induction machine and for the rotor use uniformly distributed flux barriers and a bw/bp ratio of, say, 0.3. The change of the mesh during the design optimisation, thus, was found to be not a problem.

3.5.4 Conclusions on the Powell and quasi-Newton methods

In Figs. 3.6 and 3.7 some further results are given of the quasi-Newton and Powell methods for the two case studies. Here the trend of the function values and the stator inner diameter with each iteration are shown.

From these results as well as the results of Table 3.1 and from the optimisation results of Chapter 4, the following conclusions can be drawn about the Powell and quasi-Newton methods. Note that these conclusions are based on the unconstrained design optimisation of the reluctance machine and are not necessarily valid for difficult constrained optimisation problems or for the design optimisation of other electrical machines.

(i) The Powell algorithm is very fast, initially, to optimise the variables; even after the first or second iteration most of the variables are relatively close to their optimum values (see Fig. 3.6). However, the latter depends very much on which variables are optimised first according to the initial set of unit directions. It is also clear from Fig. 3.6 that, although the method is initially fast, it is not efficient in finally finding the optimum.

(ii) The Powell algorithm seldom chooses new directions to be added to the list of vector directions. This may indicate that the unit directions are not poor directions at all. Mathematically, this implies that the unit directions can simply be used throughout the optimisation process. Powell (1964) also mentioned that as the number of variables increases there is a tendency of his method for new directions to be chosen less often.

(iii) Table 3.1 shows that the number of iterations using the Powell method is much less than that of the quasi-Newton method, but that the number of solutions is higher. This points out the penalty of the Powell method namely the use of a high number of line minimisations, each requiring a few solutions.

(iv) The advantage of the quasi-Newton method is the relatively low number of line minimisations used, making the number of solutions less. With this method, thus, accurate line minimisations can be afforded.

(v) The quasi-Newton algorithm proved to be slow initially in optimising the variables (see Fig. 3.7). Generally it was found, and this is also shown in Fig. 3.7, that after *n-1* iterations (*n* gradient vectors or *n-1* Hessian updates, where *n* is the number of variables) the method becomes fast in optimising the variables. Closer to the optimum, however, additional iterations are performed as shown in Fig. 3.7 due to the approximation of eqn (3.11). The latter is the weakness of the finite-difference quasi-Newton algorithm and is also the reason for the high number of iterations used, as shown in Table 3.1.

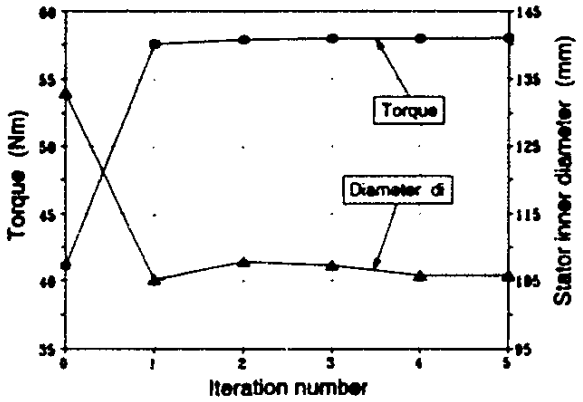

(a) Maximisation of the torque

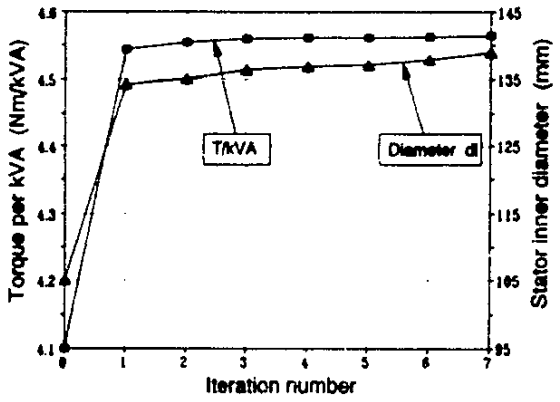

(b) Maximisation of the torque/kVA

Fig. 3.6. Trends of the performance parameters and stator inner diameter in the design optimisation of the RSM using the *Powell* method

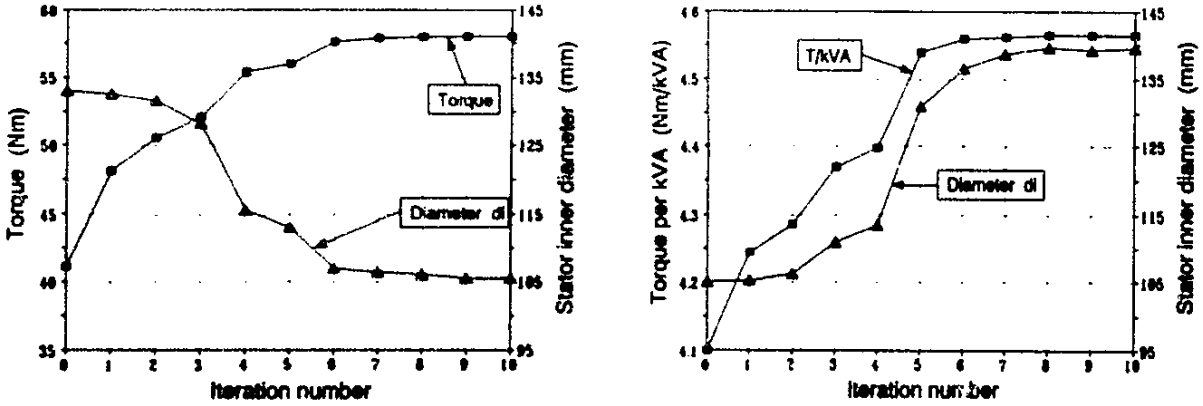

(a) Maximisation of the torque (b) Maximisation of the torque/kVA

Fig. 3.7. Trends of the performance parameters and stator inner diameter in the design optimisation of the RSM using the *quasi-Newton* method

3.6 Summary

In this chapter the line minimisation technique and the optimisation algorithms are described that are used to optimise the design of the RSM. Both the Powell and quasi-Newton methods proved to be effective in the design optimisation of the machine. In general it was found that the quasi-Newton method is equal or slightly faster in calculation speed than the Powell method. An important conclusion, thus, is that a gradient optimisation algorithm, such as the quasi-Newton method, can be used with success, using the nonlinear finite element field solution to calculate the objective function value. It is shown in this chapter (and the point will further be amplified in Chapter 4) that it is feasible in terms of computation time to do a total (stator and rotor) optimum design of the RSM using the finite element method directly in the optimisation process.

4 Optimised Structures

The different performance calculation methods of Chapter 2 and the optimisation algorithms of Chapter 3 are used in this chapter to optimise in multi-dimensions the design of the RSM. The aim of the chapter is to evaluate from calculations and also from measurements the performance capability of the RSM in the 3 - 10 kW power level. The performance capability of the RSM in the higher power levels is dealt with in Chapters 5 and 6. This chapter also gives considerable attention to the explanation and the understanding of the various optimum designed RSMs.

4.1 Variables to be optimised

The aim of the optimisation study in this chapter is to optimise the design of the RSM in the same volume as that of a standard 5.5 kW induction machine. The reason for the latter is to compare to some extent the performance of the optimised RSM with that of the induction machine. It is furthermore comfortable to do performance tests at this power level to confirm the calculated results. The RSM is thus optimised according to certain design criteria per given core outer diameter and given core axial length.

The design optimisation is done primarily for a 36-slot stator, but a 48-slot machine is also investigated. The stator windings used are all chorded windings and the number of turns in series per phase is kept constant in the analysis. The latter can be changed afterwards to meet the voltage requirement of the machine at a certain speed at full load.

The airgap length is also not varied in the analysis and is taken the same as that of the induction machine. It is shown by Kamper (1994) and is also found from further investigation that the optimum airgap length of the RSM for different design criteria is much less than the mechanical constraint on a minimum airgap length.

Furthermore, semi-closed stator slots are used throughout the design optimisation of the RSM. Large open slots will let flux pulsations rise in the rotor surface and possibly in the rotor iron segments. This will lead to an increase of the iron losses of the machine. Too narrow slots will make winding the machine difficult and will increase the leakage flux of the machine.

The other parameters not varied in the optimisation are the web widths and rib heights of the rotor (see Fig. 4.1). These are taken as thin as mechanically possible in the analysis. A rule of thumb for the punching of a lamination is to make the widths and heights of the saturation bridges not less than the thickness of the lamination itself, which is 0.5 mm in this case. From this and from mechanical strength analysis the web widths are all taken equal to 1.0 mm and the rib heights equal to 0.75 mm. In Chapter 6 the mechanical strength of the rotor lamination is considered in further detail.

A linearised cross-section of a 4-pole reluctance machine structure studied in this chapter is shown

in Fig. 4.1. Four flux barriers and two cutouts per pole (thus six barriers per pole) are used for the reluctance rotor. The question may arise: why six barriers per pole? There is a limit on the maximum number of barriers per pole that can be used. To limit iron pulsation losses in the rotor iron segments the barrier pitch must be larger than the tooth pitch, i.e. bp > tp (see Fig. 4.1). This means that in terms of the number of stator slots, N_{sl}, and the number of pole pairs, p, the number of barriers per pole, N_{bp}, must be

$$N_{bp} < \frac{N_{sl}}{2\,p} \,. \tag{4.1}$$

To ensure that iron losses are almost not present in the rotor iron segments, the number of barriers per pole is in general taken as ⅔ the number of slots per pole in the analysis, i.e.

$$N_{bp} = \frac{N_{sl}}{3\,p} \,. \tag{4.2}$$

Hence, for a 4-pole, 36-slot stator, $N_{bp} = 6$. The latter is realised in the rotor structure of Fig. 4.1 as four inner flux barriers and two outer cutouts per pole. Note that with eqn (4.2) there is freedom to vary (optimise) the barrier and cutout positions in the optimisation procedure subject to the constraint that bp > tp.

The variables (dimensions) of Fig. 4.1 to be optimised are *yh*, *tw* and *di* of the stator and *iw*, *ow*, *ip*, *op* and *cp* of the rotor. The barrier and cutout positions are varied in terms of mechanical degrees measured from the d-axis. The cutout depth, *cd*, is determined according to the outer barrier dimensions and the cutout position to obtain a more or less constant width outer iron segment. For more clarity, typical stator and rotor structures and some dimensions are shown in Figs. 4.2 and 4.3.

The other rotor structure studied is an eight flux barrier per pole rotor with uniformly distributed flux barriers and equal barrier widths, as shown in Fig. 4.4. In this case a 48-slot stator is used.

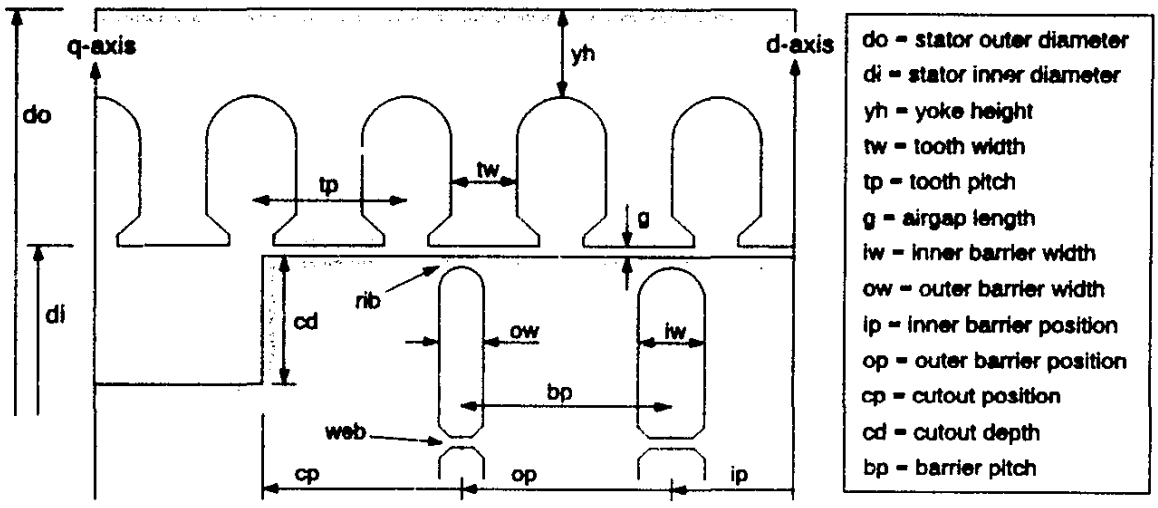

Fig. 4.1 Linearised cross-section of the stator and rotor structure of the RSM

4.2 Performance parameters and constraints

To investigate the performance characteristics of the RSM, the design of the machine is optimised by maximising different performance parameters (objective function values) of the machine. These parameters or function values are the torque, the efficiency, the torque per kVA and constrained torque per kVA. The constrained torque per kVA is done similarly to eqns (3.13) and (3.14), subject to a torque constraint of $T \geq 35$ Nm, which is the rated torque of a 4-pole, 5.5 kW induction machine.

In the design optimisation either the copper losses or the current density are kept constant. With no thermal model used in the design optimisation, the current density and copper losses are taken equal to the full-load values of that of a standard 5.5 kW induction machine to ensure that the temperature of the machine is within limits. The full-load current density of the standard 5.5 kW induction machine is $J = 6$ A/mm² and the full-load total copper losses about $P_{cu} = 700$ W. Note that the dissipation of heat in the reluctance machine will be better than in the induction machine. This is due to the fact that almost all the losses of the RSM are in the stator, which is close to and thermally in good contact with the outer cooling surface of the machine. The maximum flux densities are also checked if these are less than certain maximum values to ensure that the iron losses are within limits.

4.3 Understanding the optimum designed RSMs

It is important to understand beforehand what the RSM will look like when the machine is optimised according to the design criteria of torque, efficiency or torque/kVA. In the following sections the effects of these three criteria on the design of the machine are explained

4.3.1 Optimum RSM designed for maximum torque

The design of the maximum torque RSM can be understood from the torque equation of the machine. The torque is given by eqn (2.7) as

$$T = \frac{3}{4} p \, \Delta L \, \hat{I}_s^2 \sin(2\phi) \, . \tag{4.3}$$

ΔL can be expressed from eqns (2.28) - (2.31) as

$$\begin{aligned} \Delta L &= \frac{K_m}{g_d'} \left(1 - \frac{g_d'}{g_q'} \right) \\ &= \frac{m \, W^2 \, K_{w1}^2 \, d_i \, l \, \mu_0}{\pi \, p^2 \, g_d \, k_{sd} \, k_c} \left(1 - \frac{1}{\sigma} \right) . \end{aligned} \tag{4.4}$$

The current $\hat{I}_s$ of eqn (4.3) is given by eqn (2.9) for a given rms current density, J, as

$$\hat{I}_s = \sqrt{2} \, J \, A_{cu} \, n_s / z \, . \tag{4.5}$$

By substitution of eqns (4.4) and (4.5) into eqn (4.3) the torque can be expressed as

$$T = K_1 J^2 \left(\frac{d_1 A_{cu}^2}{k_{sd}} \right) \left(1 - \frac{1}{\sigma} \right) \tag{4.6}$$

where

$$K_1 = \frac{3 m W^2 K_{w1}^2 / \mu_0 n_s^2 \sin(2\phi)}{2 \pi p g_d k_c z^2} . \tag{4.7}$$

For the explanation of the maximum torque design the current angle, ϕ, and the Carter factor, k_c, of eqn (4.7) are taken as constants. ϕ, for example, can be taken as equal to 65°, as discussed in section 2.5; k_c also varies little in the design optimisation and can be assumed as some constant.

From eqn (4.6), with a constant, rated current density, J, it is clear that the maximum torque of the machine will be very much dependent on the first term in brackets. With the torque proportional to the square of the copper area, the optimisation algorithm will try to make this area and thus the slot area as large as possible, i.e. try to make the yoke height, tooth width and the inner stator diameter relatively small. On the other, hand the torque is also proportional to the inner stator diameter and the algorithm will try to make this variable larger. Furthermore, changing the slot area will have an effect on the saturation factor k_{sd}. A large slot area with a small yoke and thin teeth will increase the saturation factor due to the higher current in the machine and the less stator iron used. Also, making the flux barrier widths of the rotor relatively large will increase k_{sd}. Note that the saturation of the machine also influences the inductance ratio σ of eqn (4.6). There are thus optimum values for the stator and rotor dimensions that will maximise the first term, amongst others, of eqn (4.6).

To show what the optimum values of these variables are, the RSM is optimised using the FE and AMC calculation methods of Chapter 2 and the optimisation algorithms of Chapter 3. The results of these design optimisations are given in Table 4.1. The FE method is used to optimise all the variables of the stator and rotor structure of Fig. 4.1 to maximise the torque of eqn (4.6). The detailed results of the FE optimisation are given and discussed in section 4.4.

In the AMC optimisation method the same stator structure as Fig. 4.1 is assumed, but the rotor structure is taken as round with uniformly distributed flux barriers and equal barrier widths (section 2.6, Fig. 2.6). A six barrier per pole rotor is assumed. The AMC method is based on taking L_{mq} and the bw/bp ratio of the machine constant in the optimisation procedure. The initial L_{mq} value is calculated from eqn (2.33) as $L_{mq} \approx 15$ mH, with

$W = 132$, $K_{w1} = 0.901$, $l = 133.4$ mm,
$d_o = 203.2$ mm and $g_d = 0.34$ mm.

The L_{mq} value, however, is also varied in Table 4.1 to observe the effect of this on the optimum design of the machine. The bw/bp ratio is taken from Chapter 2, section 2.6(ii) as bw/bp = 0.33.

The rotor structures of the FE and AMC calculation methods differ, so strictly the results of these methods in Table 4.1 cannot be compared. However, both methods will show the same tendencies for the optimum values of the *stator* dimensions.

The AMC results of Table 4.1 show that the optimum stator dimensions for the three constant q-axis inductances (shown in italics in Table 4.1) differ relatively little from each other. This confirms that the value of L_{qm} taken in the AMC calculation method is not so critical when optimising the design of the RSM, as will also be clear from the other results in this section.

Both the AMC and FE methods show that the normalised value of d_i is relatively small (≈ 0.47), resulting in a large copper area. The latter was expected from eqn (4.6). The saturation factor is very high due to the large copper area and large current flowing in the machine. There is relatively close agreement between the optimum dimensions of the two calculation methods. The penalty of the AMC method is that cross magnetisation is not taken into account. Cross magnetisation lets the saturation factor k_{sd} increase further and prevents the copper area of the machine from becoming too large.

	tw (mm)	yh (mm)	di (mm)	di/do	k_{sd}	A_{cu} (mm²)	L_{dm} (mH)	L_{qm} (mH)
AMC (10)	4.57	14.3	92.6	0.46	3.14	54.4	41.5	*10*
AMC (15)	4.93	15.7	97.6	0.48	2.68	47.3	51.0	*15*
AMC (20)	5.2	16.8	101.8	0.5	2.36	41.8	60.3	*20*
FE	4.39	15.0	96.2	0.47	-	52.8	38.7	8.1

Table 4.1. Results of the maximum torque for given current density design

The torque of the RSM may also be maximised by keeping the copper losses constant. In this case eqn (2.10) must be used for $\hat{I}_s$ instead of eqn (2.9). Equation (4.6) thus changes to

$$T = K_2 P_{cu} \left(\frac{d_i A_{cu}}{k_{sd}} \right) \left(1 - \frac{1}{\sigma} \right) \tag{4.8}$$

where

$$K_2 = \frac{m W^2 K_{w1}^2 l \mu_0 n_a^2 \sin(2\phi)}{4 \pi p^2 g_d k_c z^2 q \rho_t (l + l_e)} . \tag{4.9}$$

The torque in this case is directly proportional to the copper area A_{cu}. This means that the first term in brackets of eqn (4.8) will become a maximum with less copper area than in the case of eqn (4.6); consequently *tw*, *yh* and *di* will be larger. In Table 4.2 the optimisation results for the maximisation of the torque of eqn (4.8) are given. As expected the copper area is much less than in the case of Table 4.1 with the normalised value of, amongst other things, *di* larger (≈ 0.52). The saturation factor is now also less due to less current in the machine. The effect of this can be seen in the much higher value for L_{dm}. Note that the AMC and FE methods show the same tendency of change in the

	tw (mm)	yh (mm)	di (mm)	di/do	k_{sd}	A_{cu} (mm²)	L_{dm} (mH)	L_{qm} (mH)
AMC (10)	5.5	17.8	105.7	0.52	2.28	36.8	64.6	10
AMC (15)	5.76	18.7	109.2	0.54	2.12	32.5	71.7	15
AMC (20)	6.0	19.5	112.4	0.55	1.98	28.7	78.7	20
FE	5.49	18.6	105.1	0.52	-	35.5	61.2	11.2

Table 4.2. Results of the maximum torque for given copper losses design

optimum values between Tables 4.1 and 4.2.

Equations (4.6) and (4.8) together with the results of Tables 4.1 and 4.2 give some understanding of the design of the RSM when the torque is maximised. A remaining question, however, may be what effect other values than rated values for J and P_{cu} will have on the optimum design of the RSM. This has been investigated to some extent by the author (results not given here). For higher values of J and P_{cu} the copper area, A_{cu}, is reduced in the optimisation to prevent over-saturation. With lower values, A_{cu} is allowed in the optimisation to increase due to less saturation. It was found, however, that the optimum dimensions change relatively little, but that the torque varies considerably. The latter can be explained from eqns (4.6) and (4.8). The optimum is to use typical rated values for J and P_{cu} to obtain the highest torque with the losses of the machine still within limits.

4.3.2 Optimum RSM designed for maximum efficiency

In a small electrical machine, such as in the sub 10 kW power level the copper losses dominate as the greatest part of the losses. The efficiency of the machine may then be taken as approximately

$$\eta \approx \left(1 + \frac{P_{cu}}{\omega_r T}\right)^{-1} . \qquad (4.10)$$

If the design of the small electrical machine is optimised in terms of its efficiency for given full-load copper losses, then eqn (4.10) shows that the efficiency of that machine will be a maximum where the torque of the machine is a maximum. This will therefore give more or less the same optimum designed machine as in the case where the torque for given copper losses is maximised (section 4.3.1). The results of Table 4.3 confirm this, as the optimum dimensions are close to those of Table 4.2. Note, however, that the latter will not be so in the case of large machines where the iron losses are relatively large at base speeds.

The efficiency may be maximised further by making the copper losses also a variable in the design optimisation. Maximum efficiency is generally obtained at lower than rated values of copper losses with the output power of the machine then less.

	tw (mm)	yh (mm)	di (mm)	di/do	k_{sd}	A_{cu} (mm²)	L_{dm} (mH)	L_{qm} (mH)
AMC (10)	5.49	18.5	104.8	0.52	2.23	36.0	65.6	10
AMC (15)	5.77	19.5	108.9	0.54	2.05	31.2	73.8	15
AMC (20)	6.0	20.3	112.4	0.55	1.92	27.4	81.3	20
FE	5.31	18.8	108.1	0.53	-	34.9	64.9	10.7

Table 4.3. Results of the maximum efficiency for given copper losses design

4.3.3 Optimum RSM designed for maximum T/kVA

An equation for the T/kVA of the RSM can be derived by taking the rms supply voltage, V_s, as being approximately equal to (see Fig. 2.3, eqn 2.4 and assume ω_r is constant)

$$V_s = \frac{V_q}{\sqrt{2}} = \frac{E_q}{\sqrt{2}} = K_3 L_d \hat{I}_s \cos(\phi) , \qquad \text{with} \qquad K_3 = \omega_r/\sqrt{2} . \tag{4.11}$$

By dividing the torque equation (eqn 2.6) by this voltage and the current, the T/kVA can after simplification be written as

$$\frac{T}{kVA} = K_4 \left(1 - \frac{1}{\sigma}\right) \sin(\phi) , \qquad \text{with} \qquad K_4 = \frac{p}{\omega_r} . \tag{4.12}$$

It must be emphasised that eqn (4.12) is just an approximation because the equation is suggesting wrongly that $\phi = 90°$ will maximise the T/kVA. This is due to the approximation of eqn (4.11) where it is assumed that $V_d \approx 0$. Nevertheless, eqn (4.12) gives a good indication of what the maximum T/kVA machine will look like. The equation shows that an optimum RSM designed for maximum T/kVA will have a large current angle, ϕ, a high inductance ratio, σ, and thus a high power factor (eqn 2.21). For a given current density and with much less current necessary (there is no requirement for high current or high torque) the slot area of this machine will be small and the machine will be out of saturation. Hence, L_d and thus σ will be high. A high σ also enforces a smaller L_q which will require the barrier widths to be large. It is expected that the airgap diameter *di* of this machine will be large due to the smaller required slot area, and more importantly, the fact that L_{dm} is a direct function of *di* (eqn 2.25). A large *di* also makes it possible to use large barrier widths.

The optimised results for the maximum T/kVA design with the bw/bp = 0.33 are given in Table 4.4. There is a remarkable difference in the inner diameter, the copper area, the saturation factor and the d-axis inductance with the corresponding values of Tables 4.1 - 4.3.

Much the same results are obtained with bw/bp = 0.5, as given in Table 4.5. This can be explained by the fact that the machine is completely out of saturation and a different bw/bp ratio will hardly

have an effect on the maximum L_{dm} value and the optimum stator dimensions. What gives confidence in the AMC method is that the method shows very much the same tendency of change in the optimum dimensions (except for the *yh*) as the FE method.

The penalty of the AMC method of keeping L_{qm} constant, however, is now very clear from the large deviations in the copper area A_{cu} and the value for L_{dm}. Keeping L_{qm} constant in the design optimisation means that L_{qm} is not effected by saturation and the optimisation algorithm will maximise L_{dm} and σ by getting the machine out of saturation. However, it is known from using flux barrier rotors with saturation bridges that if the machine comes out of saturation, L_{qm} increases rapidly (see e.g. Fig. 2.4(b)) and σ decreases. Some degree of saturation will still be maintained, as the relatively low value for L_{dm} and the large value for A_{cu} (large current) of the FE method of Tables 4.4 and 4.5 indicate.

bw/bp = 0.33	tw (mm)	yh (mm)	di (mm)	di/do	k_{sd}	A_{cu} (mm²)	L_{dm} (mH)	L_{qm} (mH)
ALC (10)	6.29	21.3	131.7	0.65	1.11	15.6	162.9	*10*
AMC (15)	6.12	21.26	134.7	0.66	1.1	14.4	168.6	*15*
AMC (20)	5.95	20.6	138.4	0.68	1.09	13.3	173.7	*20*
FE	6.2	15.6	140.0	0.69	-	20.0	118.2	14.4

Table 4.4. Results of the maximum T/kVA design (bw/bp = 0.33)

bw/bp = 0.5	tw (mm)	yh (mm)	di (mm)	di/do	k_{sd}	A_{cu} (mm²)	L_{dm} (mH)	L_{qm} (mH)
AMC (10)	5.89	20.7	136.5	0.67	1.16	14.4	161.3	*10*
AMC (15)	5.83	20.46	139.1	0.68	1.14	13.4	167.5	*15*
AMC (20)	5.75	19.84	141.9	0.7	1.13	12.6	172.2	*20*
FE	6.2	15.6	140.0	0.69	-	20.0	118.2	14.4

Table 4.5. Results of the maximum T/kVA design (bw/bp = 0.5)

4.3.4 Summary

Sections 4.3.1 - 4.3.3 shows and explains from a stator design point of view what the different optimised RSMs will look like. It is clear that the simple AMC calculation method can be used with confidence to predict the optimum stator dimensions. Little has been said about the rotor design in these sections, but more will be clear from section 4.4. The finite element calculation results of Tables 4.1 - 4.5 are given just for comparative purposes and are discussed in detail in section 4.4.

4.4 Results of optimised RSM structures

In this section the detailed results are given and discussed of the different optimum RSMs designed with the finite element method. The machines are optimised by maximising the different performance parameters (function values) as given in section 4.2. In section 4.1 altogether eight variables to be optimised to maximise the function values are given. In addition to these variables the current angle, ϕ, is also selected as a ninth variable to be optimised.

In Table 4.6 the optimum dimensions as well as the performance results of six RSMs are given. For the maximisation of the torque of the RSM, two machines are optimised. The first machine, machine 1, is optimised with the current density set equal to a given full-load value. The second machine, machine 2, is optimised with the copper losses equal to a full-load value. Machine 3 is optimised by maximising the efficiency of the RSM, also with the copper losses kept constant. Machine 4 is optimised in terms of the T/kVA of the RSM. Machine 5 is also optimised in terms of the T/kVA but with a constraint on the output torque. Machine 6 is different from machines 1 to 5 as it has 48 stator slots and an eight barrier/pole rotor with equal barrier widths. Only five variables of the latter machine are optimised namely *tw*, *yh*, *di*, *bw* and the current angle, ϕ. Machine 6, like machine 2, is optimised by maximising the torque per copper losses of the machine. The optimum stator and rotor structures of the machines are shown in Figures 4.2 to 4.4.

The above six machines are optimised using the finite element method directly in the optimisation process. The Powell optimisation algorithm is used throughout the design optimisation of the machines and the results are confirmed by using the quasi-Newton method. In the following paragraphs these machines are discussed briefly.

Machine 1: From Table 4.6 it can be seen that machine 1, compared to the other machines, has a very low inductance ratio, σ, a low power factor and a low inductance difference, $\Delta L = L_d - L_q$. This can be explained by the fact that σ and ΔL are not constants but vary with current, and thus A_{cu}, due to saturation and cross magnetisation. The high current of machine 1 due to the large A_{cu} saturates the machine deeply as is shown in Table 4.1. This lowers specifically the d-axis inductance of the machine, explaining the low σ and low ΔL values.

Note that the inner flux barrier width, *iw*, is much larger than the outer flux barrier width, *ow*, a tendency which is common for all the machines. This can perhaps be explained by the fact that the q-axis flux concentration is at its highest close to the d-axis pole position of the rotor, and the large *inner* flux barriers are just 'trying' to reduce this flux. Table 4.6 furthermore shows that the positions of the inner and outer flux barriers are basically the same for all the machines.

Machine 2: The airgap diameter of machine 2 is, as expected from eqn (4.8) and Table 4.3, larger than that of machine 1, but still on the small side ($d_i/d_o = 0.52$) compared to induction machines (typically for induction machines $d_i/d_o = 0.6$). This machine has a much higher σ, ΔL and power factor than machine 1 due to the smaller A_{cu}, less current and therefore less saturation. The optimised structure of machine 2 is shown in Fig. 4.2.

	Machine 1	Machine 2	Machine 3	Machine 4	Machine 5	Machine 6
Criterion	T	T	η	T/kVA	T/kVA	T
Constraint	J=6 A/mm²	P_{cu}=700 W	P_{cu}=700 W	J=6 A/mm²	T≥35 Nm	P_{cu}=700 W
Figure	-	Fig. 4.2	-	Fig. 4.3	-	Fig. 4.4
N_{sl}	36	36	36	36	36	48
N_{bp}	4	4	4	4	4	8
W	132	132	132	132	132	128
Chording	7/9	7/9	7/9	7/9	7/9	10/12
Variables ↓	Optimum values of variables					
yh (mm)	14.96	18.6	18.78	15.57	19.1	18.39
yh/di	0.155	0.177	0.174	0.111	0.165	0.168
tw (mm)	4.39	5.49	5.31	6.2	6.92	4.22
tw/tp	0.523	0.6	0.563	0.5	0.68	0.59
di (mm)	96.2	105.1	108.1	140.0	115.8	109.7
di/do	0.473	0.517	0.532	0.689	0.57	0.54
bw/bp	-	-	-	-	-	0.318
iw (mm)	6.69	5.76	6.52	10.39	6.92	-
ow (mm)	2.73	2.87	3.48	3.53	2.88	-
ip (°)	7.46	7.79	7.89	7.87	7.88	-
op (°)	18.95	19.25	19.31	18.53	19.02	-
cp (°)	30.93	32.52	32.26	25.06	28.48	-
cd (mm)	3.13	2.89	2.77	13.2	6.32	-
♦ (°)	65.4	63.7	66.3	70.4	61.0	66.3
Parameters ↓	Performance results at 1500 r/min					
T (Nm)	57.4	58.1	57.3	22.9	35.0	58.64
η (%)	88.6	89.6	89.7	88.2	89.6	89.6
P_{out} (kW)	9.02	9.13	8.99	3.6	5.5	9.21
P_{cu} (W)	818	721	720	314	376	721
P_{iron} (W)	296	291	260	119	214	293
P_{factor}	0.606	0.682	0.709	0.81	0.745	0.701
kVA	16.8	14.94	14.14	5.03	8.24	14.66
I_s (A) (rms)	28.7	22	21.8	10.8	13	22.2
J (A/mm²)	6.07	6.95	7.02	6.13	6.13	7.03
L_d-L_q (mH)	30.6	50.0	54.2	103.8	81.8	53.9
σ=L_d/L_q	3.61	4.63	5.1	8.13	6.42	4.95

Table 4.6. Dimensions and performances of different optimised RSMs

Machine 3: It is explained in section 4.3.2 why machine 3 will be similar to machine 2. As can be seen from Table 4.6 the stator and rotor dimensions and the performance of this machine are close to those of machine 2.

Machines 1 to 3 of Table 4.6 show remarkably high power densities with about the same copper and iron losses as those of the standard induction machine. This explains the high efficiencies of these machines. The advantage of the high power density of the RSM is discussed in further detail in Chapter 5. The torque per rotor volume (TRV) is also exceptionally high. Machine 2, for example, has a TRV of almost 50 kNm/m^3, which is higher than the range for high-performance industrial servos (20-45 kNm/m^3).

Machine 4: Machine 4 shows all the expected results of section 4.3.3, namely a high σ, a high ΔL and a high power factor. The machine is out of saturation due to the small A_{cu} and the low current which also explains the low iron losses of the machine. There is no requirement for high power density, therefore the output power is low compared to machines 1 to 3. The inner diameter is relatively large (d_i/d_o = 0.69) as are the inner barrier width and cutout depth dimensions. Note that the current angle is also larger than the current angles of machines 1 to 3 as explained by eqn (4.12). The optimised structure of machine 4 is shown in Fig. 4.3.

Machine 5: While machine 4 of Table 4.1 has a low output power, machine 5 is optimised with a constraint on the output torque, namely to be same as that of the standard 5.5 kW induction machine. It can be seen that the efficiency of this machine is higher than that of a standard 5.5 kW induction machine, but the power factor is lower - the product of efficiency and power factor is more or less the same. The latter implies that the same inverter rating will be required. The stator inner diameter of this machine is much less than that of machine 4 just to obtain more copper area and higher current to raise the output torque above the constraint value. This machine is optimised with different weighting factors (eqns 3.13 and 3.14) using both the Powell and the quasi-Newton methods. The results of these optimisations are found to be very much the same.

Machine 6: Finally machine 6, which is different in stator and rotor structure (see Fig. 4.4), is optimised according to the same criteria as machine 2. From Table 4.6 it can be seen that the performance results of machines 2 and 6 are very similar. Machine 6 has a slightly higher power factor and σ due to the higher number of barriers used. Also the optimum stator parameters of machine 6 are almost the same as those of machine 2. The fact that the performance results of machines 2 and 6 are very much the same may indicate that the number of stator slots and the type of flux barrier rotors used do not have a *significant* effect on the performance of the machine. The latter, however, must be investigated further. The number of elements in this case are 2356, the vector potential unknowns 1378 and the finite element program solution time 6 to 7 minutes. The number of elements per pole for this machine is higher due to the higher number of flux barriers used.

Two general remarks must be made about the six machines of Table 4.6:

- The efficiencies of all the machines are relatively high for the power level considered. This is an advantage of the RSM which is discussed further in Chapter 5.

- The optimum current angles are all between 60 and 70°. This confirms again the high current angles where optimum performance of the machine is obtained.

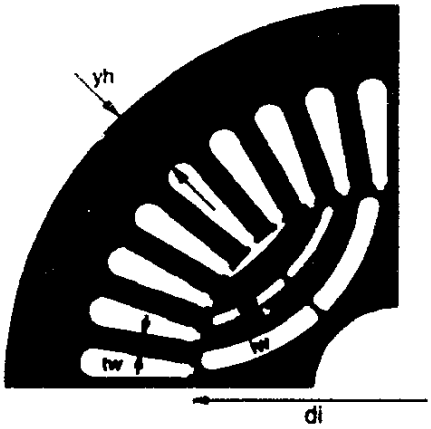

Fig. 4.2. Stator and rotor structure of the RSM designed for maximum torque (machine 2, Table 4.6).

Fig. 4.3. Stator and rotor structure of the RSM designed for maximum torque/kVA (machine 4, Table 4.6)

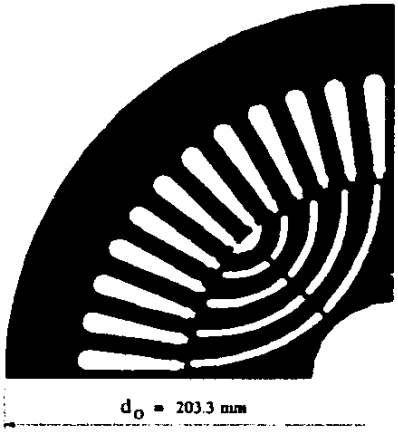

Fig. 4.4. Stator (48 slots) and rotor structure of the RSM designed for maximum torque (machine 6, Table 4.6)

4.5 Additional optimisation results

The 48-slot stator and 8-barrier/pole rotor of the RSM of Fig. 4.4 are also optimised in terms of maximum torque and maximum torque/kVA for a given current density. This is done to determine if this machine, with its different stator and rotor structure, shows the same tendency of change in dimensions as machines 1 and 4 in Table 4.6.

This machine is optimised using both the AMC and FE calculation methods to compare the optimisation results with each other. The optimised results are given in Table 4.7. Machine 7 is designed for maximum torque and machine 8 for maximum T/kVA. With the use of the AMC method in the optimisation process, the bw/bp ratio and the current angle ϕ are not optimised but are constants (shown in brackets in Table 4.7).

The change in the optimum stator dimensions and current angle between machines 7 and 8 for the FE optimisation is similar to that between machines 1 and 4 of Table 4.6. The AMC optimisation results also show this tendency to some extent - see particularly the change of the stator inner diameter. The AMC results compare well with the FE results in the case of machine 7, but less well in the case of machine 8. The latter is also found and explained in section 4.3.3.

To get more accurate results for machine 8 the Hybrid Magnetic circuit / Finite element method (HMF method), explained in section 2.7, is used. A total of 9 finite element field solutions were used to obtain more accurate values for the bw/bp ratio and the current angle ϕ of the machine. As can be seen slightly better results are obtained with this method.

	Machine 7		Machine 8		
Criterion →	T		T/kVA		
Constraint →	*J=6 A/mm²*		*J=6 A/mm²*		
Variables ↓	Optimum values of variables				
	FE method	AMC method	FE method	AMC method	HMF method
yh (mm)	14.65	14.63	16.9	20.8	19.6
yh/di	0.141	0.152	0.12	0.149	0.14
tw (mm)	3.32	3.49	3.92	4.33	4.3
tw/tp	0.49	0.55	0.428	0.475	0.47
di (mm)	103.6	96.1	139.9	139.2	139.8
di/do	0.51	0.473	0.69	0.685	0.69
bw (mm)	3.3	2.47	5.22	5.44	5.13
bw/bp	0.408	*(0.33)*	0.477	*(0.5)*	0.47
ϕ (°)	65.7	*(65)*	72.1	*(65)*	69.6

Table 4.7. FE, AMC and HMF optimisation results of the RSM structure of Fig. 4.4

4.6 Measured results

Machine 2 of Table 4.6 has been build in a standard 5.5 kW induction machine frame with the rotor skewed by one stator slot pitch. Photos of the stator and rotor of this machine are shown in Appendix E.

For the test of machine 2 the drive system of Fig. 4.5 is used. The machine is controlled by a transputer system with current and position feedback and an analog current regulator together with an IGBT inverter. Naturally sampled PWM (5 kHz) was used for the analog current regulator, with the steady-state error between the reference and actual signal made zero in the transputer control system (Wiley, 1995). Fibre-optic coupling was used between the current regulator and the inverter. Tests were conducted on the machine to compare the finite element calculations with measurements.

In the finite element calculations the d-axis current, I_d, is kept constant while the q-axis current, I_q, is varied to vary the torque, the power factor and the efficiency of the machine. The variation of the terminal stator current components, I_{d1} and I_{q1}, with variation in Iq is also determined from these calculations. I_{d1} and I_{q1} are *dq*-axis currents that include core loss current components as shown in Fig. 2.3. The calculated results are shown in Figures 4.6 - 4.8 where the torque, efficiency and power factor are plotted versus the q-axis current I_{q1}. In Fig. 4.6 the calculated variation of I_{d1} with I_{q1} is also shown. Note again that I_d is kept constant in the analysis and that the slight variation in I_{d1} is due to the core loss current component (Fig. 2.3).

The terminal d-axis current, I_{d1}, of Fig. 4.6 is used in the control system of Fig. 4.5 as the desired terminal d-axis current for the RSM drive. At a speed of 1000 r/min, the machine is loaded, in other words I_{q1} is varied, and the shaft torque, efficiency and power factor versus I_{q1} are determined as

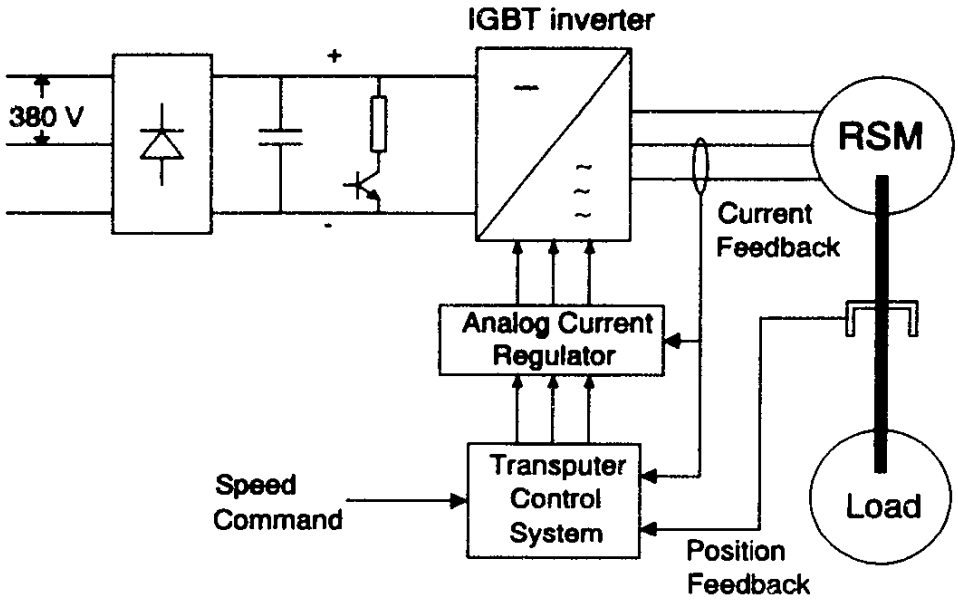

Fig. 4.5. The RSM drive system

shown in Figures 4.6 - 4.8. The power factor is measured as the fundamental average input power divided by the fundamental kVA supply. The efficiency is measured as the shaft power divided by the fundamental average input power.

In Figures 4.6 and 4.7 the close agreement between the calculated and measured shaft torque and efficiency confirms the remarkably high torque and high efficiency of machine 2 of Table 4.6. There is also a relatively close agreement between the calculated and measured fundamental power factor as shown in Fig. 4.8.

Finally, a very good correlation is obtained between the calculated and measured shaft torque versus current angle, ϕ_1, (Fig. 2.3) with 1.0 p.u. current flowing in the machine, as shown in Fig. 4.9. Both calculations and measurements show an optimum current angle of, say, 64°.

4.7 Conclusions

It is clear from the results in this chapter that it is advantageous to use the AMC method in the design optimisation of the RSM. The HMF method is also advantageous to use as the method requires only a few finite element field solutions. Although the AMC method is an approximate method, it proves to some extent that the finite element results are correct. Both the AMC and HMF methods, with low computational burdens, can be used to do first-order design optimisations of the RSM.

The finite element design optimisation results point out that the RSM has outstanding characteristics of high power density and high torque per rotor volume when designed for maximum torque or maximum efficiency. It is therefore advantageous to design the RSM (for given copper losses) for maximum torque or maximum efficiency.

When designing the RSM for maximum torque or maximum efficiency per given copper losses, typical normalised values of some of the important dimensions of the RSM can be used as initial values for the optimisation process. These are the following for 4-pole machines:

di/do = 0.55;	*tw/tp = 0.55;*
yh/di = 0.17;	*bw/bp = 0.33;*
ϕ = 65° (maximum T);	*ϕ = 70° (maximum η);*

It has been found from all the design optimisation results that the power factors of the optimum RSMs are on the low side. This affects negatively the kVA rating and the efficiency of the inverter. The low power factor characteristic of the RSM is explained in Chapter 5.

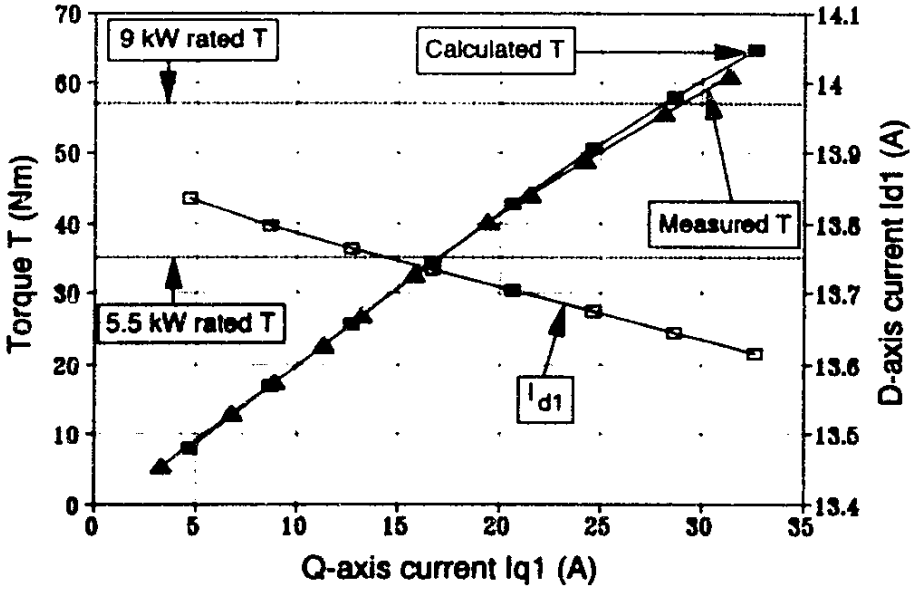

Fig. 4.6. Calculated and measured torque of machine 2

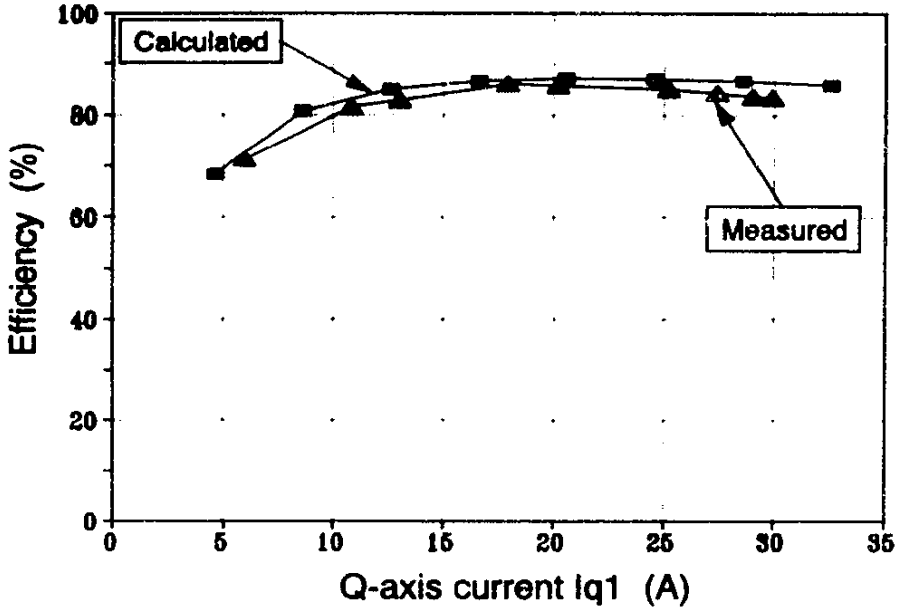

Fig. 4.7. Calculated and measured efficiency at 1000 r/min of machine 2

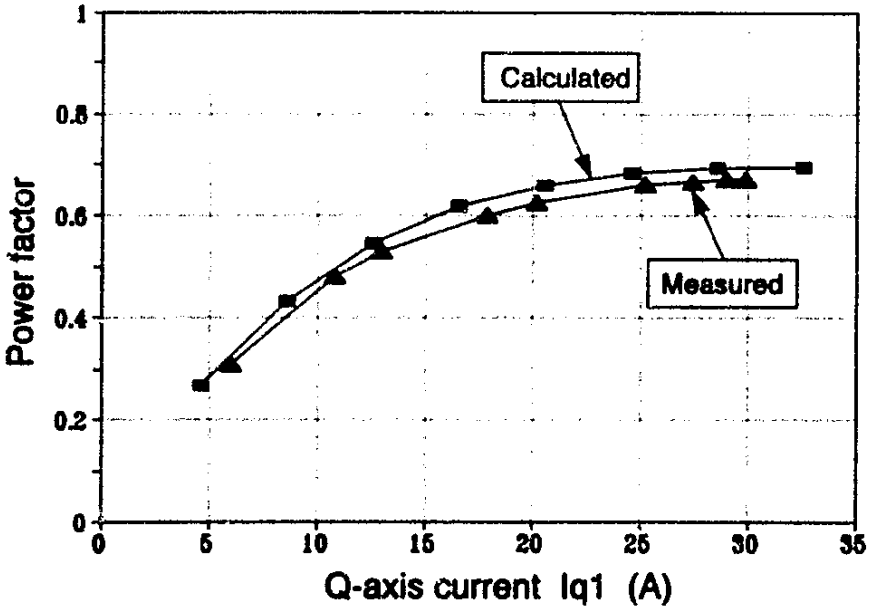

Fig. 4.8. Calculated and measured power factor of machine 2

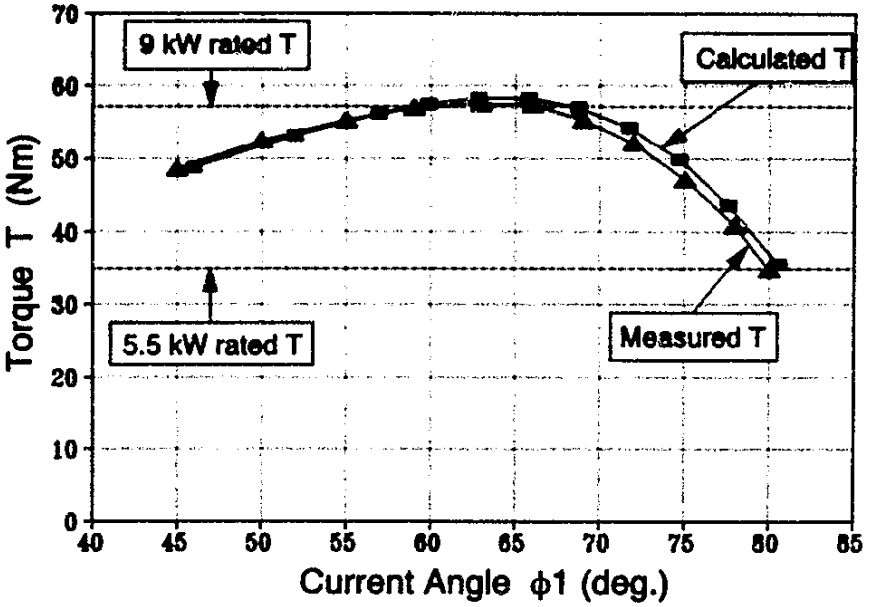

Fig. 4.9. Calculated and measured torque of machine 2 with 1.0 per unit current (I_{s1} = 22.2 A rms)

5 Considerations concerning Goodness Factors

It was shown in Chapter 4 that the RSM has the outstanding performance characteristics of high power density and high efficiency. The power factor, on the other hand, was found to be on the low side compared to the equivalent induction machine. These results were found in the 3 - 10 kW power range.

The question, therefore, to be answered is why the RSM has such a high power density and low power factor compared to the induction machine. Another question is what the performance capability is of the RSM at higher power levels. This chapter considers these questions by deriving goodness factors for the RSM and the induction machine and explaining the fundamental difference between these machines.

With the high power density and high efficiency found for the current-controlled RSM, some electrical machine analysts may classify the RSM as a good machine. On the other hand, some may still reckon that the RSM is in general a bad machine due to its low power factor. It depends on if only the machine or the machine and its supply (the inverter in this case) are under consideration. An example of where only the machine is considered is the well-known publication of Laithwaite (1965) on the goodness of the electrical machine. This chapter focuses on different goodness factors (concerning the machine and its supply) for the RSM and the induction machine. The goodness factors for the RSM give a better understanding of the results of Chapter 4.

5.1 The efficiency goodness factor

If only the electrical machine is considered (without its supply) then a goodness factor for the machine may simply be its efficiency or else the ratio of the output power to the losses of the machine. The latter ratio is used for the efficiency goodness factor, namely

$$G_{eff} = \frac{P_{out}}{P_{loss}} . \tag{5.1}$$

If all the losses except the copper losses of the machine are ignored (this is a reasonable assumption for the small electrical machine) then the goodness factor of eqn (5.1) can be approximated as

$$G_{eff} = \frac{P_{out}}{P_{cu}} . \tag{5.2}$$

5.1.1 Efficiency goodness factor for the RSM

By using the torque equation of the RSM (eqn 2.7), the efficiency goodness factor of eqn (5.2) for the reluctance machine becomes

$$G_{eff(RSM)} = \frac{\frac{3}{4}\omega_r (L_{dm} - L_{qm})\, \hat{I}_s^2 \sin(2\phi)}{\frac{3}{2}\hat{I}_s^2 R_s} = \frac{1}{2}\sin(2\phi)\left(\frac{X_{dm} - X_{qm}}{R_s}\right). \tag{5.3}$$

The goodness factor of eqn (5.3) is still a dimensionless quantity. Eqn (5.3) can be expressed further by taking the current angle, ϕ, as a constant (say $\phi = 65°$) and by writing the reactances in terms of reluctances and the resistance in terms of a slot resistance, namely

$$G_{eff(RSM)} = K\,\omega_r \left(\frac{\frac{k_L W^2}{\Re_d} - \frac{k_L W^2}{\Re_q}}{k_r W^2 r_s}\right) = K'\,\omega_r \left(\frac{1}{\Re_d r_s} - \frac{1}{\Re_q r_s}\right) \tag{5.4}$$

where k_L is an inductance machine constant (from eqns 2.25 and 2.26),
$\Re_d$ and $\Re_q$ are the d- and q-axis magnetic reluctances respectively (from eqns 2.25 and 2.26),
k_r is a resistance machine constant (eqn A.4)
and r_s is the resistance of all the conductors per slot in parallel (eqn A.4).

The goodness factor of eqn (5.4) thus defined is a function of the inverse of the product of resistance and reluctance. This inverse product is precisely the definition that Laithwaite (1965) gives for the goodness of an electrical machine. Laithwaite, as in eqn (5.4), ignores the iron and mechanical losses in his derivation of a goodness factor for the electrical machine. Laithwaite did not indicate directly that defining the goodness of an electrical machine in this way is in fact the same as considering the efficiency of the machine because

$$\eta = \frac{1}{1 + 1/G_{eff}}. \tag{5.5}$$

From the goodness factor of eqns (5.3) and (5.4), it is clear that the penalty of the reluctance machine is the existence of the q-axis magnetic circuit. The stator resistance is also detrimental to the goodness of the machine. The goodness of the reluctance machine is thus dependent on two magnetic circuits and one electrical circuit. One can visualise or understand the operation of the reluctance machine as a coupling between two magnetic circuits and one electrical circuit, as shown in Fig. 5.1. Note that there is also coupling between the two magnetic circuits due to cross magnetisation or cross coupling. This is not shown in Fig. 5.1.

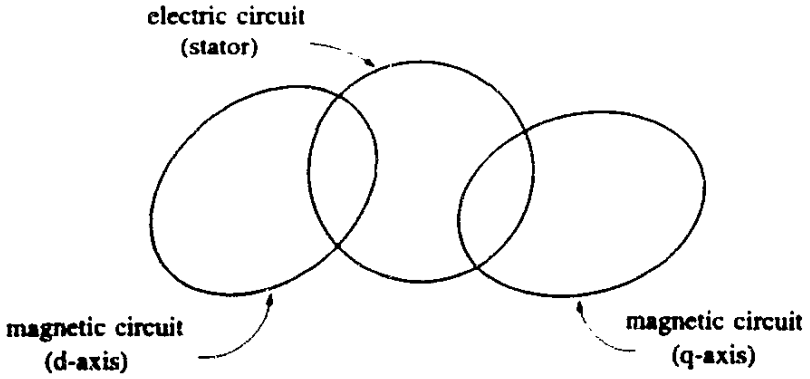

Fig. 5.1. Linking of magnetic and electric circuits of the reluctance machine

5.1.2 *Efficiency goodness factor for the induction machine*

In deriving an approximate goodness factor for the induction machine, the per phase equivalent circuit of Fig. 5.2 for the induction machine is used. Here, the core losses as well as the rotor leakage inductance are ignored. The torque of the induction machine can be written from the space phasor diagram of Fig. 5.2(b) in the reference frame fixed to the magnetising flux-linkage space phasor as (Vas, 1990, p. 50)

$$\begin{aligned} T_{IM} &= \tfrac{3}{2}\, p\, \hat{\lambda}_m\, I_r \\ &= \tfrac{3}{2}\, p\, L_m\, I_m\, I_r \\ &= \tfrac{3}{4}\, p\, L_m\, \hat{I}_s^2 \sin(2\phi) \end{aligned} \tag{5.6}$$

where $\hat{\lambda}_m$ is the amplitude of the magnetising flux linkage space phasor,
L_m is the three-phase magnetising inductance,

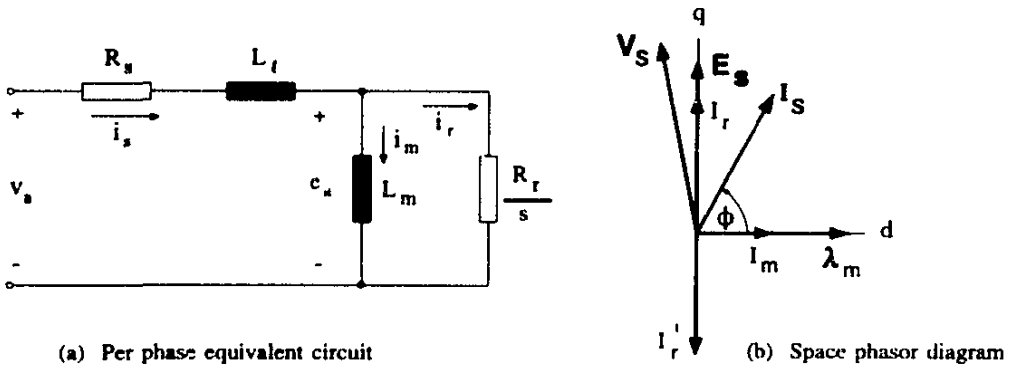

(a) Per phase equivalent circuit (b) Space phasor diagram

Fig. 5.2. Approximate per phase equivalent circuit and space phasor diagram of the induction machine

I_m is the steady-state main flux producing stator current component

and I_r is the steady-state torque producing stator current component.

If the iron and mechanical losses are ignored again, the efficiency goodness factor for the induction machine can be derived similarly to eqns (5.2) and (5.3) as

$$G_{eff(IM)} = \frac{P_{out}}{P_{cu}} = \frac{\omega_r (1 - s) \frac{3}{4} L_m \hat{I}_s^2 \sin(2\phi)}{\frac{3}{2} \hat{I}_s^2 R_s + \frac{3}{2} k_i \hat{I}_s^2 R_r} = \frac{1}{2} \sin(2\phi) \left(\frac{X_m}{R_s + k_i R_r} \right) (1 - s) \tag{5.7}$$

where $k_i = (I_r / \hat{I}_s)^2$.

s is the slip

and R_r is the rotor resistance referred to the stator winding.

The factor k_i depends on the ratio R_r/X_m and is ≈ 0.8 for small induction machines and ≈ 0.9 for large induction machines. Equation (5.7) gives one expression for the efficiency goodness of the induction machine. Laithwaite (1965) uses two separate goodness factors for the induction machine, the one relating to the primary circuit and the other one to the secondary circuit.

The similarity between eqns (5.3) and (5.7) is clear. The difference is that the penalty of the induction machine is an electric circuit, namely that of the rotor, while that of the reluctance machine is a magnetic circuit, namely the q-axis magnetic circuit. The operation of the induction machine can be defined from eqn (5.7) as a coupling between two electrical circuits and one magnetic circuit, as shown in Fig. 5.3.

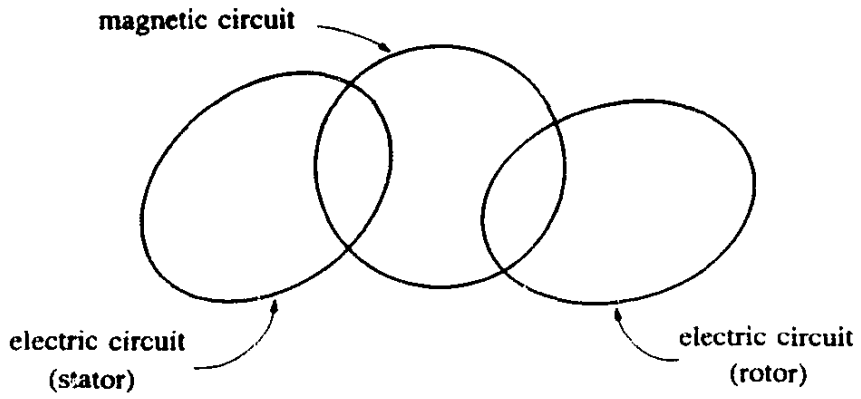

Fig. 5.3. Linking of magnetic and electric circuits of the induction machine

5.1.3 Comparison of the efficiency goodness of the RSM and the induction machine

It follows from the above that the fundamental difference between the reluctance and induction machines is that the reluctance machine makes use of a q-axis magnetic circuit on the rotor to generate torque while the induction machine makes use of a q-axis electrical circuit on the rotor. The use of an electric circuit, however, goes hand-in-hand with copper losses which become higher as the machine becomes smaller, i.e small in diameter. In this respect the goodness factor of the induction machine will significantly drop when the machine becomes small.

The reluctance machine, on the other hand, will not experience *this* penalty when the machine becomes small. The penalty of the reluctance machine, namely the q-axis reactance (eqn 5.3) or q-axis inductance (eqn 2.26), is fairly independent of the variation of the rotor diameter and thus the outer diameter of the machine. The latter is so because the g_q'/d_i ratio of eqn (2.26) is fairly independent with rotor diameter for a constant bw/bp ratio (see section 2.6(ii)). The penalty of the q-axis inductance of the RSM will therefore be similar for small and large reluctance machines.

Both reluctance and induction machines suffer from the copper losses of the stator electric circuit, which also become relatively higher as the machine becomes smaller in diameter. The latter means that the goodness factor of the reluctance machine will also drop as the machine becomes small but not as much as that of the induction machine. The induction machine suffers from the copper losses of two electrical circuits but the reluctance machine from only one.

The goodness factors of eqns (5.3) and (5.7) thus describe qualitatively the characteristics of the reluctance and induction machines. It must, however, be emphasised that iron losses are not considered in these goodness factor formulae.

5.2 The power density goodness factor

The goodness factor G_{eff} of section 5.1 cannot be used alone to define the goodness of the electrical machine from a machine point of view. When two machines have the same G_{eff} but the one machine is twice as large as the other, then surely there must be a difference in the goodness of these machines from a user point of view. The power to volume ratio or power density as a goodness factor,

$$G_{pd} = P_{out} / \text{vol} ,$$

must therefore also play a role in defining the goodness of the electrical machine.

5.2.1 Power density goodness factor for the RSM

A formula for the power density goodness factor can be obtained by dividing the torque times the speed of the RSM by the stack volume, i.e.

$$G_{pd(RSM)} = \frac{\frac{3}{4}\,\omega_r\,(L_{dm} - L_{qm})\,\hat{I}_s^2\,\sin(2\phi)}{\frac{\pi}{4}\,d_o^2\,l} .$$

Furthermore, using eqns (2.9), (2.28) and (2.30) leads to

$$\begin{aligned} G_{pd(RSM)} &= \frac{k_1\,(1/g_d' - 1/g_q')\,d_i\,l\,A_{cu}^2\,J^2\,\sin(2\phi)}{d_o^2\,l} \\ &= k_1\left(\frac{1}{g_{d(nor)}'} - \frac{1}{g_{q(nor)}'}\right)\left(\frac{A_{cu}\,J}{d_o}\right)^2\sin(2\phi) \end{aligned} \qquad (5.8)$$

where $g_{d(nor)}' = g_d'/d_i$ and $g_{q(nor)}' = g_q'/d_i$ are the normalised values of the d- and q-axis effective airgap lengths.

Note that the power density goodness factor of eqn (5.8) is independent of the length of the machine. The normalised values of the effective airgap lengths will not vary much with frame size (outer diameter) for the same design optimisation. The reason for this is that the normalised airgap length $g_{d(nor)} = g_d/d_i$, the normalised barrier width $bw_{(nor)} = bw/bp$ (affecting g_q) and the saturation factors k_{sd} and k_{sq} of eqn (2.27) will not vary much with diameter.

The power density goodness factor G_{pd} of eqn (5.8), therefore, can be *roughly approximated* by

$$G_{pd(RSM)} = k_2\left(\frac{A_{cu}\,J}{d_o}\right)^2\sin(2\phi) . \qquad (5.9)$$

Hence, with a constant current density and constant current angle, the power density of the RSM will greatly improve as the stator outer diameter d_o becomes larger, because the slot copper area A_{cu} varies more or less with the square of the outer diameter.

However, the current density generally decreases with increasing d_o (or frame size) to keep the copper losses of the larger machine within limits. Typically for small machines J = 6 A/mm² and for medium sized machines J = 4 A/mm². Also, the current angle ϕ increases slightly with frame size to have lower magnetising currents and less saturated machines to limit the iron core losses. Typically for the RSM ϕ may increase from 65 to 70°.

In spite of the lower current density and larger current angle of the larger machine, one would expect from eqn (5.9) that the power density of the RSM will improve with frame size. An example of the increase of the power density of the RSM with outer diameter will be given in Chapter 6.

Finally, the power density goodness factor of eqn (5.8) can also be expressed in terms of given copper

losses. By using eqn (2.10) instead of eqn (2.9) for the current $\hat{I}_s$, eqn (5.8) becomes

$$G_{pd(RSM)} = k_3 \left(\frac{1}{g_{d(nor)}} - \frac{1}{g_{q(nor)}} \right) \left(\frac{P_{cu} A_{cu}}{d_o^2 (l + l_e)} \right) \sin(2\phi) \quad . \tag{5.10}$$

Note that $P_{cu} \propto J^2 A_{cu}(l + l_e)$ so that G_{pd} is independent of the length of the machine.

5.2.2 *Power density goodness factor for the induction machine*

A power density goodness factor can also be obtained for the induction machine in the same way as in eqn (5.10). The copper losses of the induction machine are

$$P_{cu(IM)} = P_{cu(stator)} (1 + \alpha)$$

where

$$\alpha = \frac{P_{cu(rotor)}}{P_{cu(stator)}}$$

and

$$P_{cu(stator)} = \frac{3}{2} \hat{I}_s^2 R_s \propto J^2 A_{cu(stator)} (l + l_e) \quad .$$

Using these equations the power density goodness factor for the induction machine is

$$G_{pd(IM)} = k_3 \left(\frac{1}{g_{(nor)}} \right) \left(\frac{P_{cu}}{d_o^2 (l + l_e)} \right) \left(\frac{A_{cu(stator)} (1 - s)}{1 + \alpha} \right) \sin(2\phi) \quad . \tag{5.11}$$

This equation looks similar to eqn (5.10) for the RSM. It is clear that the power density goodness of the RSM is penalised by the factor $1/g'_{q(nor)}$ of eqn (5.10), due to the existence of the q-axis magnetic circuit. The penalty of the induction machine from eqn (5.11) is the factor $(1 - s)/(1 + \alpha)$, due to the rotor electric circuit.

5.2.3 *Comparison of the power density goodness of the RSM and the induction machine*

The power densities of the RSM and induction machine can be compared by assuming the same P_{cu}, d_o, $l + l_e$ and ϕ in eqns (5.10) and (5.11). If both machines also have the same current density, then the copper area of the RSM will be $(1 + \alpha)$ larger than the stator copper area of the induction machine. This implies from the last terms in brackets of eqns (5.10) and (5.11) that with $\alpha = 1$ the power density of the RSM, as a first approximation, will be more than 4 times that of the induction machine. However, the first term in brackets of eqn (5.10) of the RSM is greatly affected by saturation and cross magnetisation, as the machine is deep into saturation when designed for the same amount of copper losses as that of the induction machine. The first term in brackets of eqn (5.10) is typically 50% that of the first term in brackets of eqn (5.11). Hence, it is more realistic to expect

that the power density of the RSM will be a factor 2 higher than that of the induction machine. This explains the high power density of the RSM in comparison with the induction machine.

In the 10 kW power level it has been shown in section 4.4, Table 4.6 that $G_{pd(RSM)} = (1.7)\, G_{pd(IM)}$. This factor will become less as the machines become larger, because the penalty of the rotor copper losses of the induction machine becomes less with increasing diameter.

The above comparison between the RSM and induction machine was made on the basis of the same amount of copper losses. For the larger RSM the iron losses will become a problem because the machine is deep into saturation when designed for the same amount of copper losses.

5.3 The power factor goodness factor

In sections 5.1 and 5.2 it is shown that from an electrical machine point of view the RSM is a good machine in comparison with the induction machine. However, there is a disadvantage from a supply point of view. The reluctance machine makes use of magnetic circuits, represented as magnetising inductances in the equivalent circuit, to generate torque. This gives rise to a relatively large phase angle between the supply voltage and the current; larger than in the case of the induction machine where an electric circuit, represented as a resistance in the equivalent circuit, is used to generate torque.

The problem, thus, of the reluctance machine is the difficulty to get the current into the machine due to the relatively high inductive equivalent impedance. This requires more leading supply voltage resulting in a low power factor that in turn affects the inverter rating.

The power factor as a goodness factor, $G_{pf} = P_{in}/kVA$, thus defines the goodness of the electrical machine from a supply point of view. It must be used in some way or other together with the other goodness factors to define the overall goodness of the electrical machine.

A simple, approximate expression for the power factor goodness of the RSM can be obtained by ignoring the copper and iron losses of the machine. This implies that the efficiency is unity. The power factor goodness, therefore, is approximately

$$G_{pf(RSM)} = \frac{P_{out}}{kVA}\left(\frac{1}{\eta_{RSM}}\right) \approx \frac{P_{out}}{kVA}. \tag{5.12}$$

An approximate expression for P_{out}/kVA of the RSM can be obtained by multiplying the T/kVA of eqn (4.12) with the mechanical speed of the machine. The power factor goodness of eqn (5.12) then becomes

$$G_{pf(RSM)} = \left(1 \quad \frac{1}{\sigma}\right) \sin(\phi) \ . \tag{5.13}$$

A similar expression for the power factor goodness of the induction machine can be obtained by ignoring the stator copper losses and iron losses of the machine. The rotor copper losses are not ignored so that the efficiency is (1 - s). By assuming that

$$\hat{V}_s = \hat{E}_s = \omega_r L_m \hat{I}_m = \omega_r L_m \hat{I}_s \cos(\phi)$$

from Fig. 5.2(b), the P_{out}/kVA of the induction machine can be approximated as

$$P_{out}/kVA_{(IM)} = \frac{\frac{3}{4}\omega_r (1 - s) L_m \hat{I}_s^2 \sin(2\phi)}{\frac{3}{2}\left(\omega_r L_m \hat{I}_s \cos(\phi)\right) \hat{I}_s} \tag{5.14}$$

$$= \sin(\phi)\ (1 - s) \ .$$

With the efficiency of the machine equal to (1 -s), it follows from eqn (5.14) that

$$G_{pf(IM)} = \sin(\phi) \ . \tag{5.15}$$

This is correct, because the power factor angle in this case is the angle between the phasors $\mathbf{E}_s$ and $\mathbf{I}_s$ of Fig. 5.2(b).

Equations (5.13) and (5.15) clearly draw attention to the low power factor goodness of the RSM in comparison with the induction machine. With $\sigma \approx 5$ and assuming the same current angles for both machines, the $G_{pf(RSM)} \approx (0.8)G_{pf(IM)}$. This implies that with a power factor of 0.85 for the induction machine, the power factor of the RSM will be ≈ 0.68.

5.4 The overall goodness factor

In the preceding sections three goodness factors are mentioned which define the goodness of the electrical machine in some respects. The goodness factors that define the goodness of the electrical machine from a machine point of view are the efficiency goodness factor, G_{eff}, and the power density goodness factor, G_{pd}. From a supply point of view the power factor goodness factor, G_{pf}, defines in one respect the goodness of the electrical machine. The overall goodness of the machine can hence be defined simply as the product of these three goodness factors, i.e.

$$G = G_{pf}\, G_{eff}\, G_{pd}$$

$$= \left(\frac{P_{in}}{kVA}\right)\left(\frac{P_{out}}{P_{loss}}\right)\left(\frac{P_{out}}{Vol}\right) \ . \tag{5.16}$$

Note that P_{loss} of eqn (5.16) includes all the losses of the machine and not just the copper losses as

in eqn (5.2). The latter is important because in medium and large machines the iron losses are relatively large due to the rapid increase in iron mass as the machine becomes bigger.

The goodness factor G_{eff} of equation (5.16) can be replaced by the *efficiency* of the machine (see eqn 5.5) so that the overall goodness factor defined differently then becomes

$$\begin{aligned} G' &= \left(\frac{P_{in}}{kVA}\right)\left(\frac{P_{out}}{P_{in}}\right)\left(\frac{P_{out}}{vol}\right) \\ &= \left(\frac{P_{out}}{kVA}\right)\left(\frac{P_{out}}{vol}\right) \\ &= G_{pva}\, G_{pd} \end{aligned} \tag{5.17}$$

This goodness factor makes a great deal of sense because for a certain amount of output power it 'asks' how big the machine is in terms of m^3 and how big the inverter is in terms of kVA. It is shown in section 5.3 that P_{out}/kVA of the RSM is lower than that of the induction machine, but in section 5.2 that P_{out}/vol is higher. The RSM is thus in comparison with the induction machine a good machine from a machine point of view, but not as good from an inverter point of view.

5.5 Summary

The expressions for the goodness factors of the RSM are used to give a better understanding of the operation, the advantages and the penalties of the machine. They are used to explain the difference between the RSM and the induction machine and to explain the goodness of the RSM at the higher power levels.

The advantage of a high power density and disadvantage of a low power factor of the RSM can be directly attributed to the use of a passive rotor with magnetic asymmetry. A passive rotor implies a rotor without losses, consequently the stator power can be raised, resulting in a considerable increase in the power density. A passive rotor also implies that use is made of magnetic circuits, represented as magnetising inductances in the equivalent circuit, to generate torque. This makes the inductive equivalent impedance seen by the supply relatively high, causing the power factor of the RSM to be low.

The induction machine makes use of an active rotor where the rotor MMF always opposes the q-axis stator MMF. The use of an active rotor, however, is accompanied by losses which limit the power ratings of the stator and rotor electric circuits and thus the power density of the machine.

6 Optimum RSMs in the Medium Power Range

In this chapter the different goodness factors of Chapter 5 are calculated for optimum-designed RSMs in the medium power range. Large RSMs are not considered as the focus is on the possibility of using the RSM for traction applications. The aim is to investigate the extent to which the goodness or performance of the optimum RSM improves or attenuates as the machine becomes bigger. In Chapter 5 it has been shown by means of analytical expressions that the efficiency and power density goodness factors improve with frame size. This chapter will show, amongst other things, what this improvement with frame size actually is for optimum RSMs. The aim is further to compare the goodness of the RSM with that of the standard induction machine.

6.1 Design optimisation

As in Chapter 4, standard induction machine frame sizes are used for all the RSMs to compare the goodness factors with those of the induction machine. Altogether six machines are optimised in induction machine frames from 5.5 to 250 kW, using the finite element method directly in the optimisation process as described in Chapter 3. The induction machines are all different with a different number of stator and rotor slots and single- or double-layer stator windings. For the RSMs, however, the same type of stator and rotor structures are used. The stators all have 48 slots with 4-pole, double-layer windings. The rotors have eight flux barriers per pole with the flux barriers uniformly distributed. The barrier widths are all equal to make the design optimisation faster. The structure of the RSM is the same as machine 6 of Table 4.6 and is shown in Fig. 4.4 and Fig. 6.1. The airgap lengths of the RSMs are taken to be the same as those for the standard induction machines.

The reluctance machines are optimised by maximising the *efficiency* and the *power density* of the machines *for the same amount of copper losses* as those of the corresponding frame size, standard induction machines. In other words the goodness factors G_{eff} and G_{pd} of Chapter 5 for given copper losses are maximised in the optimisation.

No constraints were put on the core losses of the machines in the design optimisation. Afterwards, wherever the sum of the copper and iron losses ($P_{cu} + P_c$) exceeds a constraint, the current I_s (actually J) and the current angle ϕ are optimised to maximise the power density or efficiency of the machine subject to the ($P_{cu} + P_c$) constraint. The Powell algorithm together with the quadratic penalty function method (section 3.4) are used for this constrained optimisation.

The five variables of the machines that are optimised in the design optimisation are the tooth width (*tw*), yoke height (*yh*), stator inner diameter (*di*), barrier width (*bw*) and current angle (ϕ).

Typical optimised stator and rotor structures of the RSM designed for maximum power density per given copper losses are shown in Fig 6.1.

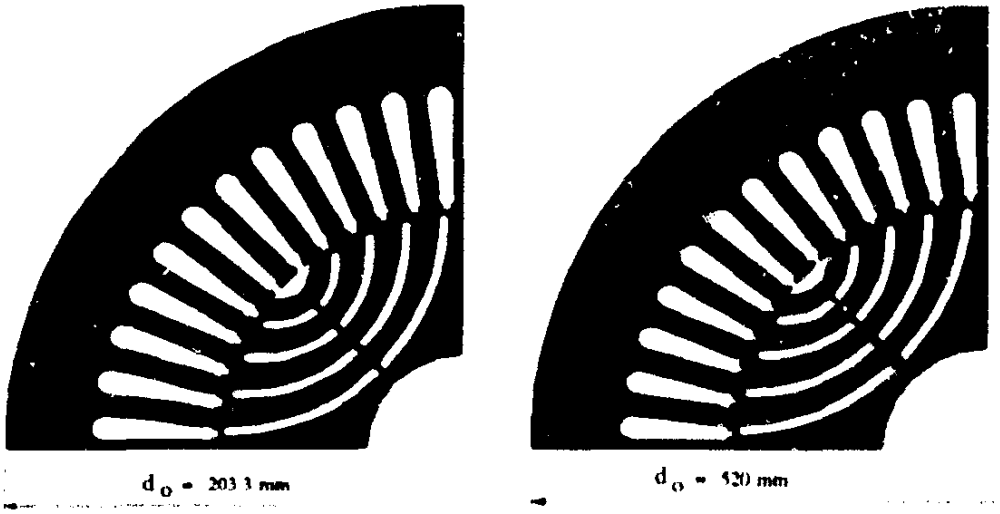

(a) 58 Nm RSM (5.5 kW IM frame) (b) 2.25 kNm RSM (250 kW IM frame)

Fig. 6.1. Structures of optimum RSMs designed for maximum power density

6.2 Mechanical strength aspects

Before considering the optimisation results, the mechanical strength of the RSM rotor is discussed. The mechanical strength of the RSM rotor is one of the aspects of the RSM over which, rightly, there is a question-mark. The iron pieces of the lamination are held together by means of ribs and webs and these ribs and webs must be as thin as possible to improve the performance of the machine. The use of webs (not just ribs) greatly improves the mechanical strength of the rotor against centrifugal forces. In addition, the higher the number of barriers used, the weaker and more pliable the lamination becomes and thus the more difficult to handle.

In Chapter 4 the web widths and rib heights used were prescribed by the punching ability and were taken in the analysis to be just more than the lamination thickness, namely 1.0 mm and 0.75 mm respectively. These widths and heights are adequate for small rotors to withstand the centrifugal forces on the outer iron pieces, but not for medium or large rotors. A mechanical strength analysis on the small rotors of the RSMs of Chapter 4 has shown that these rotors are very strong from a safety factor point of view and can withstand speeds of up to 5000 r/min. As the rotor becomes larger in diameter, however, the centrifugal forces increase with the *3rd* power of the rotor diameter. It is then unrealistic to keep the web widths and rib heights the same as for the smaller rotor, unless some other means are used to overcome the mechanical strength problem.

In order to ensure a certain minimum fatigue safety factor at twice base speed (i.e. 3000 r/min), the webs and ribs are enlarged as the rotor diameter becomes larger. An approximate mechanical strength analysis was used to calculate the required web widths and rib heights of the 8 barrier/pole rotors. The rotor structure of the 2.25 kNm RSM of Fig. 6.1(b) shows how large the webs and ribs become

for a large diameter rotor. The inner web width is 7.23 mm and the inner rib height is 2.0 mm for a rotor diameter of 292 mm. This diameter is close to three times the rotor diameter of the RSM in the 5.5 kW induction machine frame, which is 105 mm.

The penalty of the larger RSM, thus, is the mechanical constraints of the rotor which require relatively large webs and ribs, if no other means are used, to keep the iron pieces in place. This affects the torque and power factor performance of the larger RSM negatively.

6.3 Calculated results of goodness factors

In Fig. 6.2 the calculated results of the different goodness factors for the RSMs and the induction machines are shown. The goodness factors are plotted versus the frame sizes of standard induction machines, i.e. the goodness factors of the machines are given versus the rating (in kW) of the induction machines. Five induction machine frame sizes are selected, namely 5.5 kW, 11 kW, 37 kW, 90 kW and 250 kW. In Tables 6.1 and 6.2 the detailed design and performance data of the optimised RSMs are given.

Power density:

In Fig. 6.2(a) the torque density (Nm/stack-volume) versus frame size of the different machines is shown. The torque density of the RSMs outperforms completely that of the standard induction machines. It is also shown that the torque density improves with frame size.

In Fig. 6.3 the torque density is plotted versus the outer diameter of the machine. This figure proves the increase of the torque density (and the power density) of the RSM with outer diameter, as explained by eqns (5.8) and (5.9) of Chapter 5. Note that the torque density and power density are independent of the length of the machine.

The power density goodness factor in Fig. 6.2(b) increases with frame size. However, with constraints on the (P_{cu} + P_c) losses, the power density of the RSM reduces considerably (shown in dotted lines). The constrained results are also given in Tables 6.1 and 6.2. These results show how the RSM power density performance drops with the machine in the flux weakening mode (larger current angles) to keep specifically the iron losses within limits. Note from Tables 6.1 and 6.2 how large the iron losses of the large RSM become. Notwithstanding the drop in the power density of the RSM, it is still better than that of the induction machine for the same amount of total losses.

Efficiency:

The efficiency goodness factor G_{eff} of Fig. 6.2(c) improves with frame size for both machine types due to the lower penalties of the stator and rotor resistances (eqns 5.3 and 5.7). G_{eff} of the RSM is higher than that of the induction machine due to the higher output power per losses of the machine.

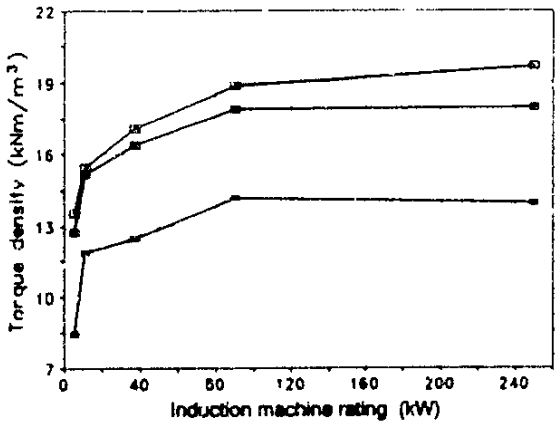

(a) Torque density

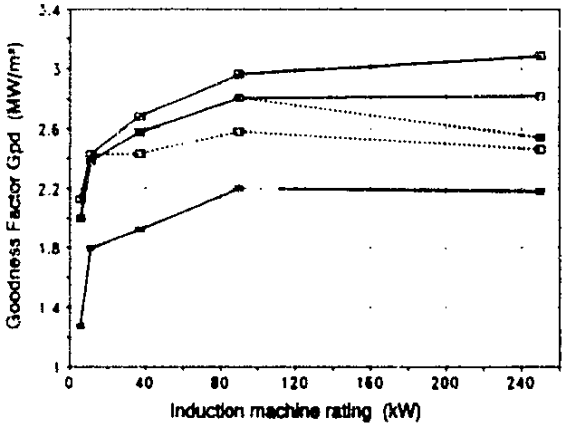

(b) $G_{pd} = P_{out} / vol$

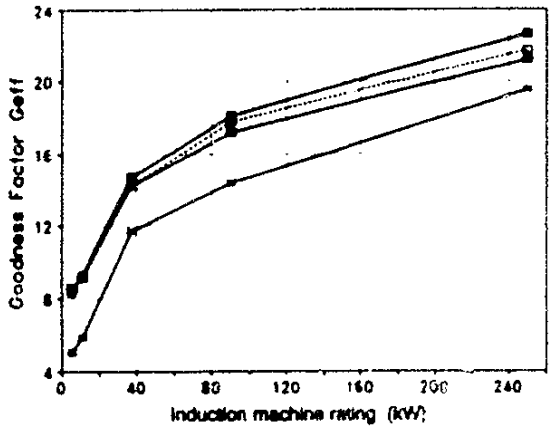

(c) $G_{eff} = P_{out} / P_{loss}$

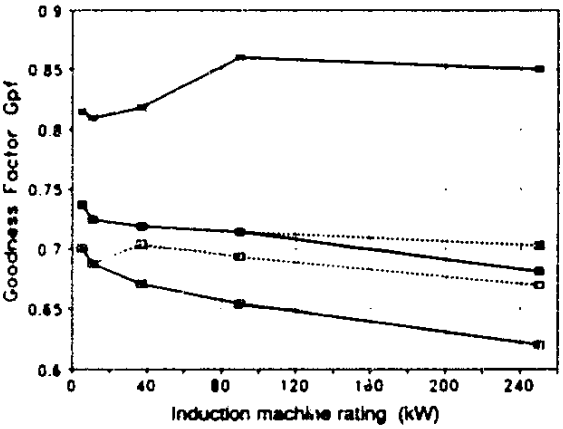

(d) $G_{pf} = P_{in} / kVA$

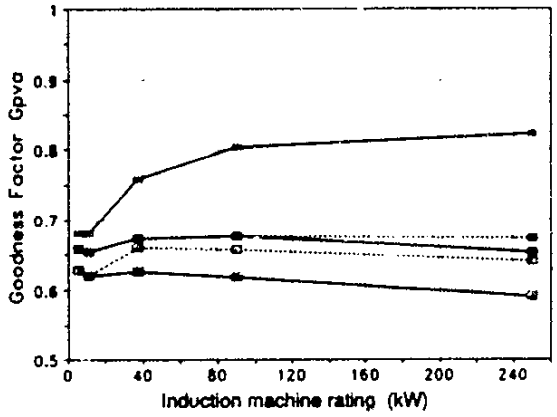

(e) $G_{pva} = P_{out} / kVA$

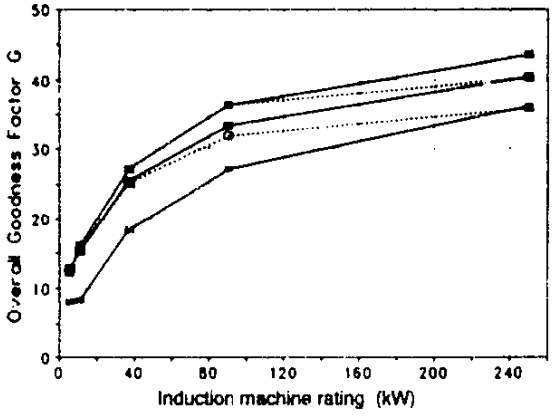

(f) $G = G_{pf} G_{eff} G_{pd}$

Fig. 6.2. Goodness factors versus frame size (dotted lines for constraints on $P_{cu} + P_c$)
* Induction machine ■ RSM optimised for maximum efficiency
RSM optimised for maximum power density

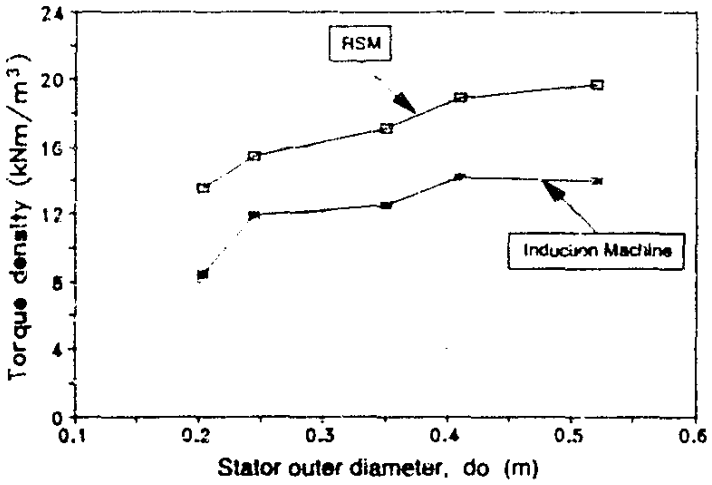

Fig. 6.5. Torque density versus outer diameter

Power factor:

The variations of the power factor goodness, G_{pf}, with frame size are shown in Fig. 6.2(d). It is clear that the power factor of the RSM is considerably lower than that of the induction machine, as explained in section 5.3.

It is seen that G_{pf} of the induction machine slightly increases with frame size while that of the reluctance machine drops. The increase in G_{pf} of the induction machine is due to the relatively lower rotor resistance and the increase in the magnetising inductance due to the lower saturation of the larger machine. This makes the impedance of L_m and R_r of the equivalent circuit of Fig. 5.2(a) more resistive. Consequently there is an improvement in the power factor.

The drop in the power factor of the RSM with frame size is mainly due to the lower stator resistance, making the supply voltage phasor more leading with respect to the current phasor. In addition, the increase in the web widths and rib heights to maintain mechanical strength makes L_q higher and the inductance ratio lower. The increase in the normalised airgap length $g_{(nor)} = g/d_i$ with frame size, as given in Tables 6.1 and 6.2, also will have a decreasing effect on L_d and thus the power factor. The latter, however, is true for the induction machine also.

Note that when the RSM is designed for maximum power density or maximum efficiency for the same amount of copper loss as that of the induction machine, the machine will be deep into saturation. This affects the power factor negatively.

Output power per kVA:

It is explained in section 5.3 that the output power per kVA goodness factor, $G_{pva} = P_{out}/kVA = \eta P_f$, of the RSM will be lower than that of the induction machine. This is proved by the G_{pva} calculated results in Fig. 6.2(e). The goodness factor G_{pva} versus frame size shows an improvement for the

	Machine 1	Machine 2	Machine 3	Machine 4	Machine 5
IM frame size	5.5 kW	11 kW	37 kW	90 kW	250 kW
Constraint P_{cu} (kW)	0.7	1.05	1.82	3	5.5
g di	0.00298	0.00277	0.00326	0.0034	0.0039
do (mm)	203.2	244.5	350	410	520
l (mm)	133.4	130.5	200	310	540
do/l	1.52	1.87	1.75	1.32	0.96
Variables ↓	**Per unit values of variables**				
yh/di	0.159	0.164	0.165	0.171	0.168
tw/tp	0.547	0.558	0.542	0.544	0.526
di/do	0.562	0.561	0.57	0.574	0.594
bw/bp	0.352	0.373	0.382	0.379	0.39
ϕ (°)	69.4	69.7	71	71.2	70.8 (*71.8*)
Parameters ↓	**Performance results at 1500 r/min** (*constraint on $P_{cu}+P_c$, optimising ϕ and J*)				
T (Nm)	55.1	92.9	315.3	732	2059 (*1853*)
η (%)	89.6	90.3	93.6	94.8	95.8 (*95.8*)
P_{out} (kW)	8.65	14.59	49.5	115	323 (*291*)
P_{cu} (kW)	0.72	1.08	1.87	3.08	5.66 (*4.55*)
P_c (kW)	0.25	0.41	1.19	2.41	6.16 (*5.81*)
$P_{cu}+P_c$ (kW)	0.97	1.49	3.06	5.5	11.82 (*10.36*)
P_{factor}	0.737	0.724	0.719	0.714	0.682 (*0.7*)
kVA	13.14	22.3	73.6	170	495 (*433*)
J (A/mm²)	6.88	6.83	5.38	5.28	4.88 (*4.44*)
$\sigma=L_d/L_q$	5.73	5.56	5.79	5.78	5.23 (*5.69*)

Table 6.1. Design and performance results of optimum RSMs designed for maximum *efficiency* for given copper losses (values in brackets hold for the constraints on $P_{cu} + P_c$)

induction machine but not for the RSM. G_{pva} of the induction machine improves because both the power factor and the efficiency of the machine improves with frame size, as shown in Figs. 6.2(c) and (d). This is not the case for the RSM as the power factor drops with frame size (Fig. 6.2(d)). The results of Fig. 6.2(e) indicate the advantage of the induction machine to the supply system, namely the lower kVA power per output power required than the RSM.

The G_{pva} of the RSM can be improved if the machine is designed for maximum G_{pva} subject to a constraint on the output power that is e.g. the same as that of the induction machine. An example of this is machine 5 of Table 4.6.

Overall goodness factor

The overall goodness factor, G, of eqn (5.16) is shown in Fig. 6.2(f) for the different machines. It is interesting to see that the overall goodness factor G of the larger RSMs is still better than that of

	Machine 1	Machine 2	Machine 3	Machine 4	Machine 5
IM frame size	5.5 kW	11 kW	37 kW	90 kW	250 kW
Constraint P_{cu} (kW)	0.7	1.05	1.82	3	5.5
g/di	0.0031	0.00286	0.00338	0.00355	0.0041
do (mm)	203.2	244.5	350	410	520
l (mm)	133.4	130.5	200	310	540
do/l	1.52	1.87	1.75	1.32	0.96
Variables ↓	Per unit values of variables				
yh/di	0.168	0.17	0.17	0.172	0.17
tw/tp	0.588	0.584	0.581	0.582	0.581
di/do	0.54	0.543	0.549	0.549	0.561
bw/bp	0.317	0.332	0.319	0.319	0.325
ϕ (°)	66.27	65.7	65.4 (*71.5*)	65 (*72*)	64.8 (*72*)
Parameters ↓	Performance results at 1500 r/min (*constraint on $P_{cu}+P_c$, optimising J and ϕ*)				
T (Nm)	58.6	94.6	328.4 (*291.4*)	772 (*671.6*)	2253 (*1796*)
η (%)	89.6	90.2	93.4 (*93.7*)	94.5 (*94.7*)	95.5 (*95.6*)
P_{out} (kW)	9.21	14.87	51.6 (*45.8*)	121.3 (*105.5*)	354 (*282*)
P_{cu} (kW)	0.722	1.08	1.88 (*1.57*)	3.09 (*2.54*)	5.67 (*4.0*)
P_c (kW)	0.314	0.505	1.46 (*1.16*)	3.16 (*2.48*)	8.68 (*6.5*)
$P_{cu}+P_c$ (kW)	1.04	1.585	3.34 (*2.74*)	6.25 (*5.02*)	14.35 (*10.5*)
P_{factor}	0.701	0.688	0.671 (*0.708*)	0.654 (*0.694*)	0.62 (*0.67*)
kVA	14.7	23.9	82.3 (*69.1*)	196 (*161*)	599 (*440*)
J (A/mm²)	7.03	6.71	5.26 (*4.89*)	5.03 (*4.63*)	4.56 (*3.89*)
$\sigma=L_d/L_q$	4.95	4.77	4.69 (*5.61*)	4.5 (*5.48*)	4.06 (*5.14*)

Table 6.2. Design and performance results of optimum RSMs designed for maximum *power density* for given copper losses (values in brackets hold for constraints on $P_{cu} + P_c$)

the induction machine, despite the low power factor of the RSM. The reason for this can be attributed to the high power density goodness of the RSM.

Two important aspects must be mentioned about the graphs of Fig. 6.2. The first is that the goodness factors for the induction machines are those of *standard* induction machines. It may differ for optimum designed vector controlled induction machines. Secondly, the goodness factors for the RSM are for one type of stator and rotor structure and may differ for other structures.

6.4 Normalised values of dimensions

The normalised values of the dimensions of the optimum RSMs designed for maximum efficiency and maximum power density are given in Tables 6.1 and 6.2. They are calculated by using the stator inner diameter and the tooth and barrier pitches as the base values. The normalised value of the stator inner diameter is calculated with the stator outer diameter as the base value.

From Tables 6.1 and 6.2 it can be seen that the normalised values of the optimum dimensions of the RSMs are similar for the different machines in the small to medium power range. This is expected to some extent as the airgap flux density, the tooth and rotor iron segment flux densities and the yoke flux density will not change much with frame size. Consequently, the normalised values of the tooth width and barrier width will stay very much the same (see in this regard eqns C.10 and C.12). The same is valid for the yoke height (yh) for a more or less constant yoke flux density (see eqn C.16).

This result of the more or less constant normalised values is significant. It implies that once a small machine is optimised according to certain criteria, one can tell immediately what the optimum dimensions will more or less be for a larger machine with the same stator and rotor structure.

6.5 Iron losses

The machines of Table 6.1 are optimised by maximising the output power per losses of the machine. This implies that the optimisation will be sensitive, amongst other things, to the iron losses of the machine. The machines of Table 6.2, on the other hand, are optimised by maximising the output power per given copper losses of the machine, regardless of what the iron losses are. To reduce the iron losses the current angles of the machines of Table 6.1 are increased, making the d-axis current and the saturation level of the machines less. The result of this can be seen in the better inductance ratios and power factors of the machines of Table 6.1. Also from the machines of Table 6.2 where there is a constraint on the total losses, the current angles are increased and the current density decreased to reduce the iron losses; consequently the inductance ratios and power factors are improved.

6.6 Conclusions

From the results of this chapter the following conclusions can be drawn:

- It is shown that the torque and power density goodness and efficiency goodness of the RSM improve as the machine becomes bigger. The general idea that the goodness of the reluctance machine will not improve with frame size is found to be untrue.

- The results of Fig. 6.2 show that optimising the design of the RSM in terms of its efficiency gives the best results overall. The overall goodness factor of the RSM is the highest when the machine is designed for maximum efficiency.

- It seems from Fig. 6.2(b) that there is an upper boundary in the medium power range, say 100 kW, from where the power density goodness factor of the RSM slowly starts to drop due to the constraints on the total losses, specifically the iron losses.

- The disadvantage of the large RSM is the problem of the mechanical strength of the rotor.

7 Summary with Conclusions and Recommendations

The contribution of the thesis can be summarised as the development of a finite element-based design optimisation method for the reluctance synchronous machine (RSM) and the evaluation of the steady-state performance capability of this machine in motoring mode under current vector control.

The proposed design optimisation method uses the finite element calculation method directly in the optimisation algorithm to optimise the design of the machine in multidimensions. The absolute optimum-designed machine can at best be obtained by using the finite element method in the optimisation process. An approximate magnetic circuit calculation method is also developed and used in the optimisation algorithm to verify to some extent the finite element optimisation results.

The performance capability of the RSM is evaluated by optimising the design of the machine according to different criteria. An RSM has also been built and tested to verify the finite element calculations and to prove some important characteristics of the RSM. The performance characteristics of the RSM in comparison with those of the induction machine are explained by means of goodness factors that are derived for both machines. The performance of optimum RSMs in the medium power range is also investigated and compared with standard induction machines.

The results and conclusions found in the thesis about the optimum design and performance of the RSM are summarised in the sections below. Recommendations for further research work necessary are made in section 7.6.

7.1 Calculation of performance parameters

In the optimisation process the finite element program is called many times by the optimisation algorithm to optimise the design of the machine. This necessitates that as few finite element field solutions as possible be used to calculate the performance data of the machine each time the finite element program is called. In the thesis it is shown how this can be done for the RSM as only one set of finite element field solutions (a set consists of 5 field solutions) is required to calculate all the equivalent circuit parameters and the performance data of the machine, taking into account the effect of saturation, cross magnetisation and skew.

An approximate magnetic circuit (AMC) calculation method is developed that can be used, instead of the finite element method, in the optimisation to optimise specifically the stator design of the machine. The use of the proposed AMC method proved to be worthwhile. The method is a very simple, fast and reasonably accurate method that can be used to show and explain design tendencies but also to do preliminary stator design optimisations. The correlation between the finite element and the AMC optimisation results suggests that designers could use this method in an initial study.

Another calculation method is proposed for use in the design optimisation of the machine, namely the hybrid magnetic circuit – finite element (HMF) method. This method makes use of both the AMC and finite element calculation methods. The idea is to identify from finite element analysis, at some stages in the optimisation process, those parameters of the RSM that are difficult to calculate accurately by means of analytical equations or lumped circuit analysis. The aim is thus to get more accurate results, while still keeping the computational burden low. An example is given in Chapter 4, where only 9 field solutions were used in the optimisation of the RSM.

7.2 Optimisation algorithms

In the thesis the algorithms of Powell and the quasi-Newton method are used for the unconstrained design optimisation of the machine. The difference between these two methods is that the Powell method is a non-gradient method which requires only function evaluations, not derivatives, while the quasi-Newton algorithm is a gradient method which requires that the vector of first partial derivatives be calculated. The reasons for using these methods are, amongst others, to determine if a gradient method can be used to optimise the design of the machine and to verify the optimum design results by using two completely different optimisation algorithms.

In the quasi-Newton method the first partial derivative of the function is determined by the forward-difference approximation. The step size of the forward-difference approximation is critical because it determines the quality of the derivative. In Chapter 3 and Appendix D an optimum, *relative* step size is determined that is used throughout the design optimisation.

The focus of the optimisation study was more on the unconstrained condition, although constrained optimisation was also done by using penalty functions. The objective function is modified by adding terms or functions that assign a positive 'penalty' for increased constraint violation.

Some results found from the use of the proposed finite element design optimisation method are the following:

- It was found that both the Powell and quasi-Newton methods give the same optimum values for the variables. This gives confidence in the results specifically if it is taken into account that the two algorithms are totally different: the one is a gradient and the other a non-gradient method.

- The computation time per finite element program solution is about 5 minutes on a SUN 1000 workstation using an average of 1800 elements per pole and 1100 vector potential unknowns. This implies that the design optimisation problem requiring, say, 100 solutions can be solved in a day. It was found that for the optimisation of 10 variables the number of solutions required typically vary between 100 and 150 with the computation time between 8 to 12 hours. The latter obviously depends on the load of the workstation, the starting vector point and the termination criterion.

- In the proposed finite element optimisation the mesh changes as the optimisation progresses. There is thus a possibility that some of the elements become badly shaped or ill conditioned and that accuracy is lost. This, however, was not experienced by the author as the variables (dimensions of the machine) do not change that much in the search for the optimum.

- Both the Powell and quasi-Newton methods proved to be effective in the design optimisation of the machine. In general it was found that the quasi-Newton method is equal or slightly faster in calculation speed than the Powell method.

Two important conclusions regarding the proposed design optimisation method are the following:

- It is feasible in terms of computation time to do an overall (stator and rotor) unconstrained or constrained optimum design of the RSM using the finite element analysis method directly in the optimisation procedure. As the power and speed of workstations and computers are increasing by the day, it seems that the finite element-based design optimisation of the electrical machine will become popular as it is the most accurate way of optimising the design of the machine.

- It is shown that optimisation algorithms which require the function's gradient, or first partial derivatives, to be computed can be used with success using the nonlinear finite-element field solution to calculate the function value. This opens the door for designers to use gradient methods in finite element design optimisations.

7.3 Optimisation results in the 3 - 10 kW power level

The different performance calculation methods and the optimisation algorithms are used to optimise in multidimensions the design of the RSM. The aim was to evaluate from calculations but also from measurements the performance capability of the RSM in the 3 - 10 kW power level. Considerable attention is given to the explanation and the understanding of the various optimum designed RSMs. The design of the machine is optimised by maximising different performance parameters (objective function values) of the machine. These parameters or function values are the torque, the efficiency and the torque per kVA of the machine.

From the design optimisation the following results are found:

- The airgap diameter of the optimum RSM designed for maximum torque is relatively small, as $d_i/d_o = 0.52$ compared to that of the induction machine where $d_i/d_o \approx 0.6$.

- The optimum RSMs designed for maximum torque or maximum efficiency show remarkably high power densities with about the same copper and iron losses as that of the standard induction machine. This explains the high efficiencies of these machines. The torque per rotor volume (TRV) is also exceptionally high. For example, the optimum RSM designed for

maximum torque has a TRV of almost 50 kNm/m^3 which is higher than the range for high-performance industrial servos (20 - 45 kNm/m^3).

The RSM, thus, has the outstanding characteristics of high power density and high torque per rotor volume when designed for maximum torque or maximum efficiency. It is therefore advantageous to design the RSM (for given copper losses) for maximum torque or maximum efficiency.

- The optimum current angles of the designed RSMs are all between 60 and 70°. This confirms again the high current angles where optimum performance of the machine is obtained.

- When designing the RSM for maximum torque or maximum efficiency for given copper losses, typical normalised values of some of the important dimensions of the RSM can be used as initial values for the optimisation process. These are the following for 4-pole machines:

di/do = 0.55;	*tw/tp = 0.55;*
yh/di = 0.17;	*bw/bp = 0.33;*
ϕ = 65° (maximum T).	*ϕ = 70° (maximum η);*

- From all the design optimisation results it is found that the power factors of the optimum RSMs are on the low side. This affects negatively the kVA rating and the efficiency of the inverter.

- An optimum RSM designed for maximum torque has been built in a standard 5.5 kW induction machine frame. Photos of the stator and rotor of this machine are shown in Appendix E. With the machine under current vector control, very good correlation is obtained between the finite element calculations and the measurements of the shaft torque, efficiency and power factor of the machine. The close agreement between the calculated and measured shaft torque and efficiency confirms the remarkably high torque and high efficiency of this machine. Both calculations and measurements indicate an optimum current angle of 64° where the torque is a maximum.

7.4 Goodness factors

Goodness factors are derived for the RSM to explain the outstanding characteristics of high power density and low power factor of the machine. The expressions for the goodness factors of the RSM give a better understanding of the operation, the advantages and the penalties of the machine. Goodness factors are also derived for the induction machine to explain the difference between the RSM and the induction machine. The goodness factors of the RSM are also used to explain the goodness of the machine at the higher power levels.

The following explanations of the operation and the characteristics of the RSM are instructive:

- The fundamental difference between the reluctance and induction machine is that the reluctance machine makes use of a q-axis magnetic circuit on the rotor to generate torque while the induction machine makes use of a q-axis electrical circuit on the rotor. The use of an electric circuit, however, goes hand-in-hand with copper losses which become relatively higher as the machine becomes smaller, i.e. small in diameter.

- The advantage of a high power density and disadvantage of a low power factor of the RSM can be directly attributed to the use of a passive rotor with magnetic asymmetry. A passive rotor implies a rotor without losses; consequently the stator power can be raised with the result that there is a considerable increase in the power density. In comparison with the induction machine the RSM is thus a good machine from an electrical machine point of view.

  However, a passive rotor also implies that use is made of magnetic circuits, represented as magnetising inductances in the equivalent circuit, to generate torque. This makes the inductive equivalent impedance seen by the supply relatively high, resulting in a low power factor that affects the inverter rating. The RSM is thus not an excellent machine from a supply point of view.

7.5 Performance of the RSM in the medium power range

The different goodness factors mentioned in section 7.4 are calculated for optimum designed RSMs in the medium power range. The aim was to investigate the extent to which the goodness or performance of the optimum RSM improves or attenuates as the machine becomes bigger. The aim was also to compare the goodness of the RSM with that of the standard induction machine.

Altogether six RSMs are optimised in induction machine frames from 5.5 to 250 kW, using the finite element method directly in the optimisation process. The reluctance machines are optimised by maximising the efficiency and the power density of the machines for the same amount of copper losses as those of standard induction machines with the same frame size.

From the results of the design optimisations of the RSM in the medium power range the following aspects are significant:

- It is shown that the torque and power density goodness and the efficiency goodness of the RSM improve as the machine becomes bigger. The general idea that the goodness of the reluctance machine will not improve with frame size is found to be untrue.

- A disadvantage of the RSM in the medium power range is the constantly low power factor and low output power per kVA of the machine. This affects the kVA rating and the efficiency of the inverter, as a larger reactive power has to be controlled.

- It seems that there is an upper boundary in the medium power range, say 100 kW, from where the power density goodness factor of the RSM slowly starts to drop due to the constraints on the total losses, specifically the iron losses. With better cooling this drop in the power density goodness of the RSM can be prevented.

- The normalised values of the dimensions of the optimum RSMs are similar for the different machines in the small to medium power range. This result of the more or less constant normalised values is significant. It implies that once a small machine is optimised according to certain criteria, one can tell immediately what the optimum dimensions will be more or less for a larger machine with the same type of stator and rotor structure.

- The mechanical strength of the RSM rotor is one of the aspects of the RSM over which, rightly, there is a question-mar'.. The iron pieces of the lamination are held together by means of ribs and webs and these ribs and webs must be as thin as possible to improve the performance of the machine.

  In order to ensure a certain minimum fatigue safety factor, the webs and ribs are enlarged as the rotor diameter becomes larger This affects the torque and power factor performance of larger RSMs negatively and may limit the use of the RSM in the higher power levels.

To conclude, the thesis demonstrates for the first time the ultimate steady-state performance of the RSM in motoring mode. It shows that the RSM has a high power density and a high efficiency even in the upper-medium power range.

It is believed that the proposed finite element design optimisation method and the design optimisation results found in this thesis will help designers and manufactures to obtain maximum performance of the RSM.

7.6 Recommendations

The proposed design optimisation method of this thesis can be used to investigate the design optimisation of electrical machines. It is recommended that the following research be undertaken:

- A more detailed study is necessary on the optimum (allowed) airgap length of the RSM (this will require a mechanical strength analysis), the optimum stator slot opening, the use of single-layer windings and their effect on the performance of the machine, and finally the effect of different pole and stator slots numbers on the performance of the RSM.

- The design optimisation of the reluctance synchronous generator (RSG) must be investigated, together with a study of the performance capability of this generator.

- A detailed study is necessary, including mechanical strength analyses and performance measurements, of the larger RSMs.

- There is a limitation in the proposed design optimisation method of this thesis in that only magnetic fields have been analysed. There is a need to incorporate in the design optimisation, through finite element analysis, the calculation of the iron losses, the heating of the machine and the mechanical strength of the rotor.

- It is recommended that the proposed design optimisation method of this thesis be used for the design optimisation of other synchronous machines like the switched reluctance machine, multiphase reluctance machines and wound field and permanent magnet synchronous machines.

R References

Abdel-Razek (1981), A.A., Coulomb, J.L., Feliachi, M. and Sabonnadiere, J.C.: "The calculation of electromagnetic torque in saturated electric machines within combined numerical and analytical solutions in the field equations", *IEEE Trans. on Magnetics*, vol. 17, no. 6, pp. 3250-3252, Nov. 1981.

Abdel-Razek (1982), A.A., Coulomb, J.L. and Sabonnadiere, J.C.: "Conception of an air-gap element for the dynamic analysis of the electromagnetic field in electric machines", *IEEE Trans. on Magnetics*, vol. 18, no. 2, pp. 655-659, March 1982.

Andersen (1967), O.W.: "Optimum design of electrical machines", *IEEE Trans. PAS*, vol. 86, no. 6, pp. 707-711, June 1967.

Andersen (1992), O.W.: "Optimal design of induction motors", *Int. Aegean Conf. on Electrical Machines and Power Electronics*, vol. 2, pp. 763-768, May 1992.

Anvari (1985), H.A., Faucher, J. and Trannoy, B.: "An investigation into the influence of a cross-coupling effect on reluctance machine performance", *Int. Conf. on Electrical Machines - design and applications*, IEE, vol. 254, pp. 70-75, 1985.

Alhamadi (1991), M.A. and Demerdash, N.A.: "Modelling of effects of skewing of rotor mounted permanent magnets on the performance of brushless DC motors", *IEEE Trans. on Energy Conversion*, vol. 6, no. 4, pp. 721-729, 1991.

Barton (1992), R.R.: "Computing forward difference derivatives in engineering optimization", *Eng. Opt.*, vol. 20, pp. 205-224, 1992.

Binder (1989), A.: "Untersuchung zur magnetischen kopplung von Längs- und Querachse durch sättigung am beispiel der reluktanzmaschine", *Arch. Elektrotech.*, vol. 72, pp. 277-282, 1989.

Boldea (1991), I, Fu, Z.X. and Nasar, S.A.: "Torque vector control of axially-laminated anisotropic rotor reluctance synchronous motors", *Electric Machines and Power Systems*, vol. 19, pp. 533-554, 1991.

Bowers (1985), B.: "The early history of the electric motor", *Philips Technical Review*, vol. 35, no. 4, pp. 77-95, 1975.

Brinkman (1965), J.: "*Theoretische und experimentelle untersuchungen an einem motor mit verbesserter ausnuzung des reaktionsprinzips*", Dissertation, Fakultät für Maschinenwesen der Technischen Hochschule Carolo-Wilhelmina, Braunschweig, Jan. 1965.

Broyden (1970), C.G.: "The convergence of a class of double-rank minimization algorithms", *Journal Inst. Maths. Applics.*, vol. 6, pp. 76-90, 1970.

Brüderlin (1924), R.: "Drehfeldmaschinen mit veränderlicher reaktanz", *Archiv für Elektrotechnik*, XIII Band, pp. 12-29, 1924.

Cheong (1979), G.H.: "The truth about airgap leakage reactance in polyphase squirrel-cage induction motors", *Proc. IEE*, vol. 126, no. 10, pp. 971-978, 1979.

Cruickshank (1971), A.J.O., Anderson, A.F. and Menzies, R.W.: "Theory and performance of reluctance motors with axially laminated anisotropic rotors", *Proc. IEE*, vol. 118, no. 7, July 1971.

Davidon (1959), W.C.: "Variable metric methods for minimization", *A.E.C. Research and Development*, Report ANL-5990, Argonne National Laboratory, Argonne, Illinois, 1959.

Douglas (1956), J.F.H.: "The theory of anisotropic field structures in synchronous machines", *Trans. AIEE*, vol. 75, pp. 84-86, April 1956.

El-Antably (1985), A. and Hudson, T.L.: "The design and steady-state performance of a high efficiency reluctance motor", *IEEE-IAS Annual Meeting*, pp. 770-776, 1985.

Faucher (1979), J., Lajoie-Mazenc, M. and Chayegani, A.: "Characterization of a closed-loop controlled current-fed reluctance machine taking into account saturation", *IEEE Trans. on Industrial Applications*, vol. 15, no. 5, pp. 482-488, 1979.

Fletcher (1963), R. and Powell, M.J.D.: "A rapidly convergent descent method for minimization", *Computer Journal*, vol. 6, pp. 163-168, 1963.

Fletcher (1970), R.: "A new approach to variable metric algorithms", *Computer Journal*, vol. 13, pp. 317-322, 1970.

Flack (1994), T.J. and Volschenk, A.F.: "Computational aspects of time-stepping finite-element analysis using an airgap element", *ICEM*, Sept 1994.

Fratta (1987), A., Vagati, A. and Villata, F.: "A reluctance motor drive for high dynamic performance applications", *IEEE-IAS Annual Meeting*, pp. 295-302, 1987.

Fratta (1988), A., Vagati, A. and Villata, F.: "A.C. spindle drives: a unified approach to the filed-weakening behaviour", *Proceedings Motor-con*, pp. 44-56, June 1988.

Fratta (1992), A. and Vagati, A.: "Synchronous reluctance vs induction motor: a comparison", *Proceedings Intelligent Motion* (Nürnberg), pp. 179-186, April 1992.

Fratta (1994), A., Petrache, C., Franceschini, G. and Troglia, G.: "A simple current regulator for flux-weakened operation of high performance synchronous reluctance drives", *IEEE-IAS Annual Meeting Record*, pp. 649-657, Oct. 1994.

Fu (1991), Z.X.: "*Study of axially-laminated anisotropic rotor reluctance synchronous machine and its drive*", Ph.D. dissertation, University of Kentucky, Lexington, KY, USA, 1991.

Goldfarb (1970), D.: "A family of variable metric methods derived by variational means", *Mathematics of Computation*, vol. 24, pp. 23-26, 1970.

Greig (1980), D.M.: *Optimisation*, Longman (London), 1980, pp. 49-59.

Gill (1981), P.E., Murray, W. and Wright, M.H.: *Practical optimization*, Academic Press (London), 1981, pp. 117-133 and pp. 335-338.

Han (1977), S.P.: "A globally convergent method for nonlinear programming", *Journal of Optimisation Theory and Applications*, vol. 22, no. 3, pp. 297-309, July 1977.

Heller (1977), B. and Hamata, V.: "*Harmonic field effects in induction machines*", Elsevier (Amsterdam), 1977.

Honsinger (1959), V.B.: "Theory of endwinding leakage reactance", *Trans. AIEE*, vol. 78, no. 3, pp.417-426, 1959.

Honsinger (1971), V.B.: "The inductances L_d and L_q of reluctance machines", *IEEE Trans. PAS*, vol. 90, no. 1, Jan. 1971.

Hooke (1961), R. and Jeeves, T.A.: "Direct search solution of numerical and statistical problem", *Journal of ACM*, vol. 8, pp. 212, 1961.

Kamper (1987), M.J.: *Design criteria of squirrel-cage induction motors*, M.Eng. thesis, Univ. of Stellenbosch, pp. 93-103, 1987.

Kamper (1994), M.J. and Volschenk, A.F.: "Effect of rotor dimensions and cross magnetisation on L_d and L_q inductances of reluctance synchronous machine with cageless flux barrier rotor", *IEE Proc.-Electr. Power Appl.*, vol. 141, no. 4, pp. 213-220, July 1994.

Kamper (1995), M.J. and Mackay, A.T.: "Optimum control of the reluctance synchronous machine with a cageless flux barrier rotor", *Trans. S.A. of the South African Institute of Electrical Engineers*, vol. 86, no. 2, pp. 49-56, June 1995.

Kostko (1923), J.K.: "Polyphase reaction synchronous motors", *Journal AIEE*, vol. 42, pp 1162-1168, 1923.

Krause (1969), P.C. and Lipo, T.A.: "Analysis and simplified representations of rectifier-inverter reluctance-synchronous motor drives", *IEEE Trans. PAS*, vol 88, no. 6, June 1969.

Kübler (1961), E., Moëller, F. and Werr, L.: "*Wechselstrommaschinen*", B.G. Teubner Verlagsgesellschaft (Stuttgart), pp. 96-100, 1961.

Kurscheidt (1961), P.: "*Theoretische und experimentelle untersuchung einer neuartigen reaktionsmaschine*", Dissertation, Fakultät für Maschinenwesen und Elektrotechnik der Rheinisch-Westfälischen Technischen Hochschule, Aachen, Jan. 1961.

Laithwaite (1965), E.R.: "The goodness of a machine", *Proc. IEE*, vol. 112, no. 3, p. 538, Mar. 1965.

Lawrenson (1964), P.J.: "Theory and performance of polyphase reluctance machines", *Proc. IEE*, vol. 111, no. 8, pp. 1435-1445, Aug. 1964.

Lawrenson (1967), P.J. and Gupta, S.K.: "Developments in the performance and theory of segmental-rotor reluctance motors", *Proc. IEE*, vol. 114, no. 5, pp. 645-653, May 1967.

Lawrenson (1970), P.J.: "Calculation of machine endwinding inductances with special reference to turbo-generators", *Proc. IEE*, vol. 117, no. 6, pp. 1129-1134, 1970.

Li (1990), C. and Rahman, A.: "Three-phase induction motor design optimisation using the modified Hooke-Jeeves method", *Electric Machines and Power Systems*, vol. 18, pp. 1-12, 1990.

Lin (1951), C.Y.: "Characteristics of Reluctance Machines", *Trans. AIEE*, vol. 70, pt. 2, pp. 1971-1977, 1951.

Lipo (1967), T.A. and Krause, P.C.: "Stability analysis of a reluctance-synchronous machine", *IEEE Trans. PAS*, vol. 86, no. 7, pp. 825-834, July 1967.

Lipo (1991), T.A.: "Synchronous reluctance machines - a viable alternative for AC drives", *Electr. Mach. Power Syst.*, vol.19, pp. 659-671, 1991.

Liwschitz-Garik (1961), M. and Whipple, C.: "*Alternating Current Machines*", 2nd edition, Van Nostrand (Princeton, New Jersey), 1961.

Luo (1994), X., El-Antably, A. and Lipo, T.A.: "Multiple coupled circuit modeling of synchronous reluctance machines", *IEEE-IAS Annual Meeting* (Denver), pp. 281-289, Oct. 1994.

Matsuo (1993), T. and Lipo, T.A.: "Field oriented control of synchronous reluctance machine", *IEEE-PESC*, pp. 425-431, 1993.

Matsuo (1994), T. and Lipo, T.A.: "Rotor design optimization of synchronous reluctance machine", *IEEE Trans. on Energy Conversion*, vol. 9, no. 2, pp. 359-365, June 1994.

Miller (1991), T.J.E., Hutton, A., Cossar, C. and Staton, D.A.: "Design of synchronous reluctance motor drive", *IEEE Trans. on Industrial Applications*, vol. 27, no. 4, July 1991.

Ong (1977), C.M. and Lipo, T.A.: "Steady state analysis of a current source inverter reluctance motor drive", *IEEE Trans. PAS*, vol. 96, no. 4, 1977.

Parasiliti (1993), F. and Villani, M.: "Optimised design of a double-cage induction motor", *Int. Conf. on Electrical Machines in Australia* (ICEMA), Adelaide, pp. 81-86, Sept. 1993.

Platt (1992), D.: "Reluctance motor with strong rotor anisotropy", *IEEE Trans. on Industry Applications*, vol. 28, no. 3, pp. 652-658, June 1992.

Powell (1978), M.J.D.: "A fast algorithm for nonlinearly constrained optimisation calculations", 1977 Dundee Conf. on Numerical Analysis, *in* 'Series on lecture notes in mathematics', Springer Verlag, pp. 144-157, 1978.

Powell (1964), M.J.D.: "An efficient method for finding the minimum of a function of several variables without calculating derivatives", *Computer Journal*, vol. 7, pp. 155-162, 1964.

Press (1986), W.H., Flannery, B.P., Teukolsky, S.A. and Vetterling, W.T.: *Numerical recipes*, Cambridge University Press, pp. 294-312, 1986.

Ramamoorty (1979), M. and Rao, P.J.: "Optimisation of polyphase segmented-rotor reluctance motor design: a nonlinear programming approach", *IEEE Trans. PAS*, vol. 98, no. 2, pp. 527-535, March/April 1979.

Richter (1954), R: "*Elektriche Maschinen*", IV Band, Verlag Birkhäuser (Basel/Stuttgart), 1954.

Schittkowski (1981), K.: "The nonlinear programming method of Wilson, Han and Powell with an augmented Lagrangian type line search function", *Numerische Mathematik*, vol. 38, pp. 83-114, 1981.

Schuisky (1957), W.: "*Induktionsmaschinen*", Springer-Verlag (Wenen), 1957.

Shanno (1970), D.F.: "Conditioning of quasi-Newton methods for function minimization", *Mathematics of Computation*, vol. 24, pp. 647-657, 1970.

Singh (1992), C. and Sarkar, D.: "Practical considerations in the optimisation of induction motor design", *IEE Proceedings-B*, vol. 139, no. 4, pp. 365-373, July 1992.

Soong (1993), W.L., Staton, D.A. and Miller, T.J.E.: "Validation of lumped-circuit and finite-element modelling of axially-laminated brushless motors", *IEE Int. Conf. on Electrical Machines and Drives* (Oxford), pp. 85-90, Sept. 1993.

Talaat (1951), M.E.: "Steady-state and transient synthesis of 3-phase reluctance motors", *Trans. AIEE*, vol. 70, pt. 2, pp. 1963-1970, 1951

Thompson (1911), S.P.: "*Dynamo electric machinery*", M. Strong (New York, N.Y.), eighth edition, pp. 389 (Fig. 264), 1911.

Trickey (1933), P.H.: "The non-excited synchronous motor", *Electric Journal* (Pittsburgh), vol. 30, pp. 160-162, 1933.

Trickey (1946), P.H.: "Performance calculations on polyphase reluctance motors", *Trans. AIEE*, vol. 65, pp. 191-193, April 1946.

Vagati (1992), A., Franceschini, G., Marongiu, I. and Troglia, G.P.: "Design criteria of high performance synchronous reluctance motors", *IEEE-IAS Annual Meeting Record*, pp. 66-73, Sept. 1992.

Vagati (1994), A.: "The synchronous reluctance solution: a new alternative in A.C. drives", *Proc IEEE IECON'94* (Bologna), vol. 1, pp.1-13, 1994.

Vas (1990), P.: "*Vector control of AC machines*", Clarendon Press (Oxford), 1990.

Volschenk (1993), A.F.: "*Finite element analysis of a salient-pole generator feeding a rectifier load*", Ph.D. dissertation, University of Cambridge, March 1993.

Weh (1985), H. and Schroder, U.: "Static inverter concepts for multiphase machines with square-wave current-field distributions", *European Power Electronics Conference* (Brussels), pp. 1147-1152, 1985.

Weh (1990), H., Mosebach, W., Niemann, W. and Tareilus, A.: "Field control in synchronous machines with permanent magnet excitation in flux concentration mode", *Proc. ICEM* (Cambridge), 1990.

Wiley (1995), B., Hudson, R. and Spee, R.: "Digital enhancement of analog current regulators for three phase motor drives", *APEC*, 1995.

Williamson (1980), S. and Smith, J.R.: "The application of minimisation algorithms in electrical engineering", *IEE Proc.*, vol. 127, pt. A, no. 8, pp. 528-530, Nov. 1980.

Williamson (1994), S., Flack, T.J. and Volschenk, A.F.: "Representation of skew in time-stepped two-dimensional finite element models of electrical machines", *IEEE-IAS Annual Meeting Record*, pp. 143-148, 1994.

Xu (1991), L., Xu, X., Lipo, T.A. and Novotny, D.W.: "Vector control of a synchronous reluctance motor including saturation and iron loss", *IEEE Trans. Industry Applications.*, vol. 27, no. 5, pp. 977-987, Sept. 1991.

Zangwill (1967), W.I.: "Nonlinear programming via penalty functions", *Management Science*, vol. 13, pp. 344-358, 1967.

A Stator Winding Resistance and Endwinding Leakage Inductance

A.1 Formula for stator winding resistance

The skin effect in the stator conductors is ignored in the calculation of the stator winding resistance R_s. The formula for the per phase stator winding resistance is

$$R_s = \frac{2 W \rho_t (l + l_e)}{n_s A_{cu}/z} \tag{A.1}$$

where l_e is the average length of a coil-end
and A_{cu}/z is the active copper area of a stator conductor.

ρ_t of eqn (A.1) is the resistivity of copper at a temperature t_c and is given by

$$\rho_t = \rho_{20} (1 + Y_t (t_c - 20)) \tag{A.2}$$

where $\rho_{20} = 17 \times 10^{-9}$ ohm.m and $Y_t = 0.0039/°C$.

The relation between the number of conductors per slot, z, and the number of turns in series per phase, W, of eqn (A.1) is

$$z = W n_s / (q p) , \tag{A.3}$$

so that eqn (A.1) may also be expressed as

$$R_s = \frac{2 W^2}{q p} \left(\frac{\rho_t (l + l_e)}{A_{cu}} \right) = k_r W^2 r_s . \tag{A.4}$$

In this equation, r_s is the slot resistance or the resistance of all the conductors of a stator slot in parallel.

A.2 Formula for endwinding leakage inductance

An investigation into the analytical calculation of the endwinding leakage reactance of squirrel-cage induction machines was done by Kamper (1987). In this study a summary is given of the different considerations and computational methods of several authors concerning the calculation of the endwinding leakage reactance. The formula given by Honsinger (1959) was taken as a basis in the creation of a formula that can be used in general for single- and double-layer windings. Honsinger's formula is firstly adapted to let the formula be valid for single-layer windings. Secondly, the basic formula is adapted to correctly take into account the mutual flux linkage between the endwinding

phase groups using the method of Lawrenson (1970).

This same formula is used for the calculation of the endwinding leakage inductance of the RSM omitting only the effect of the flux coupling between the stator endwindings and the rotor endring as for the induction machine. The formula is

$$L_e = V_{(u)}\, m\, d_i \left(\frac{W\, k_d\, k_{p(u)}}{p} \right)^2 k_{c(p)} \times 10^{-8} \quad \text{henry/phase} . \tag{A.5}$$

In this equation the subscript, u, refers to the shape of the endwinding coils namely

u = 1 implies V-shaped coils,
u = 2 implies elliptical-shaped coils
and u = 3 implies rectangular coils.

The factor k_d is the ordinary distribution factor for the fundamental which is for 3-phase, 60° phase-band, integral slot windings

$$k_d = \frac{\sin(\pi/6)}{q \sin(\pi/6q)} . \tag{A.6}$$

The factor $k_{p(u)}$ of eqn (A.5) is an endwinding pitch factor for coil shape, u, and is given by

$$\begin{aligned} k_{p(1)} &= \frac{3 \sin(\pi c/6q)}{4 - (c/3q)^2} , \\ k_{p(3)} &= \sin(\pi c/6q) , \\ \text{and} \quad k_{p(2)} &= k_{p(1)} + k_{p(2)} , \end{aligned} \tag{A.7}$$

where *c* is the coil pitch in terms of number of stator slots.

The factor $k_{c(p)}$ is an endwinding factor for a *p* pole-pair machine and is given by

$k_{c(1)} = 0.51$, $k_{c(2)} = 0.595$, $k_{c(3)} = 0.64$ and $k_{c(4)} = 0.785$.

Finally, $V_{(u)}$ of eqn (A.5) is a shape factor for coil shape *u* and is for double-layer windings

$V_{(1)} = 465$, $V_{(2)} = 920$ and $V_{(3)} = 1040$,

and for single-layer windings

$V_{(1)} = 600$, $V_{(2)} = 1180$ and $V_{(3)} = 1400$.

B Finite Element Program and Calculation of Phase Flux Linkage and Fundamental Airgap Flux Density

In this appendix the finite element program, the calculation of the total flux linkage of a phase winding and the calculation of the fundamental airgap flux density are briefly described.

B.1 The finite element program

The finite element software used is not of the commercial variety. It makes use of triangular elements of the first order. Only one pole (stator and rotor) of the machine is meshed with one airgap macro-element (Abdel-Razek, 1982) comprising nodals on both sides of the airgap. A time-saving scheme has been devised (Volschenk, 1993 and Flack, 1994) that makes the use of one airgap element very attractive as a means to model rotor movement. The Newton-Rhapson method is used for the solution of the set of non-linear equations.

The finite element solution procedure has the following basic steps:

- *Mesh generation*:

  Only one stator slot of the machine is outlined in terms of xy-coordinates and meshed and mirrored to the number of slots over a pole pitch. The phase windings are then allocated to the slots. Also, one half of a pole of the reluctance rotor is outlined and meshed and mirrored to the other half pole. The stator and rotor meshes are then joined.

- *Pre-processing*:

  This step is necessary to save storage and calculation time. Sparse matrices are created and the numbering of the equations is optimised to minimise the solution time.

- *Solving*:

  The Newton-Rhapson solution procedure is used to solve for the magnetic vector potential at the different nodes. It is a solution of a set of non-linear equations due to the non-linearity of the magnetic materials.

- *Post-processing*:

  From the known nodal magnetic vector potentials, the flux linkages, inductances, etc. of the machine are calculated (see, for example, sections B.2 and B.3).

B.2 Calculation of the total phase flux linkage

With a two-dimensional finite element solution the magnetic vector potential has only a z-directed component, i.e.

$$\begin{aligned} A &= A(x,y)\cdot a_z \qquad \{\text{cartesian coordinates}\} \\ A &= A(r,\theta)\cdot a_z \qquad \{\text{cylindrical coordinates}\} \end{aligned} \tag{B.1}$$

where $\mathbf{a}_z$ is the unit vector directed in the z direction. From the known magnetic vector potential the total flux linkage of a phase winding can be calculated. This is done as follows. Using the relation

$$B = \nabla \times A \tag{B.2}$$

and Stoke's theorem, the flux through a surface S is

$$\begin{aligned} \Phi &= \int_S B\cdot dS \\ &= \int_S \nabla \times A\cdot dS \\ &= \oint_c A\cdot dl \ . \end{aligned} \tag{B.3}$$

Hence, in terms of finite elements using a first-order triangular mesh, the flux linkage of a coil with z turns, coil-area, S, and length, l, (along the z-direction) is

$$\lambda = z\,\Phi = z \sum_{j=1}^{n} \frac{\Delta_j}{S}\left(\zeta \frac{1}{3}\sum_{i=1}^{3} A_{ij}\right) l \ . \tag{B.4}$$

A_{ij} is the value of the magnetic vector potential of nodal point i = 1, i = 2 or i = 3 of the triangular element j. ζ = +1 or = -1 gives the direction of integration either into the plane or out of the plane. Δ_j is the area of the triangle element j. n is the total number of elements of the in-going and out-going areas of the coil being meshed.

From eqn (B.4) for an electrical machine with only one pole meshed, the total flux linkage of a phase winding is

$$\lambda_{phase} = \frac{2\,p\,z\,l}{n_a\,S} \sum_{j=1}^{u}\left(\frac{\Delta_j\,\zeta}{3}\sum_{i=1}^{3} A_{ij}\right) \tag{B.5}$$

where u is the total number of elements of the meshed coil areas of the phase in the pole region.

B.3 Calculation of the fundamental airgap flux density

From eqns (B.1) and (B.2) the flux density vector can be expressed in terms of cylindrical coordinates as

$$\mathbf{B} = \left(\frac{1}{r}\frac{\partial A_z}{\partial \theta}\right)\mathbf{a}_r + \left(-\frac{\partial A_z}{\partial i}\right)\mathbf{a}_\theta \qquad (B.6)$$

where $\mathbf{a}_r$ is the unit vector directed radially outwards, normal to the cylindrical surface, and $\mathbf{a}_\theta$ is the unit vector that points in the direction of increasing θ, tangential to the cylindrical surface. What is of interest is the radial component of the airgap flux density at e.g. the stator inner bore where $r = d_i/2$. Thus, from eqn (B.6) the magnitude of the radial airgap flux density at the stator inner surface is

$$B_r = \frac{2}{d_i}\frac{\partial A_z}{\partial \theta} . \qquad (B.7)$$

The first partial derivative of A_z with respect to θ can be determined by the finite-difference approximation, i.e.

$$\frac{\partial A_z}{\partial \theta} \approx \frac{A_z(\theta + \delta) - A_z(\theta)}{\delta} . \qquad (B.8)$$

At the stator inner surface the nodal values in terms of magnetic vector potential are known. From eqns (B.7) and (B.8), therefore, the radial airgap flux density between nodal points *n* and *n+1* on the stator inner diameter can be determined as

$$B_{r(n)} = \frac{2}{d_i}\left(\frac{A_{z(n+1)} - A_{z(n)}}{\theta_{(n+1)} - \theta_{(n)}}\right) . \qquad (B.9)$$

Note that the angles of eqn (B.9) are electrical angles. Owing to the fact that only a pole is meshed, the airgap flux density of eqn (B.9) is known for only a pole pitch, i.e. half a cycle. However, with negative periodicity where

$$\mathbf{B}(r,\theta+\pi) = -\mathbf{B}(r,\theta) , \qquad (B.10)$$

the flux density is known over two pole pitches or one cycle. What is of interest is the fundamental of the radial airgap flux density. This can be determined from a Fourier expansion of the flux density.

For the fundamental, the airgap flux density can be expressed as

$$\begin{aligned} B_{r1}(\theta) &= a_1 \sin(\theta) + b_1 \cos(\theta) \\ &= \hat{B} \sin(\theta + \theta_1) \end{aligned} \tag{B.11}$$

where

$$\hat{B} = \sqrt{a_1^2 + b_1^2} \qquad \text{and}$$
$$\theta_1 = \arctan\left(\frac{b_1}{a_1}\right). \tag{B.12}$$

a_1 and b_1 of eqns (B.11) and (B.12) are the Fourier coefficients for the fundamental and are given by

$$a_1 = \frac{2}{\pi} \int_0^{\pi} B(\theta) . \sin(\theta) . d\theta \tag{B.13}$$

and

$$b_1 = \frac{2}{\pi} \int_0^{\pi} B(\theta) . \cos(\theta) . d\theta \; . \tag{B.14}$$

From eqns (B.13) and (B.14), a_1 and b_1 can be determined using n_t nodal points on the stator inner bore over a pole pitch, as

$$a_1 = \frac{2}{\pi} \sum_{n=1}^{n_t} B_{r(n)} . \sin(\theta'_{(n)}) . (\theta_{(n+1)} - \theta_{(n)}) \tag{B.15}$$

and

$$b_1 = \frac{2}{\pi} \sum_{n=1}^{n_t} B_{r(n)} . \cos(\theta'_{(n)}) . (\theta_{(n+1)} - \theta_{(n)}) \tag{B.16}$$

where

$$\theta'_{(n)} = \frac{\theta_{(n+1)} - \theta_{(n)}}{2} \; . \tag{B.17}$$

Note that with eqns (B.15) and (B.16), the higher the number of nodal points, the greater the accuracy.

Eqn (B.12) is used to calculate the amplitude and the space angle of the fundamental radial airgap flux density. θ_1 of eqn (B.12), however, must be adjusted with some offset angle to obtain the position of the flux density space phasor with respect to the electrical d-axis position of the rotor.

C Saturation Factor and Slot Leakage Inductance

In this appendix the calculation of the saturation factor for the d-axis magnetic field is described. A formula for the slot leakage inductance is given and discussed in section C.2.

C.1 Saturation factor for the d-axis magnetic field

The saturation factor k_{sd} of the d-axis magnetic circuit is calculated by assuming only d-axis magnetic flux due to the d-axis MMF. It is thus assumed that a sinusoidal stator MMF with an amplitude equal to the d-axis MMF lies on the d-axis producing only d-axis magnetic flux. The effect of cross magnetisation is in other words ignored in this calculation method. The saturation factor k_{sd} is defined as

$$k_{sd} = \frac{F_{tot}}{F_t} \tag{C.1}$$

where F_{tot} is the total fundamental stator MMF and F_t the fundamental MMF of the slotted airgap.

With a sinusoidal MMF waveform the flux density in the airgap will have a flat distribution as shown in Fig. C.1(a) due to the non-linear B/H characteristic of the iron core. The airgap flux density waveform may differ significantly from the sinusoidal fundamental waveform and it is therefore important to do the calculations at a point in the airgap where the fundamental flux density wave intersects with the actual flux density wave. The flattened or saturated airgap flux density wave can be considered as a fundamental flux density wave plus the sum of harmonic flux density waves of orders 3, 5, 7, 9, etc. If only the prominent 3rd harmonic flux density is considered and the other higher harmonic flux densities are ignored, then the flux density waveform in the airgap will have the waveform as shown in Fig. C.1(b). Hence, a good operating point in the airgap is at the positions ⅓ or ⅔ of the pole pitch where the fundamental intersects with the actual wave. The magnetic circuit

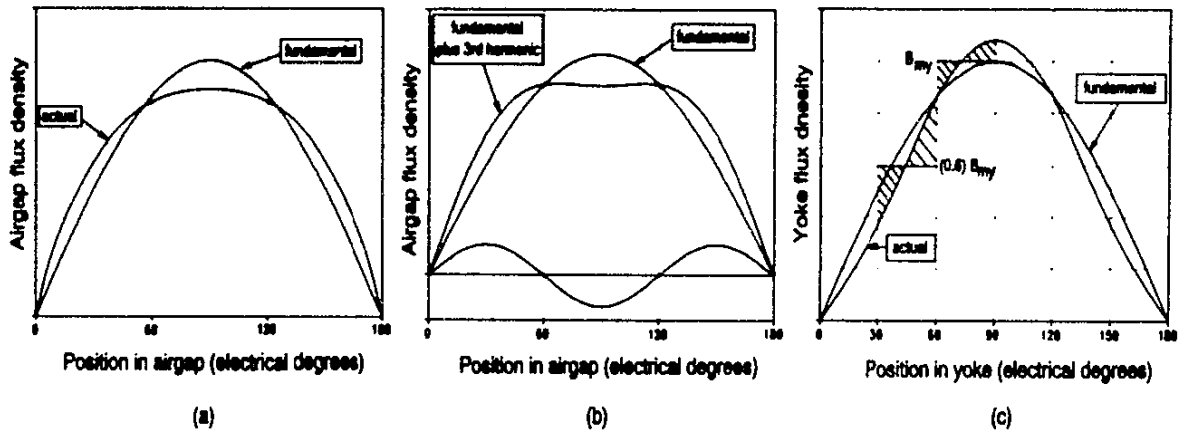

Fig. C.1. Effect of magnetic saturation on the airgap and yoke flux densities

to be analysed therefore is chosen to be that shown in Fig. C.2. Due to symmetry only half of the magnetic circuit needs to be analysed.

Next to be considered is the flux density in the yoke. If the airgap flux density waveform is sinusoidal then the yoke flux density waveform must also be sinusoidal but displaced 90° electrical in space from the airgap flux density wave. With the saturated airgap flux density waveform of Fig. C.1(a), however, the yoke flux density will have the waveform of Fig. C.1(c). With this waveform, average values for the flux densities in the different regions of the yoke are used as an approximation. These average values are shown in Fig. C.1(c). For ⅓ of the yoke region under consideration the average value for the flux density is taken as the maximum value of the fundamental yoke flux density, B_{my}. For the other ⅓ yoke region the average flux density is taken as $(0.6)B_{my}$. Another region in the yoke is defined in Fig. C.2, namely region 3. For this region the flux density is also taken as $(0.6)B_{my}$. Obviously, it would be more accurate if the yoke is divided into more than just 3 sections.

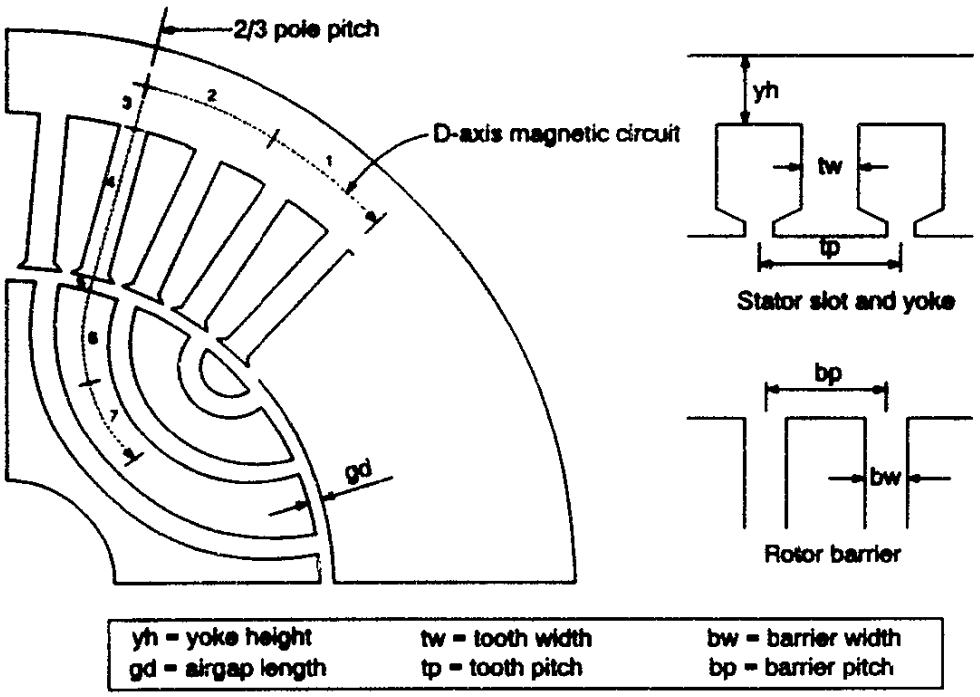

Fig. C.2. Magnetic circuit of the d-axis magnetic field

With the magnetic circuit defined, the MMFs of the different sections of the magnetic circuit can be calculated. Firstly, the amplitude of the total fundamental MMF of the polyphase winding (m > 1) can be calculated by means of the following equation (Liwschitz-Garik and Whipple, 1961, eqn 15-8):

$$F_{tot} = \frac{\sqrt{2}\, m\, W\, K_{w1}}{\pi\, p} I_m \,. \qquad (C.2)$$

In this equation I_m is the RMS value of the magnetising phase current which is also equal to

$$I_m = I_d/\sqrt{2} \tag{C.3}$$

where I_d is the steady-state d-axis fundamental stator current component. From eqns (C.2) and (C.3) the value of the total MMF at a position ⅔ of the pole pitch is

$$\begin{aligned} F_{tot(120°)} &= \frac{\sqrt{2}\, m\, W\, K_{w1}}{\pi\, p} \frac{I_d}{\sqrt{2}} \sin(120°) \\ &= \frac{\sqrt{3}\, m\, W\, K_{w1}\, I_d}{2\, \pi\, p} . \end{aligned} \tag{C.4}$$

This value of the total MMF is equal to the sum of the different MMF drops of the magnetic circuit, namely

$$F_{tot(120°)} = F_{f(120°)} + F_r + F_t + F_y \tag{C.5}$$

where $F_{f(120°)}$ is the airgap MMF at ⅔ pole pitch position,
F_r and F_t are the rotor iron segment and stator tooth MMFs respectively for ⅔ pole pitch position
and F_y is the yoke MMF.

An equation for the airgap MMF can be obtained from the following two equations for the total flux per pole of the machine, namely

$$\Phi_p = \frac{2}{\pi} F_f \left(\frac{\mu_o\, \tau_p\, l}{k_c\, g_d} \right), \tag{C.6}$$

and

$$\Phi_p = \frac{2}{\pi} B_{mf}\, \tau_p\, l , \tag{C.7}$$

where F_f is the amplitude of the fundamental airgap MMF and k_c the Carter factor, so that

$$F_f = B_{mf} \left(\frac{k_c\, g_d}{\mu_o} \right). \tag{C.8}$$

At ⅔ pole pitch position the airgap MMF is

$$F_{f(120°)} = \frac{\sqrt{3}\, B_{mf}\, k_c\, g_d}{2\, \mu_o} . \tag{C.9}$$

To calculate the tooth MMF the tooth flux density must be known. This is calculated from the airgap flux density at ⅔ pole pitch position as

$$B_t = \frac{\sqrt{3}}{2} B_{mf} \left(\frac{t_p}{t_w K_s} \right) \tag{C.10}$$

where K_s is the stacking factor. With B_t known the magnetic field strength H_t can be obtained from the B/H-curve of the lamination steel. The tooth MMF is then calculated as

$$F_t = H_t l_4 \tag{C.11}$$

where l_4 is the tooth length, i.e. the length of region 4 of the magnetic circuit shown in Fig. C.2.

If the stator slot has a round bottom and the width of the tooth top is very different from the tooth width, then the magnetic circuit of the tooth must be divided into more sections with different tooth widths and thus different flux densities.

The rotor iron segment MMF is calculated similarly to the stator tooth MMF. The flux density of region 6 of Fig. C.2 is calculated as

$$B_{r(6)} = \frac{\sqrt{3}}{2} B_{mf} \left(\frac{b_p}{(b_p - b_w) K_s} \right). \tag{C.12}$$

The flux density in region 7 of the rotor may be different from that of region 6 as the width of the iron segment may be different. The latter depends on the space available for the flux barriers and iron segments between the rotor shaft and the outer part of the rotor (see Fig. C.2 as an example). The approximate flux density in region 7 of the rotor is calculated as

$$B_{r(7)} = B_{r(6)} \left(\frac{\pi d_r}{2 p (d_r - d_{shf})} \right) \tag{C.13}$$

where d_r is the outer diameter of the rotor and d_{shf} the shaft diameter.

The field strengths for regions 6 and 7, $H_{r(6)}$ and $H_{r(7)}$, can be obtained from the B/H curve using the known flux densities of eqns (C.12) and (C.13). The rotor MMF is calculated as

$$F_r = H_{r(6)} l_6 + H_{r(7)} l_7 \tag{C.14}$$

where l_6 and l_7 are the iron lengths of regions 6 and 7 of the rotor.

The maximum value of the stator yoke flux density of the fundamental is calculated from the airgap flux density as

$$\begin{aligned} B_{my} &= \frac{\Phi_p / 2}{yh \; l \; K_s} \\ &= \frac{B_{mf} d_i}{2 p \; yh \; K_s}, \end{aligned} \tag{C.15}$$

from eqn (C.7) and replacing τ_p. Eqn (C.15) can also be expressed in terms of a normalised value for the *yh*, that is

$$yh_{(nor)} = \frac{yh}{d_i} = \frac{1}{2\,p\,K_s}\left(\frac{B_{m\ell}}{B_{my}}\right). \qquad (C.16)$$

From Fig. C.1(c) the flux density in region 1 of the yoke is B_{my} and in region 2 $(0.6)B_{my}$. The corresponding H values, $H_{y(1)}$ and $H_{y(2)}$, of these regions can be obtained from the B/H curve. For region 3 of the yoke an average flux density of also $(0.6)B_{my}$ is accepted and the magnetic length is taken as equal to yh/4. The total yoke MMF is thus

$$F_y = H_{y(1)}\,l_1 + H_{y(2)}(l_2 + l_3). \qquad (C.17)$$

With the d-axis current of the machine known the total MMF can be calculated according eqn (C.4). The MMF of eqn (C.5) must be equal to this total MMF. This means that the airgap flux density $B_{m\ell}$ must be solved for as the only unknown. The latter signifies a non-linear solution which is done by an iterative procedure using simply the bisection method. The solution procedure has the following steps:

- Obtain the dq current components, specifically I_d.
- Calculate $F_a = F_{tot(120°)}$ according eqn (C.4).
- Choose boundary values for airgap flux density:
  $B_{m\ell(1)}$=0.1 tesla and $B_{m\ell(2)}$=1.5 tesla.

→ • Set $B_{m\ell} = (B_{m\ell(1)} + B_{m\ell(2)})/2$.

- Calculate $F_b = F_{tot(120°)}$ according eqn (C.5).
- If $|F_a - F_b| \le \xi\,(F_a + F_b)/2$ then goto ➡.
- If $(F_a - F_b) < 0$ then $B_{m\ell(2)} = B_{m\ell}$; else $B_{m\ell(1)} = B_{m\ell}$.
- Goto →.

➡ • End.

Finally, with the analysis done at ⅔ pole pitch position the equation for the saturation factor k_{sd} changes to

$$k_{sd} = \frac{F_{tot(120^\circ)}}{F_{f(120^\circ)}} . \qquad (C.18)$$

This concludes the calculation of the saturation factor for the d-axis magnetic field.

C.2 Formula for slot leakage inductance

The basic equation for the stator slot leakage inductance of standard alternating current machines can be found in many alternating current machine textbooks. In terms of the symbols of this thesis the formula for the slot leakage inductance per phase is as follows (Richter (1954), Schuisky (1957), Liwschitz-Garik (1961), Kübler (1961)):

$$L_{slot} = \left(\frac{2 \mu_o l W^2}{p q} \right) (k_f \Lambda_f + k_g \Lambda_g) \quad \text{henry/phase.} \qquad (C.19)$$

k_f and k_g are correction factors for double-layer windings of the slot sections that hold air and conductors respectively. These correction factors are given by, amongst others, Kübler (1961) as functions of $\varepsilon = c/mq$ and are in equation form:

$$\begin{aligned} k_f &= 1.5\,\epsilon - 0.25 \quad \text{for} \quad 1/3 \le \epsilon \le 2/3 \\ k_f &= 0.75\,\epsilon + 0.25 \quad \text{for} \quad 2/3 \le \epsilon \le 1 \end{aligned} \qquad (C.20)$$

and

$$\begin{aligned} k_g &= 9/8\,\epsilon + 1/16 \quad \text{for} \quad 1/3 \le \epsilon \le 2/3 \\ k_g &= 9/16\,\epsilon + 7/16 \quad \text{for} \quad 2/3 \le \epsilon \le 1 . \end{aligned} \qquad (C.21)$$

Λ_f of eqn (C.19) is the permeance ratio of the slot section that holds air and Λ_g is the permeance ratio of the slot section that holds the conductors. The permeance ratios depend on the shape of the stator slot. Formulae for the permeance ratios for various slot shapes are available from a few textbooks, amongst others those by Schuisky (1957) and Liwshitz-Garik (1961). For the most general slot shape, i.e. the rectangular slot shape shown in Fig. C.3, the permeance ratios are

$$\Lambda_f = \frac{h_2}{b_s} + \frac{2 h_3}{b_s + b_g} + \frac{h_4}{b_g} \qquad (C.22)$$

and

$$\Lambda_g = \frac{h_1}{3 b_s} . \qquad (C.23)$$

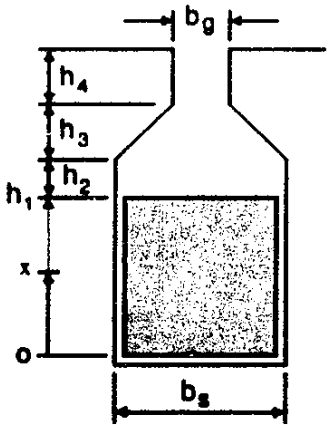

Fig. C.3. Rectangular slot shape

The permeance ratios of eqns (C.22) and (C.23) can also be used with little error for trapezoidal slots. For other slot shapes the general equation for Λ_s,

$$\Lambda_s = \int_0^{h_1} \left(\frac{A_s(x)}{A_s} \right)^2 \frac{dx}{b(x)} , \tag{C.24}$$

must be used. In this equation the conductor section areas $A_s(x)$ and A_s are

$$A_s(x) = \int_0^{x} b(x)\, dx \qquad \text{and}$$
$$A_s = \int_0^{h_1} b(x)\, dx \tag{C.25}$$

where b(x) is the slot width at position x. Equation (C.24) can be solved by dividing the conductor section of the slot into a number of small rectangular elements as described by Kamper (1987).

Finally, the calculation of the slot leakage inductance according to the above formulae does not take into account the skin effect and the effect of saturation.

D Accuracy of Computed Function Value

When only function values are available it is strictly speaking impossible to determine the accuracy of the computed function value. However, a reasonably reliable *estimate* of the accuracy of the computed function value can be obtained by using difference tables as described by Gill (1981).

To explain the difference table, the first column of the table is the computed function values f at a set of values $\{x_j\}$ where x_j is defined as $x_j = x + jb$, with $j = 0, 1, 2, \ldots, n$, and b is small. Each successive column of the table is defined as the difference of the values in the previous column. This is explained by means of the forward difference operator. The forward difference operator for the first difference column of the table, Δ^1, is defined by the relation

$$\Delta^1 f_j = f(x_{j+1}) - f(x_j) \; . \tag{D.1}$$

For the second difference column the second-order forward difference operator Δ^2 is defined as

$$\Delta^2 f_j = \Delta^1 f_{j+1} - \Delta^1 f_j \tag{D.2}$$

The higher-order differences $\Delta^k f_j$ can be defined in a similar way. Gill (1981) shows that the higher-order differences of the table (typical $k \geq 4$) start to reflect almost entirely the *differences* of the computed errors and that the differences of these columns tend to become similar in magnitude and to alternate in sign. For these columns where this general pattern is observed an estimate of the error in the computing value ε_c can be obtained. A formula for the estimation of ε_c from the k-th column of the difference table is given by Gill as

$$\epsilon_c^{(k)} \approx \frac{\max_j |\Delta^k f_j|}{\beta_k} \qquad \text{where}$$
$$\beta_k = \sqrt{\frac{(2k)!}{(k!)^2}} \; . \tag{D.3}$$

Typical values for k where the general pattern of behaviour begins are 4 or 5.

With ε_c known from the difference table, the relative error in the computed function value can be calculated as

$$\epsilon_r = \frac{\epsilon_c}{f(x)} \; . \tag{D.4}$$

h of eqn (3.11), which determines the stepsize in the forward difference approximation, is

$$h = \sqrt{\epsilon_r} \; . \tag{D.5}$$

To estimate the accuracy of the finite element computed function value, four sets of difference tables have been determined for different values of the stepsize *h* at different multidimensional vector points. Also, different dimensions (variables) of the RSM have been perturbed to study the accuracy of the computed value. These dimensions are the tooth width (*tw*), the stator inner diameter (*di*) and the inner barrier width (*iw*) (refer to Chapter 4 for further details about these dimensions). For each difference table the computed error ε_c, the relative error ε_r and the stepsize h have been calculated according to eqns (D.3) - (D.5). The torque of the machine was taken as the output function value for all the difference tables. The calculations were performed in double precision on a SUN 1000 workstation.

The results of the difference tables are shown in Tables D.1 - D.4 (see following pages). It is observed from all the difference tables that the elements of difference columns 4 and 5 show to some extent the pattern of sign alternation, although not consistently. Also, the elements of these columns are not always of similar magnitude. Nevertheless, these columns have been used to estimate ε_c and h.

Tables D.1 and D.2 show that with a smaller stepsize of $b=10^{-9}$, the calculated h values for the different dimensions becomes more in agreement with each other. The same result is observed from Tables D.3 and D.4. It can further be seen that there is little difference in the calculated h values for the two different multidimensional vector points (compare Table D.1 with Table D.3 and Table D.2 with Table D.4).

One may conclude from the results that an h value of between 10^{-5} and 10^{-6} can be used for the calculation of the first partial derivative of eqn (3.11). It has been mentioned in section 3.3 that faster optimisation results were obtained with h values between 10^{-4} and 10^{-5}.

j	f_j	Δ^1	Δ^2	Δ^3	Δ^4	Δ^5	
Tooth width (tw)							
0	0.579E+02	0.319E-06	-0.109E-09	-0.169E-09	-0.275E-09	-0.472E-09	
1	0.579E+02	0.319E-06	0.604E-10	0.106E-09	0.196E-09	0.325E-09	$\varepsilon_c^{(4)}$ = 0.519E-10
2	0.579E+02	0.319E-06	-0.455E-10	-0.904E-10	-0.129E-09	-0.955E-10	$h^{(4)}$ = 0.946E-06
3	0.579E+02	0.319E-06	0.449E-10	0.384E-10	-0.333E-10	-0.200E-09	
4	0.579E+02	0.319E-06	0.655E-11	0.717E-10	0.167E-09	0.188E-09	$\varepsilon_c^{(5)}$ = 0.832E-10
5	0.579E+02	0.319E-06	-0.651E-10	-0.949E-10	-0.217E-10	0.412E-09	$h^{(5)}$ = 1.198E-06
6	0.579E+02	0.319E-06	0.298E-10	-0.732E-10	-0.434E-09	-0.132E-08	
Stator inner diameter (di)							
0	0.579E+02	0.396E-06	0.208E-05	0.416E-05	0.624E-05	0.700E-05	
1	0.579E+02	-0.169E-05	-0.208E-05	-0.208E-05	-0.763E-06	0.318E-05	$\varepsilon_c^{(4)}$ = 0.746E-06
2	0.579E+02	0.390E-06	-0.659E-09	-0.131E-05	-0.394E-05	-0.790E-05	$h^{(4)}$ = 1.135E-04
3	0.579E+02	0.390E-06	0.131E-05	0.263E-05	0.396E-05	0.529E-05	
4	0.579E+02	-0.923E-06	-0.132E-05	-0.132E-05	-0.133E-05	-0.134E-05	$\varepsilon_c^{(5)}$ = 0.498E-06
5	0.579E+02	0.395E-06	0.582E-08	0.639E-08	0.846E-08	0.196E-07	$h^{(5)}$ = 0.927E-04
6	0.579E+02	0.389E-06	-0.569E-09	-0.207E-08	-0.111E-07	-0.341E-07	
Inner barrier width (iw)							
0	0.579E+02	0.613E-07	0.374E-10	0.674E-10	0.514E-11	-0.399E-09	
1	0.579E+02	0.613E-07	-0.299E-10	0.622E-10	0.404E-09	0.118E-08	$\varepsilon_c^{(4)}$ = 0.919E-10
2	0.579E+02	0.613E-07	-0.922E-10	-0.342E-09	-0.773E-09	-0.143E-08	$h^{(4)}$ = 1.254E-06
3	0.579E+02	0.614E-07	0.250E-09	0.431E-09	0.656E-09	0.959E-09	
4	0.579E+02	0.612E-07	-0.182E-09	-0.225E-09	-0.302E-09	-0.337E-09	$\varepsilon_c^{(5)}$ = 0.913E-10
5	0.579E+02	0.614E-07	0.433E-10	0.775E-10	0.346E-10	-0.408E-09	$h^{(5)}$ = 1.256E-06
6	0.579E+02	0.613E-07	-0.342E-10	0.429E-10	0.442E-09	0.145E-08	

Table D.1. Difference table at tw = 5.57, di = 105.6, iw = 5.8 with $b = 10^{-7}$

j	f_j	Δ^1	Δ^2	Δ^3	Δ^4	Δ^5	
Tooth width (tw)							
0	0.579E+02	0.306E-08	-0.168E-09	-0.253E-09	-0.381E-09	-0.482E-09	
1	0.579E+02	0.323E-08	0.848E-10	0.127E-09	0.102E-09	0.240E-10	$\varepsilon_c^{(4)}$ = 0.987E-10
2	0.579E+02	0.314E-08	-0.424E-10	0.253E-10	0.779E-10	-0.285E-10	$h^{(4)}$ = 1.306E-06
3	0.579E+02	0.318E-08	-0.677E-10	-0.526E-10	0.106E-09	0.526E-09	
4	0.579E+02	0.325E-08	-0.150E-10	-0.159E-09	-0.419E-09	-0.996E-09	$\varepsilon_c^{(5)}$ = 1.203E-10
5	0.579E+02	0.327E-08	0.144E-09	0.260E-09	0.577E-09	0.140E-08	$h^{(5)}$ = 1.442E-06
6	0.579E+02	0.312E-08	-0.116E-09	-0.317E-09	-0.826E-09	-0.191E-08	
Stator inner diameter (di)							
0	0.579E+02	0.413E-08	-0.379E-08	-0.747E-08	-0.115E-07	-0.189E-07	
1	0.579E+02	0.792E-08	0.369E-08	0.407E-08	0.740E-08	0.171E-07	$\varepsilon_c^{(4)}$ = 1.637E-09
2	0.579E+02	0.424E-08	-0.386E-09	-0.333E-08	-0.970E-08	-0.234E-07	$h^{(4)}$ = 5.318E-06
3	0.579E+02	0.462E-08	0.294E-08	0.637E-08	0.137E-07	0.273E-07	
4	0.579E+02	0.168E-08	-0.342E-08	-0.736E-08	-0.135E-07	-0.233E-07	$\varepsilon_c^{(5)}$ = 1.720E-09
5	0.579E+02	0.510E-08	0.394E-08	0.618E-08	0.973E-08	0.169E-07	$h^{(5)}$ = 5.450E-06
6	0.579E+02	0.116E-08	-0.225E-08	-0.355E-08	-0.713E-08	-0.131E-07	
Inner barrier width (iw)							
0	0.579E+02	0.697E-09	0.611E-10	0.106E-09	0.382E-09	0.117E-08	
1	0.579E+02	0.636E-09	-0.446E-10	-0.277E-09	-0.783E-09	-0.168E-08	$\varepsilon_c^{(4)}$ = 1.076E-10
2	0.579E+02	0.681E-09	0.232E-09	0.507E-09	0.900E-09	0.152E-08	$h^{(4)}$ = 1.363E-06
3	0.579E+02	0.449E-09	-0.275E-09	-0.394E-09	-0.621E-09	-0.120E-08	
4	0.579E+02	0.723E-09	0.119E-09	0.227E-09	0.580E-09	0.135E-08	$\varepsilon_c^{(5)}$ = 1.058E-10
5	0.579E+02	0.605E-09	-0.109E-09	-0.353E-09	-0.769E-09	-0.139E-08	$h^{(5)}$ = 1.352E-06
6	0.579E+02	0.713E-09	0.244E-09	0.416E-09	0.624E-09	0.837E-09	

Table D.2. Difference table at *tw* = 5.57, *di* = 105.6, *iw* = 5.8 (same as Table D.1) with $b = 10^{-9}$

j	f_j	Δ^1	Δ^2	Δ^3	Δ^4	Δ^5	
Tooth width (tw)							
0	0.411E+02	0.208E-05	0.226E-08	0.104E-08	0.405E-09	-0.242E-09	
1	0.411E+02	0.207E-05	0.122E-08	0.637E-09	0.647E-09	0.913E-09	$\varepsilon_c^{(4)}$ = 0.773E-10
2	0.411E+02	0.207E-05	0.581E-09	-0.107E-10	-0.266E-09	-0.330E-09	$h^{(4)}$ = 1.372E-06
3	0.411E+02	0.207E-05	0.592E-09	0.255E-09	0.636E-10	-0.169E-09	
4	0.411E+02	0.207E-05	0.337E-09	0.192E-09	0.233E-09	0.378E-09	$\varepsilon_c^{(5)}$ = 0.762E-10
5	0.411E+02	0.207E-05	0.145E-09	-0.410E-10	-0.145E-09	-0.555E-09	$h^{(5)}$ = 1.362E-06
6	0.411E+02	0.207E-05	0.186E-09	0.104E-09	0.410E-09	0.121E-08	
Stator inner diameter (di)							
0	0.411E+02	0.562E-05	0.776E-08	0.743E-08	0.791E-08	0.772E-08	
1	0.411E+02	0.562E-05	0.333E-09	-0.484E-09	0.192E-09	0.196E-08	$\varepsilon_c^{(4)}$ = 3.430E-07
2	0.411E+02	0.562E-05	0.817E-09	-0.676E-09	-0.177E-08	0.491E-09	$h^{(4)}$ = 0.914E-04
3	0.411E+02	0.562E-05	0.149E-08	0.109E-08	-0.226E-08	-0.101E-07	
4	0.411E+02	0.561E-05	0.402E-09	0.335E-08	0.780E-08	-0.946E-06	$\varepsilon_c^{(5)}$ = 3.616E-07
5	0.411E+02	0.561E-05	-0.295E-08	-0.444E-08	0.954E-06	0.383E-05	$h^{(5)}$ = 0.938E-04
6	0.411E+02	0.562E-05	0.150E-08	-0.958E-06	-0.287E-05	-0.574E-05	
Inner barrier width (iw)							
0	0.411E+02	-0.432E-06	0.310E-09	0.291E-09	0.622E-09	0.132E-08	
1	0.411E+02	-0.432E-06	0.191E-10	-0.331E-09	-0.697E-09	-0.116E-08	$\varepsilon_c^{(4)}$ = 0.833E-10
2	0.411E+02	-0.432E-06	0.350E-09	0.366E-09	0.459E-09	0.331E-09	$h^{(4)}$ = 1.424E-06
3	0.411E+02	-0.432E-06	-0.163E-10	-0.929E-10	0.128E-09	0.552E-09	
4	0.411E+02	-0.432E-06	0.767E-10	-0.221E-09	-0.424E-09	-0.507E-09	$\varepsilon_c^{(5)}$ = 0.832E-10
5	0.411E+02	-0.432E-06	0.298E-09	0.203E-09	0.837E-10	-0.201E-09	$h^{(5)}$ = 1.422E-06
6	0.411E+02	-0.433E-06	0.951E-10	0.119E-09	0.284E-09	0.532E-09	

Table D.3. Difference table at tw = 7.5, di = 133.0, iw = 3.5 with $b = 10^{-7}$

j	f_j	Δ^1	Δ^2	Δ^3	Δ^4	Δ^5	
Tooth width (tw)							
0	0.411E+02	0.208E-07	0.198E-10	0.275E-10	0.324E-10	0.461E-10	
1	0.411E+02	0.208E-07	-0.769E-11	-0.483E-11	-0.137E-10	-0.137E-10	$\varepsilon_c^{(4)}$ = 0.571E-10
2	0.411E+02	0.208E-07	-0.286E-11	0.885E-11	0.14 .E-13	-0.122E-09	$h^{(4)}$ = 1.179E-06
3	0.411E+02	0.208E-07	-0.117E-10	0.884E-11	0.122E-09	0.406E-09	
4	0.411E+02	0.208E-07	-0.205E-10	-0.114E-09	-0.284E-09	-0.617E-09	$\varepsilon_c^{(5)}$ = 0.867E-10
5	0.411E+02	0.208E-07	0.930E-10	0.170E-09	0.333E-09	0.811E-09	$h^{(5)}$ = 1.444E-06
6	0.411E+02	0.207E-07	-0.773E-10	-0.163E-09	-0.478E-09	-0.136E-08	
Stator inner diameter (di)							
0	0.411E+02	0.570E-07	0.119E-08	-0.696E-09	-0.586E-08	-0.147E-07	
1	0.411E+02	0.558E-07	0.188E-08	0.517E-08	0.882E-08	0.137E-07	$\varepsilon_c^{(4)}$ = 1.924E-09
2	0.411E+02	0.539E-07	-0.328E-08	-0.366E-08	-0.485E-08	-0.119E-07	$h^{(4)}$ = 6.843E-06
3	0.411E+02	0.572E-07	0.375E-09	0.119E-08	0.701E-08	0.230E-07	
4	0.411E+02	0.568E-07	-0.818E-09	-0.581E-08	-0.160E-07	-0.321E-07	$\varepsilon_c^{(5)}$ = 2.022E-09
5	0.411E+02	0.576E-07	0.499E-08	0.101E-07	0.161E-07	0.237E-07	$h^{(5)}$ = 7.014E-06
6	0.411E+02	0.526E-07	-0.515E-08	-0.600E-08	-0.760E-08	-0.105E-07	
Inner barrier width (iw)							
0	0.411E+02	-0.436E-08	-0.991E-10	-0.255E-09	-0.596E-09	-0.119E-08	
1	0.411E+02	-0.426E-08	0.156E-09	0.340E-09	0.594E-09	0.889E-09	$\varepsilon_c^{(4)}$ = 0.712E-10
2	0.411E+02	-0.442E-08	-0.184E-09	-0.253E-09	-0.296E-09	-0.344E-09	$h^{(4)}$ = 1.316E-06
3	0.411E+02	-0.423E-08	0.692E-10	0.423E-10	0.488E-10	0.787E-10	
4	0.411E+02	-0.430E-08	0.269E-10	-0.648E-11	-0.299E-10	0.997E-10	$\varepsilon_c^{(5)}$ = 0.750E-10
5	0.411E+02	-0.433E-08	0.333E-10	0.235E-10	-0.[illegible]E-09	-0.555E-09	$h^{(5)}$ = 1.351E-06
6	0.411E+02	-0.436E-08	0.987E-11	0.153E-09	0.425E-09	0.882E-09	

Table D.4. Difference table at tw = 7.5, di = 133.0, iw = 3.5 (same as Table D.3) with $b = 10^{-9}$

E Construction of the 9 kW Reluctance Synchronous Machine

In Figs. E.1 and E.2 the photos are shown of the stator and rotor construction of the optimum-designed 9 kW RSM assembled in a 5.5 kW induction machine frame.

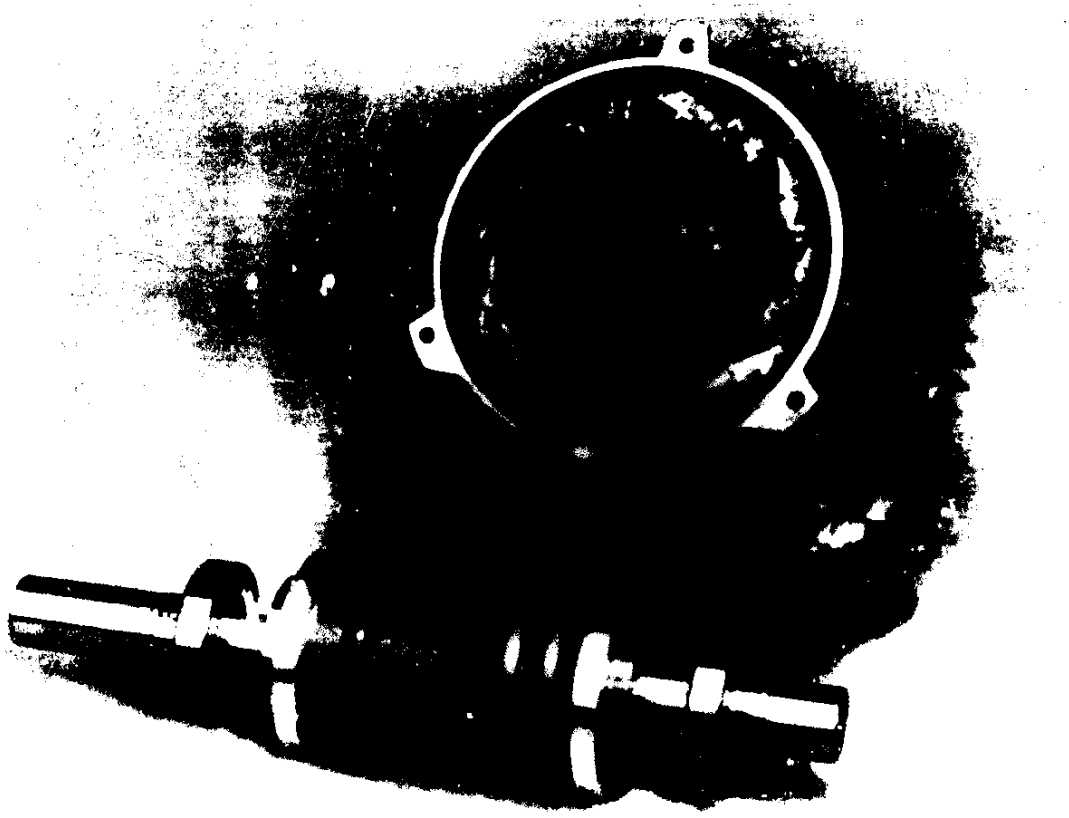

Fig. E.1 Stator and rotor of the reluctance synchronous machine

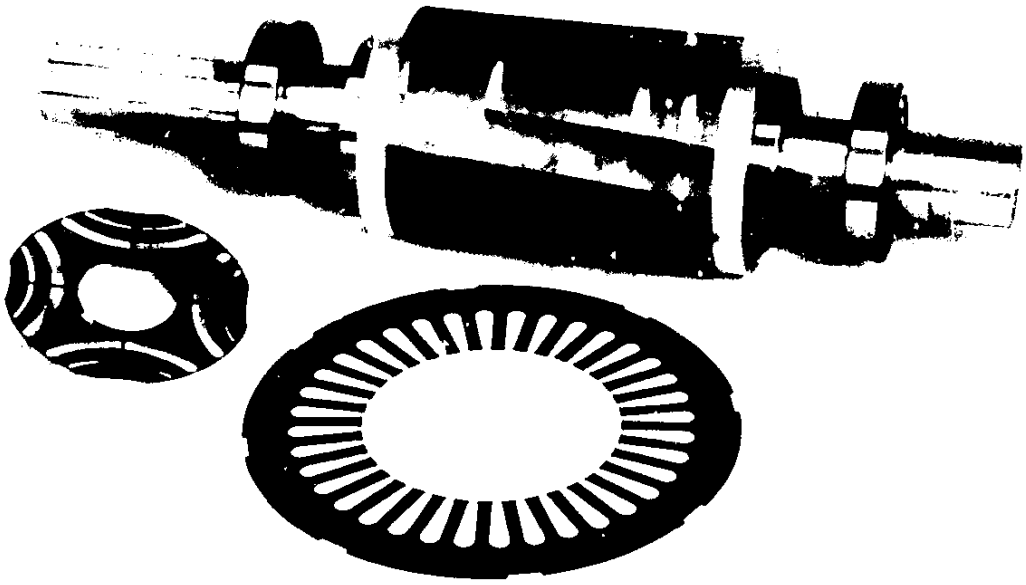

Fig. E.2 Skewed rotor with stator and rotor laminations